Univerzita Karlova
Přírodovědecká fakulta

Studijní program: Chemie
Studijní obor: Medicinální chemie

Anastasiya Zakharanka

Fyzikálně-chemické vlastnosti kyseliny oxamové a glyoxalové a jejich afinita k lanthanoidům

Physicochemical properties of oxamic and glyoxylic acids and their affinity to lanthanides

Bakalářská práce

Vedoucí závěrečné práce: RNDr. Václav Tyrpekl, Ph.D.

Praha, 2021

Charles University

Faculty of Science

Study programme: Chemistry

Branch of study: Medicinal chemistry

Anastasiya Zakharanka

Physicochemical properties of oxamic and glyoxylic acids and their affinity to lanthanides

Fyzikálně-chemické vlastnosti kyseliny oxamové a glyoxalové a jejich afinita k lanthanoidům

Bachelor´s thesis

Supervisor: RNDr. Václav Tyrpekl, Ph.D.

Prague, 2021

Prohlášení:

Prohlašuji, že jsem závěrečnou práci zpracovala samostatně a že jsem uvedla všechny použité informační zdroje a literaturu. Tato práce ani její podstatná část nebyla předložena k získání jiného nebo stejného akademického titulu.

V Praze, dne 21.06.2021

Podpis

Poděkování:

Nejprve bych chtěla poděkovat vedoucímu moje práce RNDr. Václavu Tyrpeklovi, Ph.D. za vřelou pomoc a rady, trpělivé vedení a ochotu během psaní této práce, a taky za měření SEM. Dále bych chtěla poděkovat RNDr. Ivaně Císařové, CSc. za určení krystalografické struktury, Mgr. Adamovi Alemayehu za pomoc s TGA měřeními, prof. RNDr. Ivanu Němcovi a Mgr. Soně Kohútekové za měření IR, a celému kolektivu laboratoře za vytvoření příjemného pracovního prostředí.

Abstrakt

Oblastí zájmu této práce jsou určité aspekty základních fyzikálně-chemických vlastností kyseliny oxamové a glyoxalové a jejich afinita k lanthanoidům, jako zástupci byli zvoleni cerium a gadolinium. Pro každou kyselinu byla zjištěná rozpustnost při pokojové teplotě, hodnoty pKa a jejich tepelná a fotochemická stabilita. Byla studovaná afinita kyselin k iontům lanthanoidů (III) ve vodném roztoku pomocí různých konvenčních laboratorních technik a instrumentálních metod. Dekahydráty oxalátů lanthanoidů byly syntetizovány postupy heterogenních a homogenních srážení a charakterizované klasickými analytickými technikami v pevné fázi.

Klíčová slova: srážecí reakce, kyselina oxamová, oxamáty, šťavelany (oxálaty), kyselina glyoxalová, chemie f-prvků

Abstract

This bachelor work focuses on studies of chosen aspects of the basic physicochemical properties of oxamic and glyoxylic acids and their affinity to lanthanides, cerium, and gadolinium taken as the representatives. Room temperature solubilities, pKa values, thermal and photochemical stability of the acids have been evaluated. The acids' affinity to lanthanide (III) ions in an aqueous solution has been studied using various conventional laboratory techniques and instrumental methods. Lanthanide oxalate decahydrates have been synthesized using heterogeneous and homogeneous precipitation routes and characterized using classical solid-state analytical techniques.

Keywords: oxalic acid precipitation, oxamic acid, oxamates, oxalates, glyoxylic acid, f-block metals chemistry

Contents

The list of the abbreviations used

Ln – lanthanide
REE – rare earth element
CFSE – crystal field stabilisation energy
CN – coordination number
LPC – lipid-protein complex
ROS – reactive oxygen species
MRI – magnetic resonance imaging
CT – computer tomography
PET – positron emission tomography
LBT – lanthanide binding tag
TOF-MS – time-of-flight mass spectrometry
ICP-MS - inductively coupled plasma mass spectrometry
Z – atomic number of a nuclide
A – mass number of a nuclide
nca – non carrier added
ca – carrier added
EDTMP - ethylene diamine tetramethylene phosphonate
DOTMP - 1,4,7,10-tetraazacyclododecane-1,4,7,10-tetramethylene phosphonic acid
PLLA - poly(L-lactic acid)
RSV – radiosynovectomy
α-HIBA - α-hydroxyisobutyric acid
HPIC – high performance ion chromatography
MOF - metal-organic framework
DMSO – dimethyl sulfoxide
NMR – nuclear magnetic resonance
DOTA – 1,4,7,10-tetraazacyclododecane-1,4,7,10-tetraacetic acid
DTPA – diethylene triamine pentaacetic acid
LDH – lactate dehydrogenase
EG – ethylene glycol
EDS – energy-dispersive X-ray spectroscopy
Rwp – weighted profile R-factor
GOF – goodness of fit

1. Introduction

This bachelor's work focuses on studies of the chosen aspects of the basic physicochemical properties of oxamic and glyoxylic acids and their affinity to lanthanides (cerium and gadolinium are chosen as the representatives).

The idea of the work came from the comprehensive study of the oxalic acid coordination chemistry and its extensive implementations in the lanthanide and actinide technology [1, 2]. The oxalic conversion method, which involves the metal's oxalic precipitation from the solution and subsequent thermal decomposition of the formed metal oxalate, is outstandingly important in the nuclear industry, in the preparative inorganic chemistry, analytical chemistry of the f-elements, in the applied science [3, 4, 5].

Oxamic and glyoxylic acids may be seen as the oxalic acid analogues, where amide or aldehyde functionalities, respectively, replaced one carboxylic moiety. Due to the lack of information concerning the mentioned above acids in the inorganic chemistry context, these compounds' partial characterization will be conducted. The emphasis will be put on the acids' behaviour in aqueous solutions. As well, these simple organic acids will be tested for easy lanthanide separation from aqueous solutions.

Overall, the carboxylic acids with simple structure received some attention in the context of the f-elements chemistry. For example, such compounds as fumaric, oxalic, glycolic, maleic, α-hydroxyisobutyric acids are crucial in the metal-organic 3D extended structures construction [6], in the recovery of rare earth elements from industrial waste [7], in the radiolanthanides separation and purification techniques [8, 9]. Thereby, the problematics of the oxamic and glyoxylic acids' affinity to lanthanides seems of interest.

Moreover, theoretical research concerning the lanthanides' applications in medicine and their general biochemical relevance will be carried out. The 4f metals have remarkable atomic properties and are widely used in modern technology [10, 11]; however, in the field of medicinal chemistry, these metals are a somewhat unexplored subject to study. Thereby, in the current theoretical investigation, several medicinal chemistry relevant aspects of the lanthanide chemistry will be discussed, including facts concerning the properties of non-radioactive species [12] and the characteristics of the radioactive elements employed in nuclear medicine [8].

2. Aims and objectives

Following aims and objectives were selected in presented thesis.

i) To conduct a theoretical research about lanthanides implementation in radiomedicine and evaluate their biomedical potential. Moreover, the bibliographic review about the oxamic and glyoxylic acids should be done, putting emphasis on their use in the technology of lanthanides.

ii) Since the physicochemical properties of oxamic and glyoxylic acids in aqueous solutions are poorly known their basic characterisation (pKa values, solubility) should be performed.

iii) Additionally, the stability (thermal and photochemical) of the oxamic and glyoxylic acids in aqueous solutions is to be estimated; special attention should be given to the hydrolysis/decomposition and its kinetics.

iv) The affinity of the concerned acids to lanthanides in aqueous solutions is to be examined taking cerium and gadolinium as the Ln series representatives. And as a result, the potential of both acids is to be evaluated in similar view as the 4f elements separations using oxalic acid.

v) All intermediate and final products should be characterized using classical solid-state analytical techniques (e.g., roentgen diffraction, thermogravimetry and electron microscopy).

3. Theoretical part

3.1 Lanthanides: Biochemical relevance and medical applications

The f-block elements, comprising lanthanide and actinide series, possess interesting magnetic, spectroscopic, and nuclear properties. They are suitable for a range of biomedical applications and play an important role in diagnostics, imaging, and therapy in medicine [13, 14, 11]. Besides, in the light of the increasing human exposure to lanthanides as they are widely used in modern technology, the studies on their impact on biological systems are becoming a worthy pursuit [10, 15].

3.1.1 Basic atomic and coordinative properties of lanthanides

Lanthanides (here and further abbreviated as Ln) is a term for the group of elements starting from La and further comprising the following 14 f-elements from cerium (Ce, atomic number 58) to lutetium (Lu, atomic number 71) with electronic configurations of $[Xe]4f^{0}5d^{1}6s^{2}$ (La) to $[Xe]4f^{14}5d^{1}6s^{2}$ (Lu) [16]. The f-electrons do not participate in bond formation, and the chemistry of lanthanides is governed by the 5d and 6s electrons removal [17]. Therefore, most of the lanthanides are stable as trivalent ions. Other oxidation states (+IV, +II) are somewhat rare and occur when the configuration of f^{0}, f^{7}, or f^{14} may be achieved [16]. For instance, strongly reducing dipositive (Eu^{+2}, Yb^{+2}) and strongly oxidizing tetrapositive (Ce^{+4}) ions can be distinguished in solution [18, 19] . The first and second ionization energies are almost similar throughout the series of elements ($E_1 \approx 600$ kJ/mol, $E_2 \approx 1200$ kJ/mol), and the values are comparable with those for calcium [20].

Due to the poor shielding of the 5s and 5p electrons by the 4f subshell, ionic radii of the trivalent ions decrease with increasing atomic number (from r (La^{3+}) = 1,03 Å to r (Lu^{3+}) = 0.85 Å, for CN=6[3].). This phenomenon is well known as lanthanide contraction, and it is the primary source of differences in chemical properties between the Ln series elements. For comparison, the ionic radius of calcium is about 1,00 Å for CN=6 [21]. It is seen that the lighter Ln^{3+} ions are about the same size as Ca^{2+} but logically have a higher charge-to-volume ratio. This results in higher CN preference and may result in higher complex stability and, subsequently, a higher affinity for biological binding sites [13].

One another similarity of lanthanides to calcium, or generally to the alkaline earth metals, is the formation of relatively weak complexes. Sufficiently stable species, other than the hydrated cations, can be obtained only with strongly chelating ligands when these ligands possess highly electronegative donor atoms [17].

Ln^{3+} cations bind ionically; they behave as hard Lewis' acids preferring fluorine, oxygen, and, to a lesser extent, nitrogen donors. F-orbitals are affected by ligands very slightly, and no crystal field stabilization energy (CFSE) takes place in the Ln complexes formation [17]. The strongly ionic nature of bonding leads to different coordination numbers and variable

geometries. The ionic complexes often undergo rapid ligand exchange; isomerism and slow substitution reactions are uncommon and poorly characterized. As for the possible coordination numbers, those from 6 to 12 occur, and CN = 8 or CN = 9 are often preferred [16].

3.1.2 Non-radioactive therapeutic and biochemical properties of lanthanides

Lanthanides are generally considered as elements inessential for life. These metals occur in trace amounts in living organisms and have no endogenous biological function in humans. However, lanthanides can serve as powerful biochemical probes. Their similarity to calcium ion, which is an ion of extreme biological importance, has always been known and stimulated research into the field of lanthanide medicinal chemistry.

Lanthanides in the body: biochemical effects and possible applications

Since the early 20th century, lanthanides, particularly cerium, were known to interfere with the calcium-dependent blood clotting cascade. Nevertheless, the interest in lanthanides in this context was only temporary [22] as less toxic and more efficient anticoagulants were developed fast. As a tribute to history, it is proper to mention insoluble cerium (III) oxalate, which was used to treat vomiting during pregnancy [22]. The mechanism of those antiemetic properties was not explained clearly, and its use was abandoned soon.

The successful implementations of lanthanides in healthcare include an insoluble orally administered drug called Fosrenol, chemically lanthanum (III) carbonate. It is a dietary intake phosphate binder used to treat hyperphosphatemia in patients with kidney disease who are less able to excrete phosphate [23]. Fosrenol ($LaCO_3$) proved itself to be a favourable phosphate binder as it has a high affinity for phosphate, binds it rapidly, is insoluble, and has almost no systemic absorption. Therefore it is safe to use (generally, the inability of lanthanide ions to cross cell membranes is a primary reason for their non-toxicity when ingested orally [24]).

Another efficient drug was cerium (III) nitrate used as a component of a topical cream for the burn wounds treatment [25]. The mechanism of cerium (III) action here is twofold. First of all, cerium is known to cause local soft tissue calcification as it precipitates with pyrophosphate and removes the pyrophosphate's calcification-inhibitory function [26]. It also forms the crystallization nuclei facilitating the further calcification [22]. Acting this way at the burn site, the compound facilitates the eschar formation, making it firm and impermeable. Such an eschar contains insoluble pyrophosphate and carbonate salts of Ce^{3+} and Ca^{2+}. The second action is the immunomodulatory effect of cerium. It binds the burn toxin, a high molecular weight lipid-protein complex (LPC) formed by heat-induced polymerization of several skin polypeptides. Unless being bound, the LPC causes a number of immune responses leading to immunosuppression [14, 22].

As a development of the topic of the lanthanides' impact on the immune system, it must be pointed out that their effects on immune function, in general, are contradictory. Ln ions have been reported to inhibit several cell-mediated immunity responses (e.g., lymphocyte

activation). Simultaneously, in low doses, they appear to enhance several other immune functions (e.g., the antibody formation) [14, 13].
Studies have shown that lanthanides may have an impact on lipid metabolism as well. $LaCl_3$, $GdCl_3$, and $CeCl_3$ were proved to inhibit the adipocyte differentiation in preadipocytes, and it was also proposed that lanthanides can be used as agents for slimming by promoting lipolysis [27]. Another biologically relevant case is the hydrolysis of phosphate bonds (e.g., those in the oligonucleotides) by Ln hydroxide gels. It was one of the earliest observations of metal ion catalysis of such reactions [28].

In the light of the mentioned above calcium-lanthanides similarity, the high affinity of Ln^{3+} to cartilage and bone matrix [29] is demonstrative. Ln ions may help treat the bone resorption disorders, behaving as calcium surrogates in the hydroxyapatite-like matrix of the bone [30]. This affinity can be employed in biocompatible materials development for hard tissue replacement, for example, in the orthopaedic metal implants construction [31, 32].

The anticancer potential of non-radioactive Ln species has also been investigated. Several complexes of Ln (Ce, La, Nd, Gd) with different ligands such as coumarin derivatives, 1,10-phenanthroline, citrate, and others were synthesized and explored for their cytotoxicity in malignant cells. Some compounds in definite concentrations have demonstrated antiproliferative, cytotoxic, or cytostatic effects on the *in vitro* model systems, though the trials conducted were only preclinical [22]. Moreover, by itself, individual metals (Tb) were proved to enhance some chemotherapeutic agents' anticancer activity (e.g., cisplatin). Tb (III) was found to bind the cell membrane in breast cancer cells and increase cisplatin's cellular accumulation, therefore amplifying its cytotoxicity. However, all the effects were observed only within certain concentration ranges, and a more profound understanding of the mechanisms was not achieved [33]. A noteworthy type of non-radioactive lanthanide antineoplastic complexes is redox-active (susceptible to reduction) Ln (III) complexes with texaphyrins, heterocyclic macrocycle molecules derived from porphyrins. These compounds attracted considerable interest from medicinal chemists as they may be used in cancer treatment as radio- and chemo-sensitizers [33]. The principle of their action is following. The ROS-induced oxidative damage to DNA and protein can lead to apoptosis, so manipulating the tumor cell redox balance in favor of increased oxidative stress with the considered complexes' assistance enhances the tumor cells' death rate when simultaneous chemo- or radiotherapy is being conducted [34]. In such a way, the therapeutic effect of chemo- or radiotherapy is improved.

Finally, it is suitable to consider the functional aspects of the Ln interactions with proteins. Several enzymes stimulated by Ca^{2+} or totally dependent on it were studied in this perspective [13]. In most cases, the Ln-substituted enzymes become less catalytically active, up to total competitive inhibition of their function. However, when the Ca^{2+} role in the biomolecule is not functional but structural, the enzymatic activity in most cases retains or is only slightly modified [35]. One more issue, which is easy to predict in this context, is that lanthanide ions may affect the transmembrane Ca^{2+} fluxes as they are capable of binding to different types of calcium channels in cell membranes. Therefore, nerve cells and muscle

cells' physiology is sensitive to Ln^{3+} administration: the neuromuscular transmission may be inhibited, the heart contractility may be reduced [22, 14].

Spectroscopic, magnetic properties of lanthanides useful in medicinal chemistry

Unlike spectroscopically silent Ca^{2+} ions, lanthanides may serve as useful instruments to study the Ca^{2+} dependent biological systems. Another noteworthy feature of these metal ions is that they possess beneficial magnetic properties (high magnetic susceptibilities) that may be successfully implemented analytically.

When a strong *magnetic* field is applied, a magnetically susceptible ionic species acts as a little secondary magnet, altering adjacent susceptible atoms' behavior. Consequently, NMR signals may be disturbed: chemical shift perturbations, line broadening may take place, and be a source of useful information [36].

Probably the most famous case of the Ln peculiar magnetic properties implementation is the use of Ln-based contrast agents in magnetic resonance imaging (MRI). The majority of commercially available agents are Gd^{3+} stable chelating complexes with ligands based on a polyaminocarboxylate motif. The reason for the use of gadolinium (III) is that the Gd^{3+} ion with its seven unpaired electrons (a spin quantum number of 7/2) is paramagnetic, has a relatively large magnetic moment, and a long electron spin relaxation time [37]. The contrast agents are used in about 40% of all MRI exams, and in about 60% of neuro MRI exams [36]. They markedly alter the relaxation time of water protons in tissues, which often leads to remarkable improvements in medical diagnoses. The further details will not be described as MR scanning principles explanation is beyond the scope of this work.
However, MR imaging is not the only medical imaging field where Ln may be employed. As the rare earth ions (with a few exceptions) are very efficient emitters of light upon excitation from different sources, they are instrumental in the field of scintillators. When excited by ionizing radiation that is by itself very difficult to detect, Ln^{3+} activated scintillators can efficiently convert X-rays or γ-rays into light (from UV to NIR) that standard photodetectors can quickly and cheaply detect. Therefore, Ln-activated materials can be successfully utilized as scintillators in essential and widespread imaging techniques as computer tomography (CT), and positron emission tomography (PET) [36].

The energy-converting ability of Ln is rather of import and is not limited to the mentioned above context. Lanthanides have a fascinating capability to convert a long-wavelength NIR or IR light to a shorter wavelength UV or VIS radiation. This process is known as upconversion. During this process, a sequential absorption of several (most often two) long-wavelength photons occurs, which leads to the emission of a shorter wavelength (and higher energy) photon [38]. It can be exploited in medicine in phototherapy or drug delivery. Lanthanide-based nanoparticles are an example of the employment of upconverting materials to improve release in photo-responsive capsules. The photo-triggered release is a satisfactory solution in targeted drug delivery, but one of the main problems is that the release is based on a limited range of available photochromic moieties, primarily

responsive to UV or VIS light irradiation. These wavelengths have a short penetration length, which makes these systems hardly usable in internal medical applications. Thus, upconverting materials may provide a decision: NIR light capable of deeply penetrating biological tissues is converted by lanthanide-based nanoparticles to UV/VIS radiation. It triggers the photo-responsive moieties in capsules and induces the release of the encapsulated materials [38].

An exciting example of utilizing Ln magnetic properties is ferrography techniques applied to the study of wear and arthritis in human joints. Pieces of adjacent biological tissues, cartilage particles, and bone fragments shed to the synovial fluid in an eroded joint are magnetized with Er^{3+} as it has large magnetic susceptibility and high affinity to bone and cartilage. The magnetized particles are then separated in the external magnetic field and examined. The method has the potential to be a highly sensitive monitor of the erosion of intraarticular surfaces in arthritis treatment [29].

The *spectroscopic* properties of the rare earth elements are often described as unique. In this connection, several of their electronic structure features should be noted first. The f-f transitions are spin forbidden; therefore, lanthanide ions tend to have pale colors. The f orbitals have a so-called "buried" nature in an atom's electron cloud, and their energy is only slightly affected by thermal vibrations. This results in a relatively sharp, narrow shape of the absorption bands [16]. Lanthanide ions have remarkable luminescent properties due to their unique 4f orbitals: there are many electronic energy levels, and it allows for a rich cascade of radiative and non-radiative relaxation processes in excited lanthanide ions [39]. Lanthanide luminescence is characterized by rather long lifetimes of the excited states. The long lifetimes are a particular advantage for the implementations in biological systems as they enable time gating to eliminate the effects of the short-lived background biological luminescence [28].

Ln-based luminescent probes have several bioanalytical applications. It is beneficial to use them in studies devoted to protein structures, protein-protein interactions, topology in multiprotein complexes [40]. A lanthanide binding tag (LBT) may consist, for example, of a small peptide easily incorporated into proteins with minimal impact on their structure and function [36]. Another way to employ the lanthanides' luminescent properties is to construct fluoroimmunoassays within Ln-labelled antibodies or antigens [39].

Even more interestingly, the mentioned above fluoroimmunoassays are not the only area where Ln-labelled antibodies are used. They play an important role in mass cytometry, which is a combination of the conventional fluorescence-based flow cytometry and time-of-flight (TOF) mass spectrometry [41]. The lanthanide labels (the labelled antibodies) are used as stains in single-cell suspensions: most often, they bind to the corresponding antigens in cell membranes. The lanthanide species attached are identified and quantitatively determined by analysing the cell suspension employing the Inductively Coupled Plasma Mass Spectrometry (ICP-MS). Thus, it is possible to distinguish individual cell types because different cells exhibit different antigen expression levels [36].

The reviewed features and applications are not a comprehensive list of the properties and implementations of lanthanides relevant for medicinal chemistry but rather an illustrative example of the diversity of the possibilities.
With regard to such a wide range of established and potential applications, there is a considerable amount of research being conducted in the coordination chemistry of lanthanides with amino acids, sugars, porphyrins, siderophores, various organic acids, and other naturally occurring ligands [10]. The analysis of binding modes, the determination of thermodynamic and kinetic complex stabilities is being conducted, a large amount of spectroscopic data is available. Thereby, a deeper understanding of the fundamental aspects of f-element complexation is being developed, and the awareness of possible biological implications increases.

3.1.3 Radiolanthanides and their application in nuclear medicine

Lanthanides possess several radioisotopes that have established and successfully developing nuclear medicine applications because of their favorable and diverse decay properties. Moreover, all the trivalent Ln ions have very similar chemical properties and coordination chemistry, which makes them interchangeable in the molecular carrier to meet the required decay characteristics. According to the World Nuclear Association, the use of radiolanthanides in medicine is significant: over 10,000 hospitals worldwide use radiolanthanides, and the demand for therapeutic radionuclides is constantly increasing [42].

There are three major production pathways of Ln radioisotopes. The first one consists in irradiating the appropriate stable target material by a thermal or epithermal neutron flux in a nuclear research reactor. Although there are not many suitable nuclear facilities globally, this pathway satisfies a large percentage of total radionuclide consumption [42]. It is highly efficient and offers the ability to irradiate a high volume of target material, irradiate several samples simultaneously, and produce a wide variety of radionuclides. The second, less widespread, and less efficient production method is based on the particle accelerator (cyclotron) use, where different types of particles (α-particles, protons) are accelerated to bombard the targets. The last nuclide production system is called a nuclide generator and can be considered an extension of the first pathway, as a starting long-lived parent nuclide is produced in a nuclear reactor *via* neutron irradiation, and afterward, it is loaded onto the generator system. The shorter-lived medical nuclides of interest are formed in the generator by the parent nuclide's decay and can be selectively eluted then [8].

The radiolanthanides production in nuclear research reactors is worth thorough attention as a convenient and well-studied pathway. High specific activities of the resulting radionuclides are reached within this method. Specific activity is an amount of the radioactivity or decay rate per unit mass of a particular radionuclide, expressed in Bq/g, the older unit used in medicine is Ci/g. A target material containing isotopically enriched stable Ln isotopes is irradiated with a high thermal neutron flux. The common nuclear reactions are neutron capture ${}^{A}_{Z}Ln(\mathrm{n,\gamma}){}^{A+1}_{Z}Ln$; double neutron capture

$^{A}_{Z}Ln(n,\gamma)^{A+1}_{Z}Ln(n,\gamma)^{A+2}_{Z}Ln$; neutron capture followed by ß$^-$ decay (through a very short-lived intermediate formation) $^{A}_{Z}Ln(n,\gamma)^{A+1}_{Z}Ln(ß^-)^{A+1}_{Z+1}Ln$. Additionally, the absorption of less efficient (with lower cross-sections) and more energetic epithermal neutrons (for orientation E_n(thermal) = 0,025 eV and E_n(epithermal) > 0,2 eV) [43] might sometimes result in (n,p) reaction. Within the first two strategies, only the carrier-added (*ca*) radionuclides may be produced. At the same time, ß$^-$ decay gives the possibility to obtain the non-carrier-added (*nca*) product as the Ln with another atomic number (Z) than in target material is formed, and the chemical separation is possible [44].

Endoradiotherapy

Targeted radionuclide therapy is a systemic approach where a radiolabelled compound delivers a cytotoxic radiation level to the targeted disease site in the organism. There are two major components in any radiopharmaceutical product: a radionuclide by itself and a carrier system. The latter may also be called a "targeting vector" or "an affinity component" as it ensures the targeted delivery to the desired site (e.g., receptor, antigen on the malignant cell surface) and may be represented by a particular peptide, specific antibody, or an oligonucleotide [45]. The radionuclide is usually attached to the vector via a biocompatible chelator and linker (Fig.1); highly thermodynamically, kinetically, and *in vivo* stable lanthanide chelating complexes are used to ensure that the radiolanthanide reaches the target site without being detached on its way. Those chelators are frequently based on the octadentate coordinating ligands with a polyaminocarboxylate motif (e.g., DOTA, DTPA) as it was in the case of Gd-based contrast agents in MRI imaging mentioned above; macrocyclic polyaminophosphonic acids and porphyrins are also used [46].

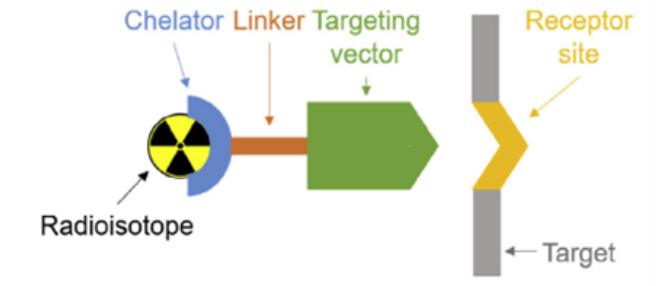

Figure 1. Schematic representation of a radiopharmaceutical product [8]

There are several criteria to be satisfied for a radiopharmaceutical to be considered as an appropriate one. The type of radiation, the energy, the penetration depth of the emitted particles, and the half-life of the isotope are extremely important as they define the drug's suitability and effectiveness. The emitted particles should destroy harmful cells efficiently but penetrate healthy tissues around as little as possible. The half-life of the nuclide must be long enough for convenient pre-hospital manipulations with the drug, but not longer than a defined limit, because longer half-lives are associated with the increase of the background patient radioactivity and lead to lower therapeutic effect. Also, the nuclide's half-life has to correspond with the biological half-life of the radiopharmaceutical [47].

Once delivered to the right location, the radionuclide fulfils its therapeutic role, e.g., destroys the tumor cell DNA by emitting α-, or ß-particles, or Auger, or conversion electrons. α-particles possess the highest decay energies in the range of 4,0 – 8,8 MeV; they are heavy and do not penetrate deeper than few cell diameters. As they originate from rather heavy nuclei, their use is less abundant with only one isotope - ^{149}Tb - that is used in preclinical tests [43]. ß$^-$ emitters are more important in medicine and more common among the radiolanthanides series; those neutron-rich nuclei are easily formed by neutron capture in the research reactors. Each Ln species from this group emits ß$^-$ particles with different energies, therefore the penetration depth is also varying from 5 to more than 150 cell diameters. Although the energy of a single emitted ß$^-$ particle is not enough to cause substantial damage in DNA, labelled molecules usually get distributed heterogeneously in a solid tumor and act through the so-called crossfire effect [8]. Several radiolanthanides emit ß$^-$ and γ simultaneously and can be suitable for both therapy and diagnosis at once. Such a dual approach is called theranostics, with γ radiation helping to track the *in vivo* localization of the radiopharmaceutical [8]. The last considered type of the emitted particles is Auger and conversion electrons that originate from the proton-rich nuclei decaying by electron capture or by internal conversion. They have a very short penetration range limited to several nm or μm, their energy depends on the electron shells involved in the transition, but usually it is very low, ranging from 20 to 500 eV. Due to their short ranges in soft tissues, radiopharmaceuticals carrying such emitters should be targeted directly into the cell nucleus [43].

Common medical radiolanthanides, their decay characteristics, production pathways, and therapeutic properties are listed in Table 1 below.

Table 1. Common medical Ln radionuclides and their basic characteristics [47, 8, 43, 42, 46]

Radio-nuclide	Common production route	Half-life $t_{1/2,}$ [d]	Type of decay	Properties, medical use, comments
^{143}Pr	$^{142}_{58}Ce$(n,γ)$^{143}_{58}Ce$(ß$^-$)$^{143}_{59}Pr$; The isotope of interest is prepared *nca*; isotopically enriched ^{142}Ce is used as target material.	13,6	ß$^-_{max}$ = 933 keV; γ$_{main}$= 742 keV	This isotope is used in therapy (targeting) but rather rarely due to its relatively long half-life. It is an advantageous isotope in terms of separation and purification, easily prepared *nca* owing to $Ce^{IV}O_2$ use as target material (efficient separation of the trivalent product from the tetravalent cerium).
^{149}Pm	$^{148}_{60}Nd$(n,γ)$^{149}_{60}Nd$ (ß$^-$)$^{149}_{61}Pm$; The isotope of interest is available *nca* in high purity	2,21	ß$^-_{max}$ = 1071 keV; γ$_{main}$= 285 keV	It is a high-specific activity isotope. It finds use in targeting some specific receptors on

	(after the proper extraction chromatography separation from neodymium).			many tumor cells. It is suitable for radiolabelling in cancer therapy; it is also suitable for *in vivo* imaging – theranostics.
^{153}Sm	$^{152}_{62}Sm$(n,γ)$^{153}_{62}Sm$; Isotopically enriched ^{152}Sm is used as target material. The *ca* product is obtained; therefore, it is unsuitable for radiolabelling. Upon longer irradiation times, the co-production of the long-lived ^{154}Eu occurs: $^{153}_{62}Sm$(ß$^-$)$^{153}_{63}Eu$ (n,γ)$^{154}_{63}Eu$. Also, the ingrowth of ^{154}Eu limits the shelf life (time the radionuclide can be safely used) of the product as the amount of ^{154}Eu that can be administered to a patient is strictly regulated.	1,95	ß$^-_{max}$ = 808 keV; γ$_{main}$= 103,2 keV	This isotope is most often used in the form of ^{153}Sm-EDTMP chelate (^{153}Sm – ethylene diamine tetramethylene phosphonate, Quadramet) with bone-seeking properties; it is used in palliative care, bone metastasis treatment. It is an important isotope for the internal radiotherapy of liver tumors; γ-photons emission can be used for imaging (theranostics). The isotope's relatively short half-life hampers the use: because of it, no purification takes place,^{153}Sm is nowadays used only as a *ca* isotope.
^{161}Tb	$^{160}_{64}Gd$(n,γ)$^{161}_{64}Gd$(ß$^-$)$^{161}_{65}Tb$; Highly isotopically enriched target material is needed, as other Gd isotopes (esp. ^{157}Gd – a neutron poison due to its large cross-section) might decrease the product's specific activity. The isotope of interest is obtained *nca* after the separation from the redundant target material.	6,9	ß$^-_{max}$= 593 keV; γ$_{main}$= 74,6 keV; Auger and conversion e$^-$ (3-50 keV)	It is a medical nuclide of increasing relevance over the last decade. It has similar radionuclidic characteristics with popular ^{177}Lu but increased therapeutic efficiency due to Auger and conversion electrons emission. This isotope is used in targeted radionuclide therapy.
^{166}Ho	1)$^{165}_{67}Ho$(n,γ)$^{166}_{67}Ho$; ^{165}Ho is an isotope with 100% natural abundance. This route leads to the *ca* product with a moderate specific activity. 2)$^{164}_{66}Dy$(n,γ)$^{165}_{66}Dy$;	1,12	ß$^-_{max}$ = 1854 MeV; γ$_{main}$= 80,6keV	It is an essential medical nuclide. The chelate of ^{166}Ho with DOTMP (DOTMP is a 1,4,7,10-tetraazacyclododecane-1,4,7,10-tetramethylene phosphonic acid) is an important

	$^{165}_{66}Dy$(n, γ)$^{166}_{66}Dy$(ß$^-$)$^{166}_{67}Ho$; This route involves double neutron capture followed by beta-decay; it leads to the *nca* product with a high specific activity. ^{166}Dy is a relatively long-lived nuclide ($t_{1/2}$= 81,6 h), so a nuclide generator system for ^{166}Ho production can be used. The described way is advantageous because no direct access to the nuclear reactor is needed, and medical radionuclide can be obtained on demand.			radiopharmaceutical for multiple myeloma treatment targeting bone marrow. Other chelates were designed and explored for bone pain palliation. ^{166}Ho loaded poly(L-lactic acid) microspheres (^{166}Ho-PLLA, commercially named QuiremSpheres) were investigated for liver tumors/metastases treatment. Isotope's γ radiation is ideally suited for imaging. The only drawback is the relatively short radionuclide's half-life, so only the hospitals within short proximity to the production site can use this radionuclide.
^{169}Er	$^{168}_{68}Er$(n,γ)$^{169}_{68}Er$; As seen from the scheme, only *ca* product is available by this route; ^{168}Er has a low cross-section (σ_{th}=1,28 barn), resulting in low specific activity product.	9,39	ß$^-_{max}$ = 350 keV; γ$_{main}$= 84 keV	This soft ß$^-$emitter is used in radiosynovectomy (RSV) – treatment of small inflamed joints in rheumatoid arthritis or other degenerative joint diseases therapy; radiotherapy usually involves an intra-articular injection of ^{169}Er in colloidal form. Due to low specific activity and exclusively *ca* form, no tumor treatment is possible, but on the other hand, this isotope can be used by patients out of the hospital without any radiation risk.
^{177}Lu	1)$^{176}_{70}Yb$(n,γ)$^{177}_{70}Yb$(ß$^-$)$^{177}_{71}Lu$; *nca* ^{177}Lu is obtained after the appropriate separation. 2)$^{175}_{71}Lu$(n,γ)$^{176}_{71}Lu$(n,γ)$^{177}_{71}Lu$ [$^{177m}_{71}Lu$];	6,65	ß$^-_{max}$ = 498 keV; γ$_{main}$= 208,4 keV	It is one of the most popular therapeutic and theranostics radionuclide. It finds implementation in radiosynovectomy(RSV),

	This direct route leading to a *ca* product is efficient and gives high specific activity product, but minor amounts of long-lived metastable ^{177m}Lu are also formed, slightly hampering its use as the amount of ^{177m}Lu present is strictly regulated. ^{177m}Lu is a nuclear isomer of ^{177}Lu – a nucleus with the same atomic and mass numbers but different energy. The transition to the ground state may occur through γ emission or internal conversion. ^{177m}Lu also decays *via* ß$^-$emission.			bone pain palliation, neuroendocrine tumors treatment, liver, ovarium, and breast cancer therapy. *nca* ^{177}Lu formed by the first production route is used for radiolabelling and targeted radiotherapy. A wide range of targeting vectors is being investigated to develop new ^{177}Lu-based radiopharmaceuticals.

Strict requirements are put on the radionuclide purity for safety reasons – to avoid the patients' exposure to too high amounts of the long-lived radioactive isotopes. Another reason for the demand for highly pure radiolanthanides is that they are needed for radiolabelling for efficient coordination because of the limited amount of the available receptors in the cell. The target material is sometimes a mixture of adjacent lanthanides with extremely similar chemical properties, and after the irradiation, significant amounts of the redundant target material stay in the end-product. Moreover, unwanted long-lived isotopes may emerge during the irradiation. If the medical nuclide is too short-lived, it may decay while being irradiated in the reactor, forming unwanted radioactive daughter isotopes - ingrowth. Therefore, different preparation strategies and irradiating times are chosen to balance the purity issues with the efficiency of the target material use; and the purification techniques become of a great import[8].

There are many different approaches to the radiolanthanides purification problematics [8, 9], but often the use of α-hydroxyisobutyric acid (α-HIBA, Fig.2) as a complexing agent takes place. This simple α-functionalized acid shows high sensitivity to Ln cation radii [9]. The typical arrangement is high-performance ion chromatography (HPIC) with cation exchange column and gradient elution with α-hydroxyisobutyric acid solutions of different pH [48]. If to consider such a system with the aqueous α-HIBA as an eluent, several equilibria take place. To put it briefly and simplified, the heavier lanthanide with higher charge density will be eluted first as it forms a more stable (with higher stability constant) complex with α-HIBA. Afterward, the solution acidification with hydrochloric acid takes place. Thus, the Ln- α-HIBA complex is broken, and the Ln species can be separated within a secondary cation-exchange column [8].

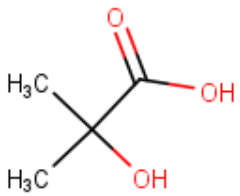

Figure 2. The structure of α-hydroxyisobutyric acid

In searching for suitable complexing agents for lanthanides' separation, different carboxylic acids such as glycolic acid, oxalic acid, lactic acid, mandelic acid, and citric acid have been tested in various laboratories [7, 49, 48]. In this connection, the studies on the affinity of the simple carboxylic acids to lanthanides seem worthwhile.

3.2 Oxalic acid in the technology of lanthanides and actinides

Oxalic acid, the simplest dicarboxylic acid, has a remarkable position in the chemistry of f-elements.
Beforehand, it is a reagent of great importance in the nuclear industry, where it is extensively used as a precipitating agent. Oxalic precipitation of actinide (III) and actinide (IV) species is a technological method for isolating and purifying actinides [50] exploited in nuclear fuel management. It is also exploited in the processing of minor, less abundant actinides to synthesize those actinides feedstock for specific uses [1]. Oxalate ion being a thermally labile ligand, provides a possibility for thermal decomposition of the precipitated metal oxalate leading to a stable oxide formation. This process, known as an oxalic conversion, is both industrially and scientifically important [51, 4].

In the nuclear environment, the experiments with unstable, radioactive actinide elements are often complicated to conduct. Therefore, actinides are commonly simulated with lanthanides to develop and improve the experimental methods in harmless conditions [52]. For example, in spent nuclear fuel processing, the plutonium in nitric acid solution is converted into plutonium dioxide (PuO_2) through oxalic conversion (Purex proces [53], PuO_2 is recycled as MOX fuel). If the precipitation step proceeds under reducing conditions, Pu (III) oxalate is precipitated. Lanthanide (III) and actinide (III) basic oxalate hydrates are isomorphic. Therefore, to gain experience, the calcination process can be studied on lanthanide (Nd, Ce) oxalates systems [54]. Both lanthanides and actinides possess f valence electrons, and they are relatively close in size and chemical properties. Thus, such an approach is reasonable and remains important in the 5f and 4f elements chemistry [55], but the similarity is rather rough. Some contemporary studies reveal that ionic and steric factors, which are the main contributors to Ln chemistry, are not equally significant for actinides: the covalent contribution to the bonding in An(III) complexes was reported [1]. Moreover, the isomorphous structural arrangements do not ensure that the processes such as thermal decomposition will necessarily follow the same mechanism [54].

In the mere lanthanides' chemistry, the oxalate method has been used for years to separate and prepare lanthanide compounds. Thanks to their low solubilities in aqueous solutions, lanthanide oxalates may be used for extracting lanthanides from mineral sources, for their gravimetric analytical determination or just for separating them from industrial wastes [2]. Isomorphism in the lanthanide oxalate series inhibits the preparation of individual Ln compounds. Still, the oxalic precipitation method efficiently decontaminates the Ln species from foreign cations such as Al, Fe, Ti, or Mn. Oxalate precipitation is also used as a part of chemical analysis for assessing Ln-species contents in variable synthetic procedures [5]. In the same fashion, as it was in the case of actinides, lanthanide oxalates can be convenient reactants for the thermal preparation of oxide lattices containing rare earth elements, which are often important inorganic materials [3].

In standard conditions, the oxalate anion is quite a strong complexing agent, stable in terms of redox properties. Often, it acts as a bis-bidentate ligand and rigidly bridges the metal centres [1, 5], but it also may exhibit various other coordination modes (Fig. 3). For this, oxalate anions as ligands are popular in the field of metal-organic frameworks (MOFs). Metal-organic frameworks are a class of crystalline porous solids composed of a three-dimensional network of metal ions that are connected and organized in space by multidentate organic molecules [56].

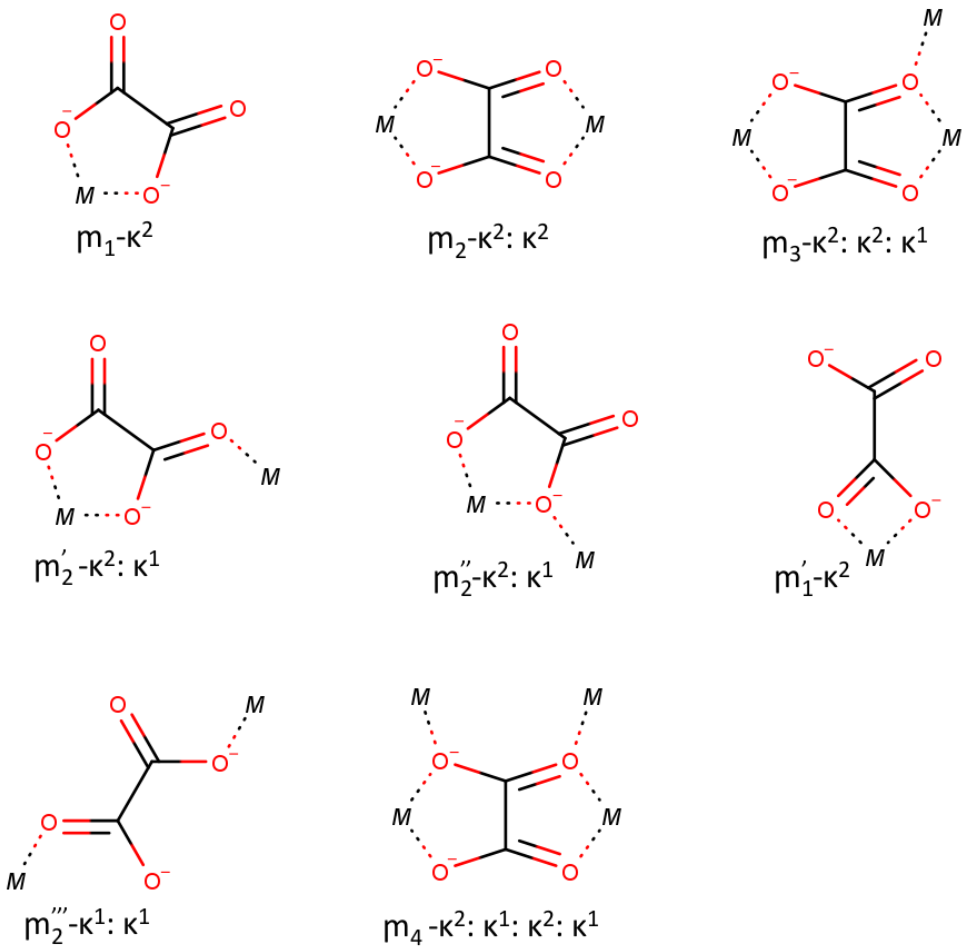

Figure 3. Several coordination modes exhibited by oxalate ligand [1, 56, 57, 6]

M- stands for metal, μ- here denotes the number of metal atoms bound to the bridging ligand (oxalate), κ- is denticity for each coordination interaction.

In order to obtain various coordination geometries, desired multidimensional structures, different advanced approaches are used. Such factors as the synthesis route, conditions, presence of additional organic or mineral cations (their charge, dimension, probable template effect), and the lanthanide nature (e.g., its ionic radius) affect the construction of the obtained framework [5, 6]. Hydrothermal or solvothermal conditions realized in the autoclave are often employed.

However, for simple lanthanide separation from aqueous solutions, there is no need for sophisticated synthesis techniques, which is one of the main advantages of the method. Oxalic precipitation was reported to be quite a robust reaction: it can proceed under relatively extreme conditions (at a wide pH range, at different temperatures) [3]. In order to design the precipitation experiment, several sources (listed below in the text) were used.

It is documented that there are two isomorphous series of compounds for lanthanides obtained at the same precipitation conditions. The elements from La to Ho form the first series that is identified as decahydrates. The heavier lanthanides, Er – Lu, were proved to form a second isomorphous series – hexahydrates [58]. In the cited paper, the authors worked in aqueous solutions, without pH control, precipitating the oxalates by the rapid addition of oxalic acid solution to the lanthanide nitrate hexahydrate solution (molar ratio acid: metal = 2:1) at 95°C. Attempts to prepare the decahydrate phases for the heavier Ln (Er-Lu) were unsuccessful even using low-temperature precipitation and lead to partially unidentified mixed-phase product formation. Some later studies confirmed that for the simple lanthanide oxalates, the transition from CN = 9 to CN = 8 occurs between Er and Ho, which corresponds with the transition from the decahydrates to hexahydrates series [5].

In this work, Gd and Ce were chosen as the lanthanide representatives. Therefore, the formation of lanthanide (III) oxalate decahydrates was anticipated.

In the nuclear industry, in the fuel reprocessing procedures, highly acidic conditions are common [53]. Nuclear fuel treatment implies complex chemistry which is beyond the scope of this work. Nevertheless, it was repeatedly reported that highly acidic solutions tend to impair the oxalic precipitation reaction, lowering its efficiency: with the increasing acidity of the media, the metal-oxalate complexes' solubilities are getting higher [2]. However, even in the precipitations pursuing the highest possible Ln recovery from the solution, it is often impractical to work at a pH higher than 2 because the purity aspects must be taken into consideration. In some cases, at pH>2, less insoluble oxalates of other metals may start to precipitate. Moreover, the co-precipitation of such species as $Al(OH)_3$, $Fe(OH)_3$ is possible [59]. Raising the system pH upper than pH=4 is naturally inefficient as the Ln^{3+} hydrolysis may already occur in this pH range.

In the majority of the examined articles on the topic of oxalate precipitation chemistry, the excess of oxalic acid was used [2, 58, 60]. As a rule, even a small excess induces a reduction in a lanthanide oxalate's solubility in the regarded solution. However, the visible precipitate is

easily formed with any molar ratio between the reactants (the acid excess, stoichiometric conditions, the excess of the metal ions) [3, 52].

To conduct a proper precipitation experiment, several solution chemistry calculations were performed.

Oxalic acid is a relatively strong diprotic acid, with its two-step dissociation equilibrium described as following [61]:

$H_2C_2O_4 + H_2O \rightarrow H_3O^+ + HC_2O_4^-$ $K_1 = 5{,}62 \cdot 10^{-2}$ (25 °C) [1]

$HC_2O_4^- + H_2O \rightarrow H_3O^+ + C_2O_4^{2-}$ $K_2 = 7{,}24 \cdot 10^{-5}$ (25 °C) [2]

$c(H_2C_2O_4) = [HC_2O_4^-] + [C_2O_4^{2-}] + [H_2C_2O_4]$ [3]

$$\alpha_0 = \frac{[C_2O_4^{2-}]}{c(H_2C_2O_4)} = \frac{K_1K_2}{[H^+]^2 + K_1[H^+] + K_1K_2}$$ [4]

In the given equations 1-4, $c(H_2C_2O_4)$ stands for analytical concentration of oxalic acid in the solution, expressions in brackets represent the individual species, respectively. α_0 is the fraction of dianion species with respect to the analytical (total) concentration of oxalic acid in the solution, expressed using two-step dissociation constants, which are not specified as their expressions are apparent.

Figure 4 shows the calculated species distribution of oxalic acid in an aqueous solution as a pH function. The calculation was performed in CurTiPot freeware [62]. The values of the oxalic acid's pKa_1, pKa_2 [61] were used to construct the graph.

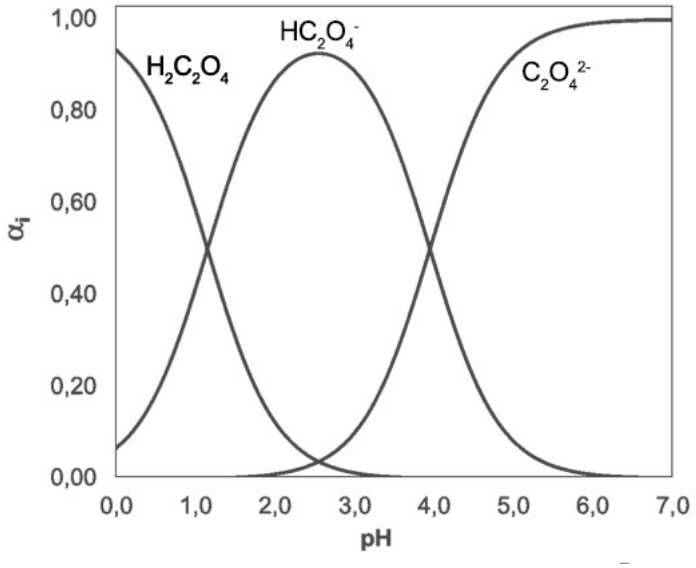

Figure 4. The calculated species distribution of oxalic acid in aqueous solution as a function of pH.

In Fig. 4, it is seen that at pH=2, the predominant species in the solution is $HC_2O_4^-$.

For a particular element, its precipitation by oxalic acid can be expressed with the following reaction:

$$2\ Ln^{3+} + 3\ H_2C_2O_4 + 10\ H_2O \rightleftharpoons Ln_2(C_2O_4)_3 \cdot 10\ H_2O + 6\ H^+ \quad [5]$$

$$K_r = \frac{[H^+]^6}{[Ln^{3+}]^2[H_2C_2O_4]^3} = \frac{(K_1K_2)^3}{K_{sp}} \quad [6]$$

$$K_{sp} = [Ln^{3+}]^2 \cdot [C_2O_4^{2-}]^3 \quad [7]$$

Herein, K_r is the reaction equilibrium constant, K_{sp} is the solubility product of the formed oxalate. Again, in equation 6, the default expression is rearranged using two-step oxalic acid dissociation constants. In handbooks, the solubility products for the oxalates of all complete series of rare earth elements are not available; often, in literature [63, 60] neodymium (III) oxalate as a reference compound is used with its K_{sp} value of $3 \cdot 10^{-27}$. With this number, regarding equation 6, we get values of $1{,}79 \cdot 10^{10}$ for K_r, which indicates a nearly complete, quantitative precipitation. Concerning the amount of oxalic acid, the stoichiometric need (denoted as H_S) can be easily calculated in accordance with equation 8:

$$H_S = \frac{3}{2}(c_{Ln^{3+}} - [Ln^{3+}]) \quad [8]$$

In the given equation $c_{Ln^{3+}}$ is the initial concentration of lanthanide element in the solution, $[Ln^{3+}]$ is its final concentration in supernatant. To explain and demonstrate the oxalate excess role in the system, we can combine the solubility product of the salt, K_{sp}, with the equation 4, aiming to count the additional amount of oxalic acid (denoted as H_E) needed to maintain a desired (arbitrary) residual Ln^{3+}concentration:

$$H_E = \frac{[H^+]^2 + K_1[H^+] + K_1K_2}{K_1K_2} \cdot \sqrt[3]{\frac{K_{sp}}{[Ln^{3+}]^2}} \quad [9]$$

The calculated H_E (for the residual concentration $[Ln^{3+}] = 1 \cdot 10^{-5}$ mol/dm^3) variation with pH is shown in Fig. 5.

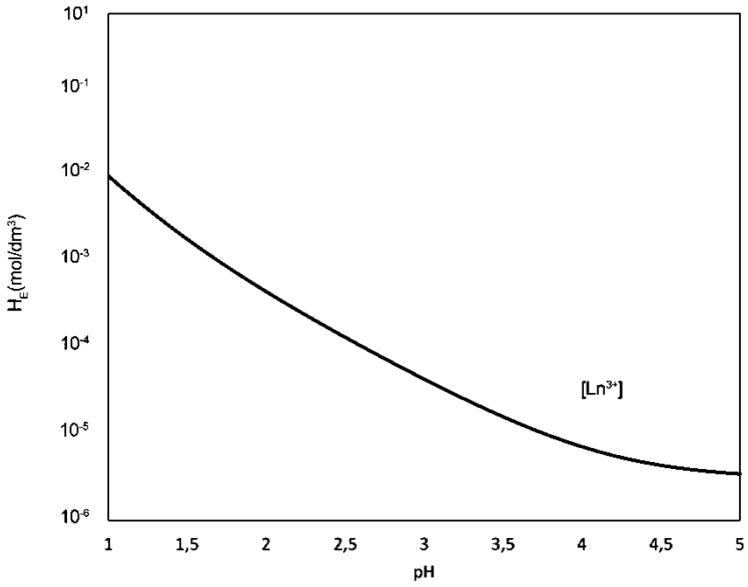

Figure 5. The calculated consumption of oxalic acid to achieve an arbitrary level of residual Ln^{3+} concentration of $1 \cdot 10^{-5}$ as a function of pH.

From the considerations above, the reason for the excess use of oxalic acid is clear. To sum up, the graph showing the efficiency (*E*) of the precipitation as the function of pH may be constructed (Fig. 6), the efficiency being formulated as following [60]:

$$E = \frac{H_S}{H_S + H_E} \qquad [10]$$

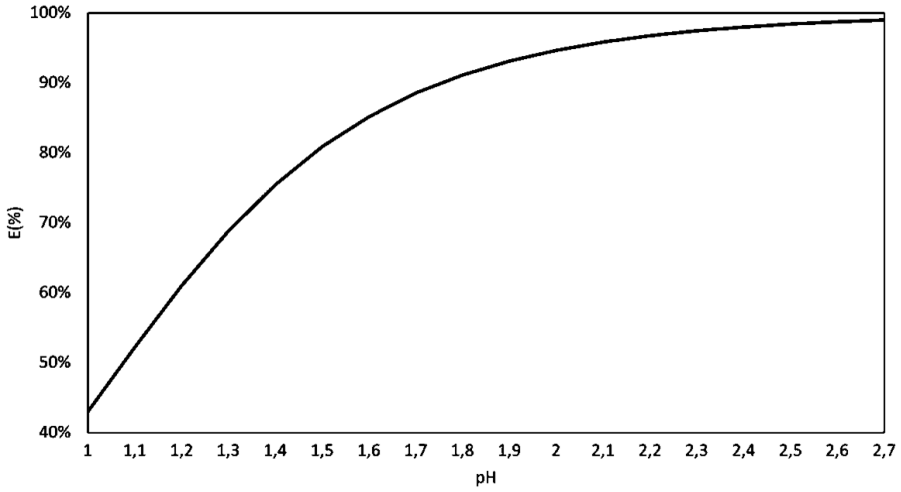

Figure 6. The oxalic precipitation efficiency as the function of pH for the solution containing no substantial amount of further precipitating or/and complexing metal ions.

Based on the aforesaid facile calculations and notes from examined literature [60], the molar ratio $[H_2C_2O_4]$: $[Ln^{3+}]$ from 2 to 3 was chosen for the experiments, which is higher than the corresponding stoichiometric requirement. The reaction was decided to be conducted in an aqueous solution without any additional pH adjustment. Although the precipitating reaction [5] is proton-productive, there is a weak acid equilibrium ($HC_2O_4^-$/ $C_2O_4^{2-}$) in the

system, which is expected to stabilize pH. In fact, the pH value stabilization was observed at approximately 1,5 – 3 (evaluated with pH paper test; the experiment is described in Chapter 4.6).

The structure of the lanthanide oxalate decahydrates has been described in literature [64, 65, 1]. The structure was solved in space group $P2_1/c$, $Ln_2(C_2O_4)_3 \cdot 10H_2O$ isomorphic series of compounds belong to the monoclinic crystal system. The Ln environment is formed by three crystallographically different oxalate anions and three water molecules. Each of the oxalate ions binds in a bidentate fashion. Three water molecules are close to the central cation: for instance, in cerium oxalate decahydrate, the distance is about 2,52 Å [51]. Thus, nine oxygen atoms around the Ln metal form a tri-capped trigonal prism. The coordination number of the Ln is nine. The LnO_9 polyhedron is distorted because the capped positions are not occupied by water molecules but by three oxygen atoms from three independent oxalate ions. The oxalate ions act as bis-bidentate, bridging (μ_2-) ligands. They connect the adjacent metal atoms, so a six-membered ring with a chair conformation is formed. The rings are connected in a fashion to form a honeycomb 2D arrangement stacked along the *b* axis – in other words, forming layers parallel to the crystallographic plane (010). The basic building unit of a lanthanide-oxalate network may be formulated as $[\{Ln(H_2O)_3\}_2(C_2O_4)_3]\infty$. The interlayer distance, as an example taking the gadolinium oxalate decahydrate, is about 4,82 Å. There are non-coordinated water molecules in the interlayer space located within the aperture of the honeycomb-like layers. To put it another way, in a honeycomb network layer, cerium-oxalate units occupy positions y=0, 1/2, 1, and so forth; in the interlayer space, free water molecules fit in the positions y=1/2, 3/4, etc. These free water molecules are "zeolitic" water, and sometimes to point this fact out, the formula of the lanthanide oxalate decahydrate is written as $[Ln_2(C_2O_4)_3(H_2O)_6] \cdot nH_2O$, n frequently equal to 4. However, several sources report that the number of interlayer water molecules may vary and depends on the synthesis conditions [1]. In literature, there is evidence of n=3,5 [66] ($Ln_2(C_2O_4)_3 \cdot 9{,}5H_2O$) for lanthanum oxalate structure; n=4,5 [1] ($Ln_2(C_2O_4)_3 \cdot 10{,}5H_2O$) for neodymium oxalate structure. Gadolinium oxalate free of uncoordinated water was also obtained under hydrothermal conditions [67]. The structure was reported to remain layered with some deformations due to the changes in the bond angles. Thereby, the oxalic acid precipitation chemistry remains of interest.

Some structural features of the lanthanide oxalate decahydrates described above are depicted in Chapter 5.5.

3.3 Glyoxylic acid

Glyoxylic acid (also 2-oxoacetic or formylformic acid) is the simplest known compound comprising both aldehydic and carboxylic functions ($C_2H_2O_3$, Fig. 7).

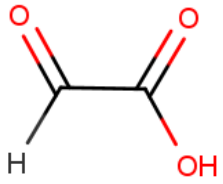

Figure 7. Molecular diagram of glyoxylic acid

This α-oxocarboxylic acid plays a significant role in organic synthesis due to its bifunctional nature [68]. It is a reagent of importance in many industrial branches [69], including the food industry (vanillin production) [70] , agrochemistry, cosmetics [68, 71]. A range of the pharmaceutical intermediates is synthesized within glyoxylic acid [72]. It is also a compound of interest in environmental chemistry issues because it is a natural component of the atmospheric aerosols [73]. Glyoxylic acid is encountered in nature and plays an essential biochemical role: in animals, it is a component of several metabolic processes; in plants and bacteria, it is a key compound in the glyoxylate cycle, which enables these organisms to convert fatty acids into carbohydrates [69, 72].

In medicinal chemistry, it is a well-known compound not only due to its biochemical function; the acid and its derivatives are also an investigation object for their potential applications. For example, the natural abundance of the acid and its relatively low toxicity [69] accounted for the development of the class of polymers with potential implementation in controlled release drug delivery [74]. Those are the polymers on the base of the esters of glyoxylic acid. The poly (alkyl glyoxylates) have beneficial chelating properties and show excellent biodegradability as they are self-immolative: they depolymerize upon a definite stimulus, ultimately generating the corresponding alkyl alcohol and glyoxylic acid hydrate, which can be normally metabolized in the body [75].

However, little is known about the glyoxylic acid interactions with metals. The data on the aqueous solution chemistry of glyoxylic acid, its features as a ligand in coordination chemistry, and its physicochemical properties relevant to this context are rather scarce.

Glyoxylic acid crystallizes in the form of monohydrate, $C_2H_2O_3 \cdot H_2O$. It is a colorless or straw yellow crystalline solid. It was reported that the hydrate water could not be removed by treatment with the dehydration agents even under the reduced pressure conditions [68]. The crystals are highly hygroscopic [76]; the compound is highly hydrophilic. It is soluble in water and alcohols (with alcohols it reacts), and in water-miscible organic solvents, insoluble in ethers and non-polar organic solvents. When dry, the monohydrate has a melting point of 50-52 °C. The acid is commercially supplied in solid form or as a 50% water solution; the solution density is 1,34 g/cm^3, 20°C [77].

The early powder X-ray diffraction studies reported that the acid monohydrate isolated from aqueous solution exists in the solid form as 2,2-dihydroxyacetic acid [78]. At the same time, the ^{1}H-NMR and ^{13}C-NMR data were published, indicating that in aqueous solutions, glyoxylic acid exists mainly as 2,2-dihydroxyacetic acid. A minor amount of linear dimeric form is also present (Fig.8) [68].

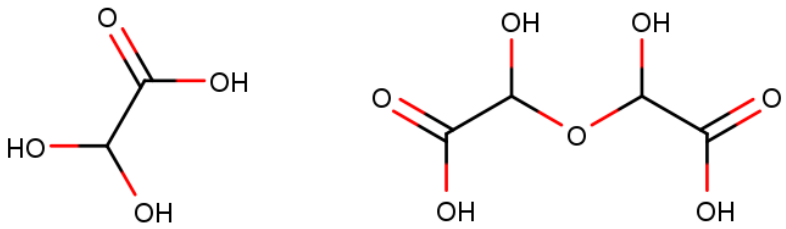

1 2

Figure 8. 2,2-dihydroxyacetic acid (1) and the linear dimer (2)

The formation of 2,2-dihydroxyacetic acid in the presence of water is a reaction typical for the aldehydic function – the geminal diol formation (Fig.9).

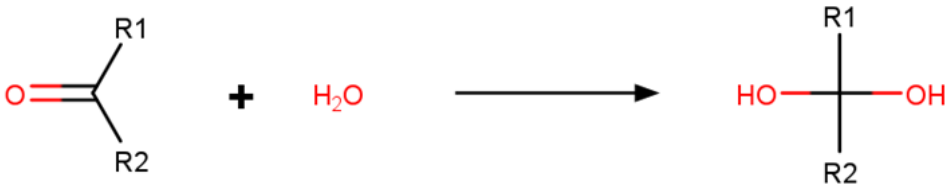

Figure 9. The gem-diol formation reaction for the two protolytic forms of glyoxylic acid: R1 = -COOH or -COO $^-$ (glyoxylic acid or glyoxylate ion form), R2 = -H

For the reaction depicted in Fig.9, the equilibrium can be formulated as follows:

$$K_H = \frac{[(R_1)(R_2)C(OH)_2]}{[(R_1)(R_2)C(O)]} \qquad [11]$$

In equation 11, K_H is the hydration equilibrium constant; the expressions in brackets represent the equilibrium concentrations of the corresponding species (gem-diol and carbonyl forms).

As the cited sources report, the prevalent species in the solution is the gem-diol form of the acid: the equilibrium position is shifted to the right in the reaction as written in Fig. 9. The K_H of this reversible hydration process was found to be $3{,}0 \cdot 10^2$ for glyoxylic acid and 15,1 for glyoxylate ion at room temperature [79].

The geminal diol formation can alter some physicochemical properties of the molecules. For example, vapor pressure is impacted: the hydrated form (diol) shows lower values than the keto-form. This is because gem diols tend to form stronger inter- and intramolecular hydrogen bonds compared to their carbonyl analogs [80]. The phenomenon of the 2,2-dihydroxyacetic acid formation is also important from the chemical point of view as this is the form in which the acid in aqueous solutions interacts with metals.

In the absence of water in the isolated state, the glyoxylic acid exists mainly as a cyclic intramolecularly H-bonded conformer (as confirmed by the vibrational spectroscopy studies) [81]. This "trans" carbonyl arrangement is depicted in Fig. 10.

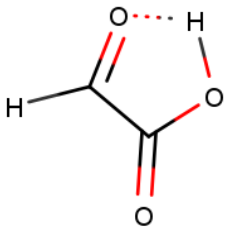

Figure 10. The scheme of the intramolecular bonding in the isolated glyoxylic acid.

Most of the reactions typical for glyoxylic acid will not be mentioned here as they belong to the organic synthesis scope, but the chemical properties possibly relevant to the problematics concerned in this work will be briefly described below. Being a carboxylic acid, glyoxylic acid reacts with bases forming corresponding salts. However, on additional heating, glyoxylic acid disproportionates to the mixture of glycolic acid and oxalic acid or their salts [68] (Fig. 11). This reaction may also proceed without the presence of a base, to a lesser extent.

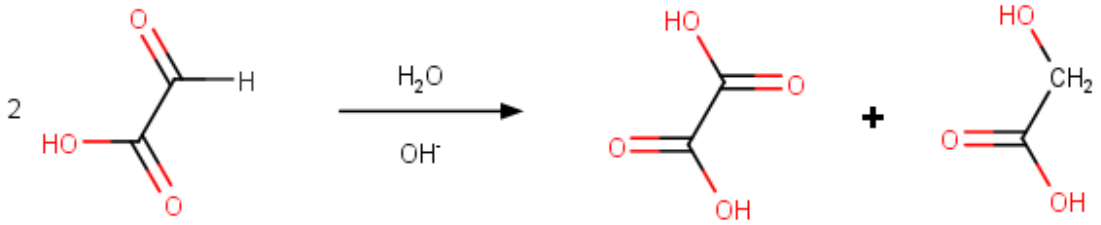

Figure 11. Disproportionation of glyoxylic acid

Glyoxylic acid has reducing properties and may be employed in technology as a non-toxic reducing agent [82]. It is stable in the air but can be oxidized to oxalic acid by nitric acid (Fig. 12).

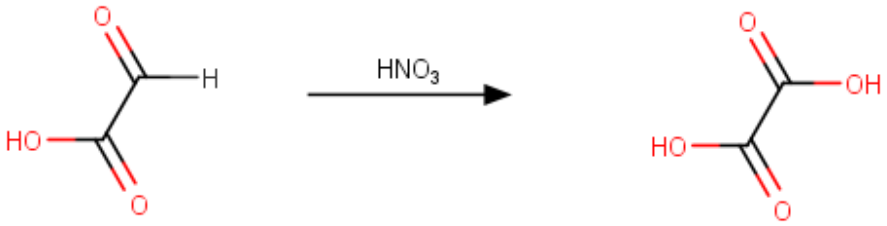

Figure 12. Oxidation of glyoxylic acid

Glyoxylic acid may form complexes with alkali and alkaline-earth metal ions: it was reported to have a chelating power of 30 mg of calcium carbonate ($CaCO_3$) per gram of its 50% aqueous solution [69]. However, more detailed data on this matter are not found in the literature. Another publication reported the formation of calcium glyoxylate hemihydrate precipitate (Figure 13; curdy, white solid is formed) in the reaction of glyoxylic acid with calcium hydroxide in molar ratio acid: base = 2: 1 in aqueous solutions in pH range 1,6-5,0 [83].

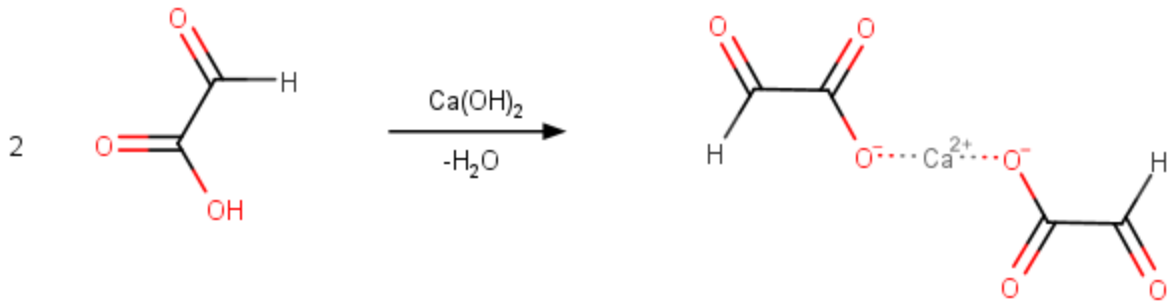

Figure 13. Calcium glyoxylate precipitation scheme

Further, the separation and purification issues may be of certain interest for this work's scope. As described in several sources, the crystallization or recrystallization of glyoxylic acid from the solution is quite a laborious process, which requires time or sophisticated equipment. The glyoxylic acid monohydrate isolation in solid-state from an aqueous solution may require reduced pressure conditions, adding the seed crystals and specific temperature program. The use of drying agents (e.g., fresh P_2O_5) can also be beneficial. As revealed by XRD diffraction studies of the crystallization products, the varying conditions of the crystallization (temperature, pressure, the choice of drying agent) lead to products with a slight variation in the proportion of hydrate water [68, 78]. Despite the crystallization process's difficulties, the properly obtained product is not just an amorphous mass of solid material but crystalline.

3.4 Oxamic acid

Oxamic acid (also 2-amino-2-oxoethanoic acid or 2-amino-2-oxoacetic acid) is the simplest known organic acid containing an amide group. Formally it is a derivative of oxalic acid - its monoamide ($C_2H_3NO_3$, Fig. 14).

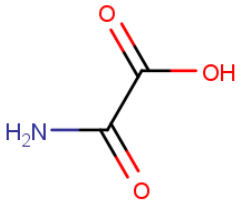

Figure 14. Molecular diagram of oxamic acid

Oxamic acid is available commercially in the form of a white, fluffy, very fine water-soluble powder. Its melting point was reported to be 209 °C; the acid decomposes at its melting point [84]. Oxamic acid is a very polar molecule, and it is very slightly soluble in nonpolar organic solvents [85]. No data concerning the acid's quantitative solubility parameters and its stability in the aqueous solution were found. According to the DrugBank website, ALOGPS (Virtual Computational Chemistry Laboratory), water

solubility is predicted to be around 108.0 mg/mL at room temperature, and the predicted pKa value is 2.49. As the available form of oxamic acid is a fine powder, several attempts were made to obtain larger crystals [86]. Small crystallites were achieved within the procedure, where oxamic acid was dissolved in the mixture of methanol and water, and the obtained saturated solution seeded with small grains of oxamic acid was slowly evaporated. Numerous attempts to obtain large crystals suitable for single-crystal X-ray diffraction studies by slow evaporation in various solvents have been carried out, but mostly unsuccessfully. However, a few crystals were obtained by a crystallization experiment conducted in ethanol [86].

As seen from the Fig.14, oxamic acid is isoelectronic with pyruvic acid ($C_3H_4O_3$), which is one of the most important biochemical compounds [87]. This fact is the underground for some oxamic acid features relevant for biochemistry and their sequent implementations. Pyruvic acid is a substrate for the enzyme lactate dehydrogenase (LDH), involved in the glycolysis. Oxamic acid, the pyruvic acid isosteric analog, was proven to be the lactate dehydrogenase inhibitor [88]. Therefore, the acid may be implemented in biotechnology in the analysis of the materials containing LDH [85], in the selective separation of this enzyme. Some early studies [84] report the anticancer activity of oxamic acid: sodium oxamate was found to be active in the glucose metabolism in carcinoma cells. The effect is probably related to the mentioned above inhibition of LDH.

Oxamic acid is a by-product in some synthetic procedures in the pharmaceutical industry [89]. It has several polymer chemistry applications, where it is exploited as a useful substrate for modification of structure and properties of polymers [90].

Despite its chemical simplicity, few data on the acid's physicochemical properties are available.
Attracted by the oxamic acid's steric similarity to pyruvic acid, Raczynska et al. [85] undertook systematic studies on both acids' geometrical properties. Prototropic tautomerism (Fig. 15) exhibited by the acids was the main subject of investigation. Keto-enol conversion of pyruvic acid is a well-known and thoroughly studied phenomenon [91], but the same cannot be said about oxamic acid. The authors [85] carried out quantum-chemical calculations on the amide-iminol tautomerism of oxamic acid. They concluded that the amide tautomer has substantially greater thermodynamic stability than the iminol tautomer, irrespective of the environment (whether it is solid-state, gas phase, or solution). At all, there is no experimental evidence for the existence of the iminol forms [86]. Three amide structures that may be theoretically determined in the gas phase or in the nonpolar environment are shown in Fig. 16.

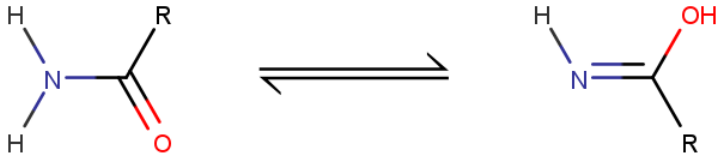

Figure 15. Amide-iminol tautomeric conversion for oxamic acid. R = -COOH

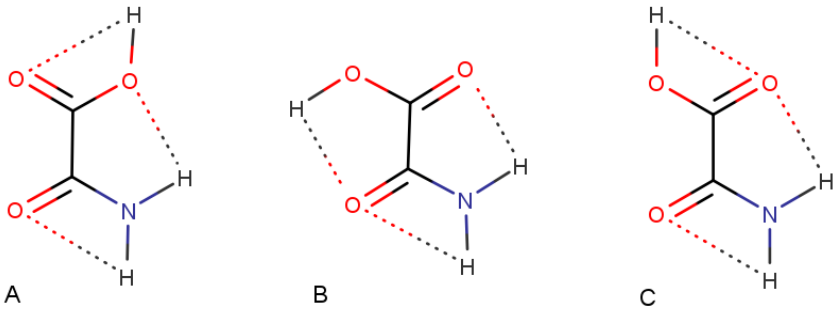

Figure 16. Intramolecular interactions for the amide structures of oxamic acid in the gas phase.

Several studies by IR and Raman spectroscopy on oxamic acid and its simple salts had been carried out relatively long ago [92, 93, 84]. The solid-state hydrogen-bonding patterns were the main interest of those studies. Dicarboxylic acids in which one of the carboxylic functions is substituted by a primary amide function are a class of compounds interesting in terms of hydrogen bonding as they exhibit proton donating groups (-OH and -NH-) and proton accepting groups (=C=O), which gives a variety of possible hydrogen bonding patterns. The deprotonated dicarboxylic acids' monoamides capable of generating the extended hydrogen-bonded motifs may be implemented as useful building blocks for crystal engineering [94]. Based on the spectroscopic studies' results, the authors [92, 93, 84] assumed that oxamic acid behaves as a linear hydrogen-bonded polymer with alternating intermolecular cyclic acid-acid and cyclic amide-amide dimers. However, this assumption is inconsistent with the latest data. In fact, the complex 2D hydrogen-bonding pattern in the acid's structure is based on the cyclic amide-acid dimeric unit (Fig. 17). So, cyclic non-centrosymmetric amide-acid heterosynthons control the packing of oxamic acid [95].

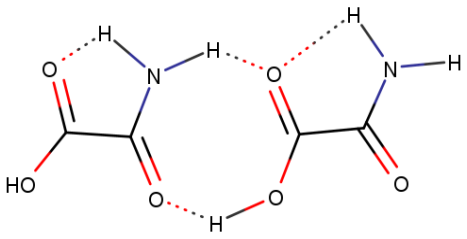

Figure 17. Hydrogen bond pattern in solid oxamic acid. The intramolecular H-bonds are also shown.

However, when it comes to the anionic motifs displayed by oxamate anion, $[OOCCONH_2]^-$, other types of hydrogen-bonded scaffolding may be met. Single-crystal XRD studies [94] revealed the preferential assembly patterns displayed by oxamate anion in several simple salts with organic cations such as piperidinium, imidazolium, and N-substituted ammonium (Fig. 18). In the same fashion as in the pure oxamic acid structure, in salts, the oxamate dimers may aggregate into infinite one-dimensional sequences. The remaining

hydrogen-bond sites are then available for cross-linking between the adjacent 1D motifs, forming layers - 2D scaffolding.

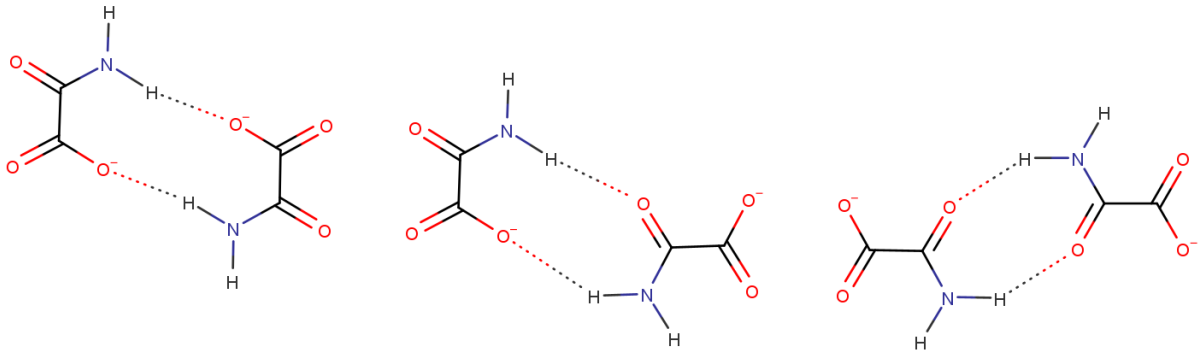

Figure 18. An example of the dimeric motifs that are present in several simple oxamate salts with organic cations.

The crystal structure of oxamic acid was reported relatively recently, in the year 2018 [86]. The anhydrous acid crystallizes in a monoclinic crystal system in space group Cc (№ 9). The molecules are close to planar, interact through carboxyl-amide H-bonds (as shown in Fig. 17), and form ribbons (not linear chains) that run along the b axis. The adjacent ribbons interact and form layers parallel to the ab plane (Fig. 19). The layers are connected and held together by van der Waals's interactions. The image in Fig.19 is adapted from the cited source.

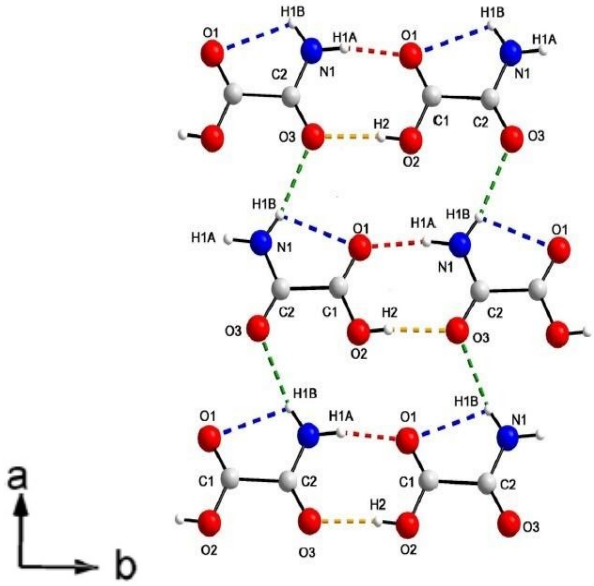

Figure 19. The oxamic acid 2D structure pattern (ab plane is shown) [86].

3.5 Oxamic acid and glyoxylic acid compounds of selected metal ions

Metal oxamates

If to expand on a topic raised in Chapter 3.4, it is proper to turn to the ligating possibilities of oxamic acid, which are interesting and versatile. Concerning the coordination modes, oxamic acid may act as a di-, tri-, or tetradentate ligand. Regarding its charge, it may act as mono- or dianion, losing the carboxylate or both carboxylate and one amide hydrogens, respectively [96]. The seven oxamate coordination possibilities described in literature are shown in Fig. 20.

After ionization of the carboxylic hydrogen (as a monoanion abbreviated as $Hoxm^-$), it may coordinate to metal ions through its carboxylate and amide oxygens (Fig. 20, a) [97, 98]. Still, as a monoanion, it can coordinate through both of the carboxylate oxygens (Fig. 20, b) [96, 99] or through one carboxylate oxygen and one nitrogen atom (Fig. 20, d) [100]. In cases a) and d), the five-membered chelate ring is formed. Still, as a monoanion, it may display the monodentate binding mode coordinating through one carboxylate oxygen atom (Fig. 20, c) [96], or it may also behave as a tridentate ligand using all oxygens present in the molecule for coordination (Fig. 20, e) [99]. After the removal of the second ionizable hydrogen (one of the amide hydrogens), the dianion form (oxm^{2-}) is attained. It may act as a bidentate ligand coordinating through one carboxylate oxygen atom and one amide nitrogen atom; the chelate ring is formed in this case (Fig. 20, f) [101]. The oxm^{2-} ion may also appear as a tetradentate bridging *μ*-ligand in binuclear or polynuclear complexes (Fig. 20, g) [98].

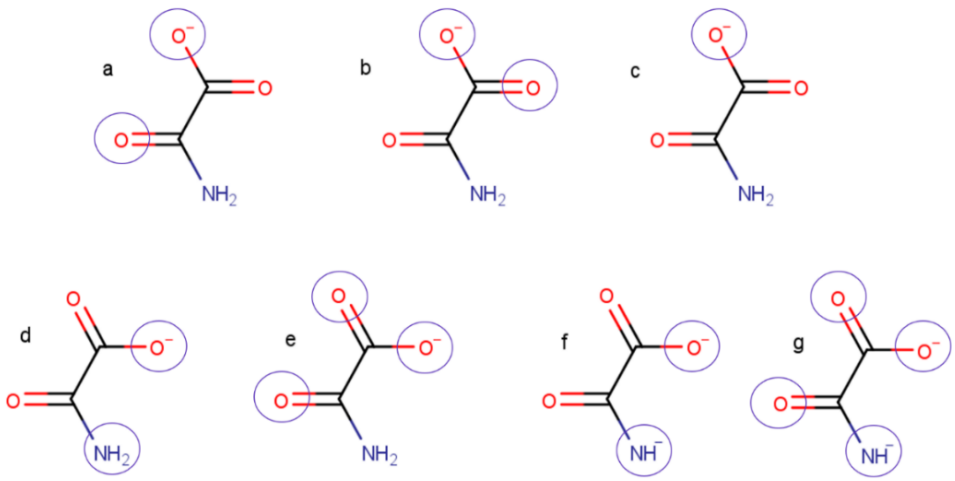

Figure 20. The ligating possibilities of oxamic acid. The circled atoms are those participating in the coordination polyhedra

Oxamates as ligands received some attention in the coordination chemistry of lanthanides [102, 103, 96]. More studies, supported by structural and spectroscopic data, are available for the oxamate complexes of transition metals [104, 105, 101, 106]. The research on the oxamic acid exploitation in polynuclear heterometallic complexes synthesis revealed no studies of this type present in literature. However, oxamic acid N-substituted derivatives are relatively

popular in crystal engineering of such systems [107], but this matter is out of this work scope.

When it comes to the complexes of divalent and trivalent transition metal cations, oxamate anion often demonstrates coordination modes that lead to the formation of five-membered chelate rings (as shown on the schemes a), d) and f) in Fig. 20). Both $Hoxm^-$ and oxm^{2-} compounds are known [106, 101]. For example, the complexes of general formula $M(H_2NCOCOO)_2 \cdot 2H_2O$ ($M = Mn^{II}$, Co^{II}, Ni^{II}, Zn^{II}) may be mentioned. As confirmed by the vibrational analysis [104], the structure of these complexes is trans-octahedral with the apical positions occupied by water molecules; oxamate anion coordinates through the amide oxygen and one carboxylic oxygen as donor atoms (Fig. 21, a). The thermal decomposition process leads to the formation of the oligomeric structures $[(C_2H_2NO_3)\ M\ (C_2H_2NO_3)]_n$, where oxamate anion bridges the metal cations forming the oligomeric chain (Fig. 21, b).

The complexes with monoanionic oxamate species are chosen as an illustration here because, in the practical part of this work, there are no experiments to be conducted in strongly alkaline media, making the dianion (oxm^{2-}) species occurrence rather unlikely and irrelevant.

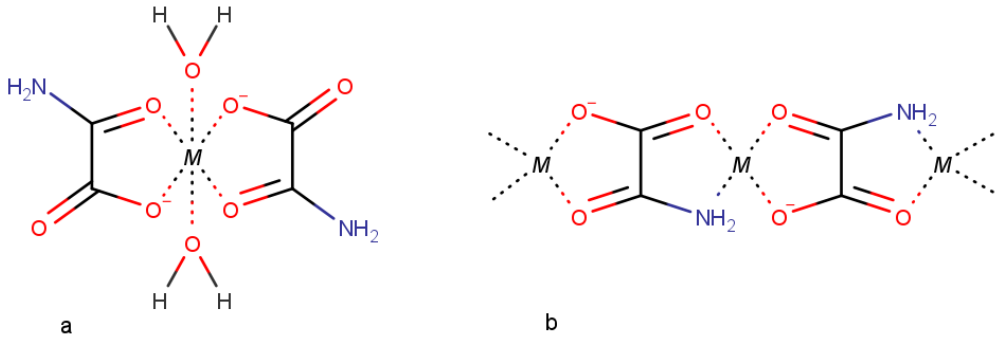

Figure 21. Trans-octahedral structure of $M(H_2NCOCOO)_2 \cdot 2H_2O$ ($M = Mn^{II}$, Co^{II}, Ni^{II}, Zn^{II}) (a) and molecular structure of the oligomer formed during thermal decomposition (b).

Eventually, it is necessary to introduce several advances in lanthanide oxamates chemistry. Different types of complexes were synthesized, but only a few were prepared with a satisfactory crystallinity degree to determine structure from the XRD patterns [108]. Both compounds of the oxamate monoanionic and dianionic forms are described [109, 103]. Oxamic acid demonstrates various coordination modes (Fig. 20) in different complexes.

The anionic complexes of general formula $K_3[Ln(oxm^{2-})_3(H_2O)_3]$ are a typical example of the compounds with double-deprotonated oxamic acid species [103, 102]. Those compounds are obtained from the systems with high pH values (pH = 11 – 13) maintained by KOH solution slow adding. The stated pH value is a rough estimation calculated from the published experimental data [102]. Noticeably, in the cited papers, much more rapidly and easily obtained stable precipitates were obtained using DMSO-water mixture rather than pure aqueous systems. However, there was no evidence of either coordinated or lattice

DMSO molecules in the prepared lanthanide oxamates, even though dimethyl sulfoxide has higher electron-donating activity than water.

The standard preparation route of $Ln(Hoxm^-)_3 \cdot nH_2O$ compounds involves mixing the corresponding metal salt (e.g., lanthanide chlorides [100] $LnCl_3 \cdot 6H_2O$ or $LnCl_3 \cdot 7H_2O$, basic lanthanide carbonates [99] $Ln_2(OH)_2(CO_3)_2 \cdot mH_2O$) maintained in water or water-ethanol mixture with a water solution or suspension of oxamic acid with or without the addition of the base (e.g., NaOH) [100]; different ratios metal: oxamate are tested and described in literature [100, 99]. Different conditions (temperature, magnetic stirring) are used in different works. The formation of the microcrystalline powder-like precipitates is reported by several researchers [100], others [96, 99] stated the method of obtaining the solid-state oxamates by the evaporation of the solutions of the respective metal oxamates to dryness in a water bath, following by the drying in an oven and a desiccator. However, relatively diluted systems (high volumes of the solvents) are used in the latter case, so resultant oxamate compounds' solubilities in both cases are difficult to be assessed. Nevertheless, many authors agree on the fact that the generally low solubility of the $oxamate^{1-}$ complexes may be an indication of their polymeric character [100, 109].

In the chemical formula of the compounds discussed above ($Ln\ (Hoxm^-)_3 \cdot nH_2O$), n is the number of the coordinated/lattice water molecules; it varies depending on the specific metal, the preparation conditions, and also differs from one paper to another.

One interesting observation made during the analysis of the published experimental data on the oxamate compounds preparation is that relating to the similar concentrations (mol/l) of oxamic acid in the water, terms "water solution" and "water suspension" are used alternately in different sources. This inconsistency may be due to the slow kinetics of the dissolution of oxamic acid in water. There is no data concerning the solubility of oxamic acid published, so oxamic acid's solubility was studied in a practical part of this work. Furthermore, the oxamic acid probable hydrolysis aspects are not taken into account in the mentioned above articles. At the same time, there are many reports [66, 110] about the oxamic acid aqueous solutions hydrolysis phenomenon. Therefore, in the current work, the lanthanide – oxamate interactions were examined, emphasizing the oxamic acid stability/decomposition aspect.

As an example of the $oxamate^{1-}$ complex, the following compound of holmium (III) may be mentioned: $[Ho\ (Hoxm^-)_3\ (H_2O)_3]_4 \cdot 2{,}75H_2O$. As revealed from the single crystal XRD studies [108], holmium atoms are nine-coordinated: nine oxygens are contributed by three bidentate oxamates and three water molecules. The coordination number of the metal is nine, even though heavier Ln usually prefer the coordination number of eight. The coordination polyhedron is a tricapped trigonal prism: three oxygens from water and three oxygens from oxamates form the prism; the remaining three oxygens from oxamates fulfil the "caps" positions outside the midpoints of the rectangular faces of the prism. This geometry is quite popular among the complexes of lanthanides with oxygen donors (Fig. 22). So, oxamic acid acts as bidentate O, O- non-bridging ligand. If to go into further structural details, it is appropriate to describe the hydrogen bonding pattern briefly. Hydrogen bonding is responsible for the formation of "polymeric" chains (perpendicular to

b axes, parallel to a-c plane) and layers. The adjacent layers in the b direction are also held together by H-bonds. The Ho coordination environment illustration in Fig. 22 is adapted from the cited article.

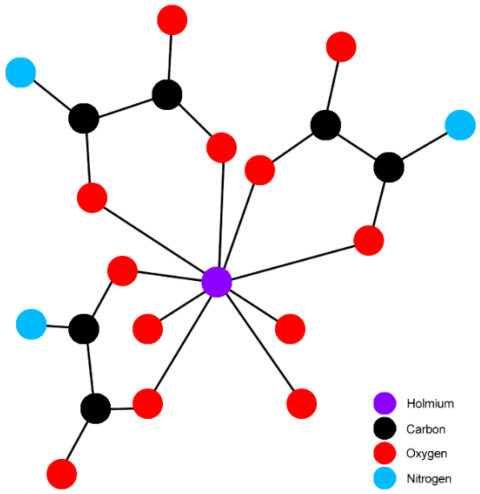

Figure 22. The coordination environment of Ho atom in [Ho ($Hoxm^{-}$)$_3$ (H_2O)$_3$]$_4$ ·2,75H_2O complex [108].

Metal glyoxylates

Glyoxylates as ligands are not popular in coordination chemistry: there are barely any studies focused on glyoxylic acid complexes in literature.

Though, several bis-hydrazine metal glyoxylates were reported [111, 112]. The series of the complexes with the suggested molecular formula of Ln(glyoxylate $^{-1}$)$_3$(N_2H_4)$_2$, where Ln (III) = La, Ce, Pr, Nd, Gd [111]; and M(glyoxylate $^{-1}$)$_2$(N_2H_4)$_2$, where M (II) = Mg, Mn, Co, Ni, Cu, Zn or Cd [112] were prepared. The coordination number of 9 was assigned for the Ln^{3+} ion in the Ln(glyoxylate $^{-1}$)$_3$(N_2H_4)$_2$ series. The coordination environment of the Ln^{3+} ion was suggested to be formed by three bidentate glyoxylates, one bridging (bidentate) hydrazine molecule, and one monodentate non-bridging hydrazine molecule; the 2D polymeric structure is expected.

However, there is no consistent and reliable data available, and even the proposed general formula of the mentioned above complexes is questionable. The authors [112, 111] report obtaining the powder-like crystalline compounds with neutral hydrazine molecules in the composition, stable in air and insoluble in water and alcohol. In all the described cases, an aqueous mixture of glyoxylic acid monohydrate and hydrazine hydrate (in excess) is mixed with the corresponding metal nitrate's water solution. The attempts to isolate solid hydrazinium glyoxylate undertaken to examine and characterize the ligand were unsuccessful and led to obtaining dark brown gel. More recently, under slightly different conditions working with M^{2+} cations of several 3d metals, other researchers obtained the metal (II) hydrazone glyoxylate dihydrates [M($OOCCH{=}NNH_2$)$_2$(H_2O)$_2$] [113]. The condensation of the aldehydic function of glyoxylic acid with hydrazine is a probable process indeed. Thus, the composition, structure, and physicochemical characteristics of

the compounds mentioned in the current paragraph are, in reality, rather poorly understood and need further investigation.

A much more interesting and well-studied case concerns the heteropolynuclear coordination compounds referred to as polyhydroxoglyoxylates. Several reports in the literature describe the synthesis and characterization (physicochemical, thermal, and spectroscopic analysis, X-ray diffractometry) of these compounds [114, 115]. In most synthetic procedures glyoxylic acid is generated *in situ* as an oxidation product of ethylene glycol (EG). An oxidizing agent is nitric acid in aqueous solution:

$$NO_3^- + 3e^- + 4H^+ \rightleftharpoons NO + 2H_2O \quad [12]$$

$$C_2H_3O_4^- + 6e^- + 7H^+ \rightleftharpoons C_2H_4(OH)_2 + 2H_2O \quad [13]$$

$$C_2H_4(OH)_2 + 2NO_3^- + H^+ \rightleftharpoons C_2H_3O_4^- + 2NO + 2H_2O \quad [14]$$

Equations 12 to 14 depict the redox reaction between the nitrate anion and EG; glyoxylate anion produced by oxidation is written straight away in its hydrated form. The molecular formulae are clarified by the structural formulae given in Fig. 23.

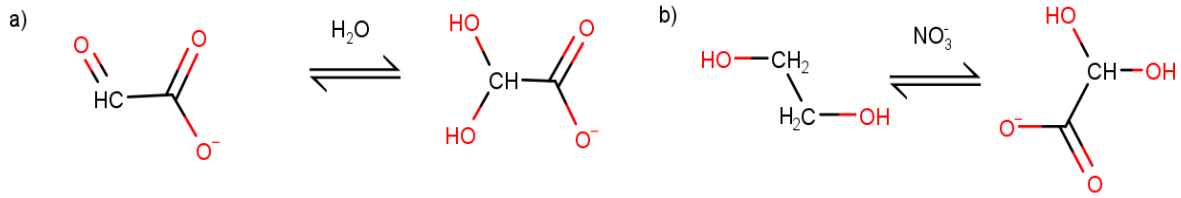

Figure 23. The glyoxylic acid hydrate formation (a) and the EG oxidation scheme (b)

As an example of the indicated type of coordination compounds, the complex with the following composition formula may be mentioned: $Co_4Fe_{10}(L)_9(OH)_{20}(H_2O)_{32}\cdot_{14}H_2O$ [114], where L is the glyoxylate dianion ($C_2H_2O_4^{2-}$, Fig. 24).

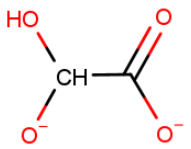

Figure 24. The glyoxylate dianion structural formula ($C_2H_2O_4^{2-}$)

The synthesis of this coordination compound is based on the *in situ* oxidation of EG by nitrate anion in water-diol mixture with the corresponding metals nitrates present in the solution, with the pH value set at 3,0 (maintained by concentrated HNO_3 drops adding) under heating. The solid, powdery, reddish-brown product is precipitated. It is a very stable compound, obtained with low crystallinity degree, practically insoluble in water and common organic solvents; its composition in the pure state does not change with time, and it can be destroyed only by strongly acidic media or by the ammonium treatment [114] (Co^{2+} forms ammine complexes) [16]. The authors concluded that the Co^{2+} and Fe^{3+} cations have a pseudo-octahedral coordination environment, as confirmed by their experimental data.

The suggested structure of the indicated heteropolynuclear coordination compound is shown in Fig. 25. The picture is taken from the cited source.

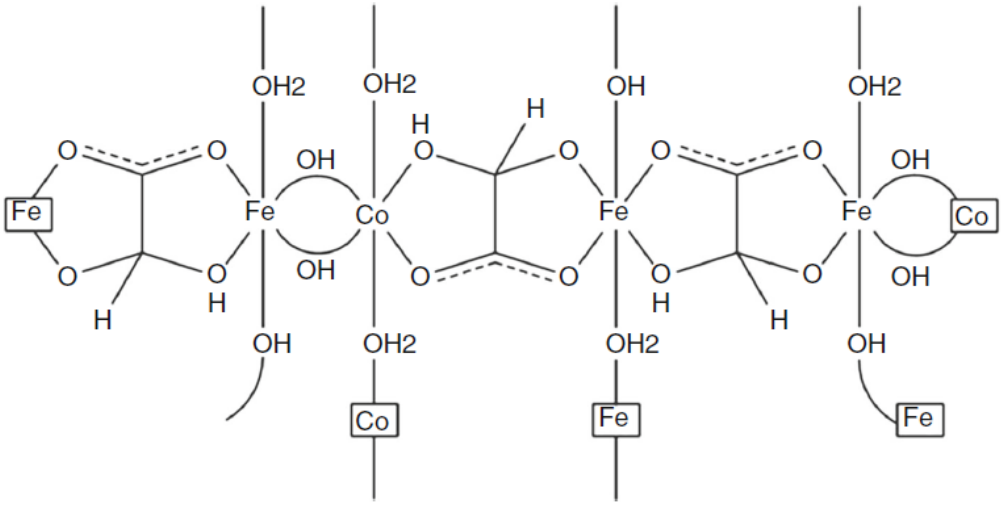

Figure 25. The proposed structure of Co(II)–Fe(III) polyhydroxoglyoxylate [114]

As it is seen from Fig. 25, glyoxylate ions in the dianion form act as bridging (μ_2 - κ^2: κ^2) tetradentate chelating ligands connecting the adjacent metal centres.

The polyhydroxoglyoxylate compounds of the discussed above type are often investigated in the context of the production of the nanosized metal oxides [116]. Actually, heteronuclear complexes' thermal decomposition is one of the simplest techniques for preparing the mixed oxide nanoparticles [115]. The synthesis route involves preparing the precursor heteronuclear metal glyoxylate complex and its subsequent thermal decomposition to obtain the desired nanoparticles. The precursor complex is prepared *via* the route involving oxidation of ethylene glycol by nitrate ions; the emerged glyoxylic acid dianion immediately chelates and bridges the metal centres and forms the insoluble coordination compound. As the main interest of the process is to prepare the oxide nanoparticles, the intermediate glyoxylate complex is often not characterized.

4. Experimental part

4.1. Materials and characterization methods

Materials
All chemicals used in the experiments are listed below. All chemicals and solvents were used as received without further purification.

Oxamic acid (Sigma-Aldrich, >98% purity), glyoxylic acid monohydrate (Sigma-Aldrich), sodium hydroxide (Sigma-Aldrich, BioXtra, ≥98% (acidimetric), pellets (anhydrous)), oxalic acid dihydrate $(COOH)_2 \cdot 2H_2O$, Sigma-Aldrich, ≥99% purity). Ce (III) nitrate hexahydrate (Sigma-Aldrich, 99,99% purity), Gd (III) nitrate hexahydrate (Sigma-Aldrich, 99,99% purity).
Nessler reagent (Potassium tetraiodomercurate, Sigma-Aldrich), $KMnO_4$ solution (0,02M, Lach-Ner).

Characterization methods
All graphs were made using a Microsoft Office Excel program if other is not specified.

Powder X-ray diffraction (XRD)
To study the phase compositions of the samples, powder X-ray diffraction was used. XRD patterns were recorded by a PANalytical X'Pert PRO diffractometer (Cu Kα radiation), equipped by a secondary monochromator and PIXcel detector using a Data Collector control software (Malvern PANalytical) at the Science Faculty, Charles University, Prague. Profile analysis was undertaken with Profex[117] open-source software and Jana2006[118].

Scanning Electron microscopy (SEM)
The morphology of the final powders was studied under scanning electron microscopes JEOL JSM-6510 and Philips CP XL 30 at the Institute of Inorganic Chemistry of the Czech Academy of Sciences. The samples were coated with a thin Au/Pd layer or as received.

Micro-Raman spectroscopy
Raman spectra were recorded on the Nexus Nicolet module attached to Nicolet 6700 spectrometer with Nd:YVO4 excitation laser (1064 nm) at the Science Faculty, Charles University, Prague. Spectra were recorded between 100 and 3700 cm−1 with 4 cm−1 step, 256 scans, InGaAs detector, and 1.3 W laser power.

Thermogravimetric analysis (TGA)
Thermogravimetric analysis (TGA) measurements were carried out at the Science Faculty, Charles University, Prague under air on a Mettler Toledo TGA 1 Stare thermal instrument

with a heating rate of 3 K min^{-1} and a gas flow of 20 mL min^{-1} in a 70 µL aluminum oxide crucible.

4.2 The acids' solubility determination experiments

In order to determine the oxamic acid solubility in water (and subsequently to try the same with glyoxylic acid), the following experimental setup was constructed. In the three-neck round-bottom flask, the saturated solution of oxamic acid in equilibrium with undissolved oxamic acid was prepared. The flask was immersed in a water bath with temperature control. An air condenser was attached to the middle neck of the flask, the side necks' openings were capped with plastic stoppers.

As the solubility of oxamic acid is an unknown quantity, the preparation of the solution was directed by the undissolved solute presence in the system. The preliminary experiments showed that the dissolution of oxamic acid in water proceeds at a low kinetic rate. Therefore, the temperature was set at 30 °C, and three days were left for oxamic to dissolve completely; the solution was periodically magnetically stirred. Then, the temperature was set at 25 °C, and the system was left to stand for three more days for the nominal dissolution equilibrium to be established. The term "nominal dissolution equilibrium" implies that no accurate thermodynamic calculations were conducted, and it is not absolutely correct to use the term "dissolution equilibrium" explicitly. This work aimed to tentatively evaluate the oxamic acid's solubility in water and express it in g per 100 g of solvent units.

A set consisting of five small pear-shaped flasks was prepared. The flasks were rinsed with a mixture of detergent and citric acid, with copious volumes of tap water, and then with deionized water; the glassware was kept in an oven at 110 °C overnight. The dried flasks were weighed. Five 2 ml samples of the oxamic acid saturated solution were taken and added to the correspondingly numbered pear-shaped flasks. The flasks with the analyzed solution aliquots were weighed, and the exact masses of the aliquots were counted. The samples were evaporated to dryness using the rotary evaporator. The solid residues in the flasks were dried in the desiccator for three days. Afterward, the flasks with the dry residues were weighed, and the oxamic acid solubility was counted from the data (Table 2, Chapter 5.1).

4.3 The oxamic acid and glyoxylic acid's pKa values determination

To assess the acid-base behavior of the examined acids, the pKa values determination was conducted by the potentiometric acid-base titration method. The titrations were monitored with a pH meter; an acid-base indicator (phenolphthalein) was added to the solutions of the analytes for easy qualitative assessment of the equivalence point. The pKa values were

read from the titration curves in accordance with the Henderson-Hasselbalch equation (Equation 15).

$$pH = pKa + log\frac{[A^-]}{[HA]} \quad [15]$$

In equation 15, $[A^-]$ is the relative concentration of the dissociated form of the acid, [HA] is the relative concentration of the undissociated form of the acid. The half-equivalence point gives pH = pKa. This simple speculation is valid for weak monobasic acids, which dissociate in the solution according to the following scheme: $HA \rightleftharpoons H^+ + A^-$.

Generally, the dissociation constant of an arbitrary dissociation step (numbered *n*) of an *m*-basic acid is given as follows:

$$K_A\ (H_nA) = \frac{[H^+][H_{n-1}A^{(m-n+1)-}]}{[H_nA^{(m-n)-}]} \quad [16]$$

For a monobasic acid:

$$K_A\ (HA) = \frac{[H^+][A^-]}{[HA]} \quad [17]$$

Glyoxylic acid is a monobasic acid with its dissociation constant described as it is given in Equation 17. Therefore, this acid was anticipated to display a titration curve with one inflection (one equivalence point). On the other hand, oxamic acid has two potentially ionizable hydrogens. A titration curve with two inflection points was anticipated. However, the appearance of the experimental oxamic acid titration curve was explicitly an appearance of a monobasic acid's titration curve (Fig. 27, Chapter 5.2). So, under the chosen experimental conditions, oxamic acid behaves as a monobasic acid, dissociating in one step, releasing only its carboxylic hydrogen.

Procedure

In a 250 ml volumetric flask, a stock titrant solution of NaOH (V = 250 ml) with approximate concentration 0,1 $mol \cdot dm^{-3}$ was prepared. The solution was kept stoppered in a volumetric flask to prevent the absorption of the atmospheric CO_2 and the formation of CO_3^{2-} ions, which may interfere with the equivalence point (the slope of the titration curve at the inflection point may be decreased). The determination of the exact concentration of this solution (the standardization of the titrant solution) was conducted. Oxalic acid dihydrate was used as a primary standard for this procedure. The biuret was filled with NaOH solution. The precisely weighed amount of the standard was quantitatively tapped out to the Erlenmeyer flask and dissolved in distilled water; phenolphthalein was used as an indicator. The obtained oxalic acid solution was titrated with NaOH till the endpoint (the color change from colorless to pink). The neutralization reaction between NaOH and oxalic acid runs according to Equation 18:

$$2NaOH + (CO_2H)_2 \rightarrow (CO_2Na)_2 + 2H_2O \quad [18]$$

The procedure was repeated three times, the exact molarity of the NaOH solution was counted. The Q-test did not exclude any values, and the average value was taken as a final exact concentration of the titrant solution. According to the goals of the current

experiment, the knowledge of the exact concentration of the titrant solution was not necessary. Nevertheless, it was determined to follow the proper chemical protocol.
The pH-meter was calibrated with the use of pH4 and pH7 buffer solutions.
The solutions of the examined acids were prepared in the titration flasks (50 ml, $9{,}5 \cdot 10^{-3}$ $mol \cdot dm^{-3}$). The concentrations and the amounts of all the solutions were chosen to be as stated for convenience reasons.
The potentiometric titrations of the oxamic acid and glyoxylic acid solutions were conducted, the pH values were read from the pH-meter display and recorded. The temperature in the laboratory was 25 °C. The titration curves are shown in Fig. 27 and 28 (Chapter 5.2).

4.4 The identification of the oxamic acid decomposition product

Several orientational tests were conducted to identify the chemical nature of the oxamic acid decomposition product. The aqueous mixture remained after all the manipulations of the solubility determination experiments was analyzed. In total, this system was heated up (using an oil bath) and cooled down several times; the highest temperature was 85 °C. The content of the flask was not protected from daylight. Several samples of the solution from the leftover two-phase mixture in a three-neck flask were taken and transferred into the test tubes. The qualitative analysis tests were conducted following a standard analytical chemistry protocol [119] . To make a first educated guess, the chemical nature of oxamic acid was considered (it is a monoamide of a dicarboxylic acid – oxalic acid). According to the preliminary suggestion, oxalate ions and ammonium ions' presence was tested.
Several drops of NaOH solution were added to the first test tube, and the test tube was gently heated. A damp universal indicator paper test detected ammonia gas evolution. To the second test tube, few drops of the Nessler reagent (an alkaline solution of potassium tetraiodomercurate (II), $K_2[HgI_4]$) were added. The formation of yellow-colored species was observed, which confirmed the presence of the ammonium cations in the analyzed solution.
In the third test tube, a reaction with $KMnO_4$ was conducted to determine the identity of the anionic species in the analyzed solution. The typical permanganate violet color disappeared in 3 seconds after adding the analytical reagent (Equation 19), confirming the oxalate ions presence in the solution.

$$2\ MnO_4^- + 16\ H^+ + 5\ C_2O_4^{2-} \rightarrow 2\ Mn^{2+} + 8\ H_2O + 10\ CO_2 \qquad [19]$$

Thereby, the presence of ammonium oxalate in the analyzed solution was confirmed.
In the course of the solubility determination experiments, single crystals were grown unintentionally on the surface of the solid phase of the system. The experiments had a slightly similar format to the single-solvent recrystallization method for crystal growth; they lasted in total for several weeks, and afterward, the system was left to stay for a month, so enough time was provided for a crystal formation, even though in an unplanned way.

RNDr. Ivana Císařová, CSc. (from the Department of Inorganic Chemistry) kindly performed the structure analysis of the grown single crystals. The analysis unequivocally demonstrated that the obtained single crystals were those of ammonium oxalate monohydrate $(NH_4)_2C_2O_4 \cdot H_2O$.

4.5 A study of the oxamic acid stability in aqueous solutions

During the solubility determination experiments (as described in Chapter 5.1), it was proven that the oxamic acid decomposition in aqueous solutions takes place under certain conditions. To specify this process, a set of experiments (described below) was designed. As the decomposition occurs in the ambient laboratory conditions, both light and temperature effects were studied.

The effect of light on the oxamic acid decomposition process
30 ml of the oxamic acid 0,1 mol·dm^{-3} solution was prepared in a beaker. The beaker was covered up with a watch glass. The beaker was naturally exposed to the daylight (no daylight isolation was used); moreover, an electric UV lamp was placed in the distance l = 100 cm from the beaker. The system was kept at room temperature during the whole course of the experiment. The samples (V = 2 ml) were taken with a Pasteur pipette in 12 h (sample 1), 36 h (sample 2), 72 h (sample 3), and 120 h (sample 4), the Petri dishes with the samples were left overnight in the oven at 40 °C. The powders were collected to the correspondingly labelled Eppendorf tubes and afterward analyzed through the XRD diffraction.

The effect of temperature on the oxamic acid decomposition process
30 ml of the oxamic acid 0,1 mol·dm^{-3} solution was prepared in a round bottom flask. A simple Liebig condenser was attached to the neck of the flask (in reflux mode). The flask was immersed in an oil bath with temperature control. The whole setup was isolated from the daylight with aluminium foil. The temperature was set to 100 °C. The samples (V = 2 ml) were again taken with a Pasteur pipette in 12 h (sample 1'), 36 h (sample 2'), 72 h (sample 3') and 120 h (sample 4'), the Petri dishes with the samples were left overnight in the oven at 40 °C, and the products were collected again to the correspondingly labelled Eppendorf tubes.

The XRD diffraction patterns of the individual samples from the "light effect study" series were compared with the pattern of the commercial form of oxamic acid powder recorded in advance. The comparison was conducted in Panalytical HighScore software. All the samples represented the identical phase – pure oxamic acid (Chapter 5.3, Fig. 29). Therefore, the stability of oxamic acid in the aqueous solution towards the light in the given timespan (5 days) was proven.
On the other hand, the XRD analysis of the samples from the "temperature effect study" series confirmed that the thermal decomposition of oxamic acid in water solutions occurs.

The chosen temperature conditions and the scheme of sampling did not enable to track the process of the oxamic acid gradual decomposition. The last three powder evaporates from the "temperature effect study" series were identified as the final decomposition product of oxamic acid - pure ammonium oxalate monohydrate (Chapter 5.3, Fig. 30).
Samples 3' and 4' (from the "temperature effect study" series) were studied by the Raman spectroscopy. As the referential compounds, commercial powder of solid oxamic acid and ammonium oxalate monohydrate (synthesized in advance) were taken. Ammonium oxalate monohydrate was prepared in amounts needed for the micro-Raman analysis by mixing 2 ml of 0,125 mol·dm^{-3} $H_2C_2O_4 \cdot 2H_2O$ with 0,1 ml of 25% aqueous ammonia solution and drying the product in an oven to evaporate water. The corresponding Raman spectra are attached in Chapter 5.4, Fig. 32; the wavenumber region 400 – 1800 cm^{-1} is shown.

The determination of the oxamic acid's thermal decomposition rate
As revealed by the preceding experiments, the elevated temperature is the reason for oxamic acid to decompose in an aqueous solution, and at T = 100 °C (reflux conditions), the complete decomposition takes less than 24 hours. To determine the rate of oxamic acid decomposition, the following experiment was conducted. 20 ml 0,2 mol·dm^{-3} solution of oxamic acid was prepared in a round bottom flask. A simple Liebig condenser was attached to the neck of the flask (in reflux mode). The flask was immersed in an oil bath with temperature control, and the solution was heated to 90 °C. The samples (V = 2 ml) were taken with a Pasteur pipette every 30 minutes. In total, five samples were taken and labelled as sample 1'', sample 2'', sample 3'', sample 4'', sample 5''. Petri dishes with the samples were left overnight in an oven at 40 °C, and the dry residues were collected to the labelled Eppendorf tubes. The resultant powders were analyzed using roentgen diffraction. In each XRD pattern, two phases were detected and determined as ammonium oxalate monohydrate and oxamic acid in Panalytical HighScore software. An example of the refined two-phase roentgen diffraction pattern is shown in Fig. 31, Chapter 5.3. The quantitative phase analysis was conducted in Profex open-source software[117]. The determined phase ratios (mass fractions) of each sample are shown in Fig. 33 and Fig. 34, Chapter 5.4. The kinetics of the oxamic acid decomposition process was evaluated (Fig. 35, Chapter 5.4).

4.6 Lanthanide oxalates heterogeneous precipitation experiments

The lanthanide (III) oxalate decahydrates precipitation experiments were designed in accordance with the considerations written in Chapter 3.2. Cerium and gadolinium were chosen as the Ln series representatives. Both of the metals belong to the so-called lighter lanthanides group. The formation of the insoluble Ln(III) oxalate decahydrate is described by Equation 5, Chapter 3.2.
0,2 mol·dm^{-3} solutions of $Ce(NO_3)_3 \cdot 6H_2O$ and $Gd(NO_3)_3 \cdot 6H_2O$ were prepared in distilled water and stored in 50 ml volumetric flasks. 50 ml 0,2 mol·dm^{-3} $H_2C_2O_4 \cdot 2H_2O$ stock solution was prepared. The oxalic acid solution was added from a dropping funnel to a

100 ml round bottom flask with the defined amount of the metal nitrate solution. The oxalate-to-metal ratio was 2 in the first series of the tests and 3 in the second series. The mixture in the round bottom flask was constantly magnetically stirred (200 rpm). The temperature in the laboratory was 23 °C. The immediate formation of the precipitate was observed in all the cases. After the precipitation, the mixtures were let stand for several hours (the exact time is not crucial) at room temperature. The resultant mixtures were centrifugated (5000 rpm, 5 min), the products were separated from the supernatant and dried on the watch glass in the exicator over P_2O_5. Four precipitation experiments (two series with two different acid-to-metal chemical amounts ratios) were carried out in total. In all the cases, the product was a white powder-like solid. The powders achieved in the first series (with the oxalate-to-metal ratio = 2) were further characterized (Chapter 5.5).

4.7 A study of the oxamic and glyoxylic acids' affinity to lanthanides (III)

In 50 ml volumetric flasks, 0,2 $mol \cdot dm^{-3}$ stock solutions of $Ce(NO_3)_3 \cdot 6H_2O$ and $Gd(NO_3)_3 \cdot 6H_2O$, and 0,1 $mol \cdot dm^{-3}$ stock solutions of oxamic acid and glyoxylic acid were prepared. Experiments to examine the acids' affinity to lanthanides in aqueous media were planned in agreement with theoretical insights described in Chapter 3.5.
Different molar ratios metal: acid (1:1,25; 1:2; 1:2,5; 1:3) were tried for both of the acids. However, as there were no macroscopically observable differences, only the referential ratio 1:3 for both acids will be described below.
In the working procedure, 1 ml of the lanthanide (III) nitrate solution was mixed with the appropriate amount of the corresponding acid in plastic laboratory vials. The vials were screwed with caps (as no gas evolution was expected), and the mixtures were left overnight under constant magnetic stirring (300 rpm).
In the case of glyoxylic acid, the solutions remained transparent the next day. Later, upon standing, no changes were detected as well. In the case of oxamic acid, the solutions looked clear the next day. However, in several weeks the liquid in the vials appeared turbid, and some of the particles settled out of the mixtures: very fine-grained suspensions were formed. The experiments had the same course both for cerium(III) and gadolinium(III) samples. The mixtures were centrifuged (5000 rpm for 5 min). The products collected by centrifugation (fine white powder) were analyzed using powder XRD diffraction to assess the crystallinity. The diffraction pattern showed that the obtained powders were cerium(III) oxalate decahydrate and gadolinium(III) oxalate decahydrate. The supernatants were left in the vials. In several days, the solutions turned turbid, and the fine white powder precipitated again. The powders were separated by the recurring centrifugation. Their XRD analysis clearly implied the lanthanide (cerium, gadolinium) oxalate decahydrate phase.
UV-VIS spectroscopy measurements were conducted to observe and tentatively estimate the acids' species coordination on the lanthanides metal centres in the solution. The stock solutions of Ce^{3+}, Gd^{3+}, oxamic acid, and glyoxylic acid (5 ml, 0,1 $mol \cdot dm^{-3}$) were prepared in small plastic laboratory bottles. The acids' solutions were used as prepared without the dilution, as the acids do not absorb the light in the chosen wavelength range.

The metals' solutions were diluted five times up to a total volume of 25 ml for each lanthanide stock solution (resulting in concentrations of 0,02 mol·dm^{-3}) in order to get to the reasonable absorbance numbers. The absorbance spectra were measured for the 0,02 mol·dm^{-3} Ce^{3+} and 0,02 mol·dm^{-3} Gd^{3+}samples. The next samples were prepared by mixing 2 ml of the 0,02 mol·dm^{-3} Ln^{3+} solutions with 1 ml 0,1 mol·dm^{-3} glyoxylic, resp., oxamic, acids' solutions. For completeness, the absorbance spectra of 0,1 mol·dm^{-3} acids' solutions were measured at the end. The obtained spectra are shown in Fig. 46, 47, Chapter 5.6. The absorbance spectra were recorded in the wavelengths ranges 190-800 nm. However, the final graphs were worked up in the range 250-400 nm (mainly UVA and UVB bands), as only this segment contains useful information.

4.8 Homogeneous precipitation of Ce (III) oxalate decahydrates

The results of the studies described in Chapter 5.4 indicated the oxamic acid thermal instability in aqueous solutions. These results prompted the idea of conducting homogeneous precipitation experiments of trivalent lanthanides' (cerium taken as a representative) oxalate decahydrates from aqueous solutions using oxamic acid as the oxalate ion precursor.

Homogeneous precipitation can be an advantageous alternative to regular, heterogeneous precipitation. Heterogeneous precipitation is a solubility-related event when a precipitating agent is being added to a solution, the chemical precipitation reaction occurs, and a rapid formation of a solid (precipitate) from an oversaturated solution takes place. In the homogeneous precipitation procedure, on the contrary, the precipitating agent is being generated in an initially homogeneous system, in a single solution, during a prolonged period. Thus, the oversaturation remains low. Controlling the oversaturation level in this way appears to be a promising way to affect the morphology of the final precipitated crystalline particles[120].

The oversaturated solution is a solution in a metastable state, and the oversaturation value is the difference between the actual immediate concentration of a specific solute and its equilibrium concentration. The oversaturation level is conventionally denoted as ΔC. Basically, oversaturation is the determinative factor in the processes of crystal nucleation and crystal growth. The relations between the growth rate, resp. nucleation rate and the oversaturation level can be denoted by the simplified Nyvlt equations[121]:

$$G = k_g \cdot \Delta C^{\,g} \qquad [20]$$

$$B = k_b \cdot \Delta C^{\,b} \qquad [21]$$

In equations 20 and 21, G (resp. B) stands for growth rate (resp. nucleation rate); k_g (resp. k_b) is the growth constant (resp. nucleation constant), a kinetic parameter that describes the overall mass transfer and is dependent on temperature and several other variables (e.g., may be affected by the presence of the impurities)[122]. Further, g is the growth order (typically 1 to 2 depending on a crystallization system), and b is the nucleation order (often 5 to 10)[123]. Concerning the g and b typical values, it can be predicted that lowering the oversaturation level will lead to a larger crystal size distribution and probably more

compact, easily filtered crystalline precipitate formation because crystals will grow faster than the nucleation events will be happening.

Indeed, such reasoning about the oversaturation problematics is greatly simplified. The topic of oversaturation control, particle size, and shape distribution control is much more extensive and complex and lies out of the scope of the present work.

Homogeneous precipitation is an advantageous method employed in many chemical synthesis routes [124, 125], as it facilitates the product morphology control, yields highly ordered products, or reduces the product contamination in the precipitations carried out in the multi-component solutions [126].

Procedure

25 ml 0,2 mol·dm^{-3} water solution of oxamic acid (n = 0,005 mol) was prepared in a volumetric flask. 10 ml 0,2 mol·dm^{-3} $Ce(NO_3)_3 \cdot 6H_2O$ water solution (n = 0,002 mol) was prepared in another volumetric flask, the pH of this solution was adjusted to 3,0 by the concentrated HNO_3 droplets addition. The prepared solutions were mixed in the round-bottom flask placed in the heated oil bath with temperature control. A Liebig condenser was attached to the neck of the flask. The reaction mixture was constantly magnetically stirred (500 rpm).

To observe the course of the homogeneous precipitation, the residual concentration of the Ce^{3+} ions in the solution was tracked. The residual concentrations were determined gravimetrically. Due to the extremely low solubility products of the lanthanide(III) oxalates (Chapter 3.2), the oxalic precipitation method was chosen for the analytical determination of the residual Ce^{3+} concentrations.

Several precipitation trials were conducted to optimize the experimental setup. In the final variant, the solution was heated to the desired experimental temperature T_{max} (90 °C in the first experiment and 100 °C in the second; the heating took 15 minutes), then the temperature was maintained constant. At the same time intervals (every 30 min after the set experimental temperature T_{max} was reached), a 5,0 ml sample was taken from the heated solution (with an automatic pipette). The sample was centrifugated; 4,0 ml of the supernatant were carefully taken with an automatic pipette and poured into the new dry, clean, weighed in advance centrifugation test tube. The fixed amount of oxalic acid dihydrate was added to the test tube. The cerium (III) oxalate decahydrate was precipitated immediately. After a minute (left for the precipitate to get finely “coagulated”), the sample was centrifugated. This time, the supernatant was partially removed with a Pasteur pipette, and the pellet in the centrifugation test tube was left in the oven (60 ˚C) for drying. The whole procedure was repeated six times (six samples in total were taken for the gravimetry analysis). At a certain moment (120 min from the experiment start), a sample of the suspension formed in the heated round-bottom flask was taken, centrifugated, the pellet of the homogeneously precipitated $Ce_2(C_2O_4)_3 \cdot 10H_2O$ was dried in the oven (60 ˚C) and subsequently examined by scanning electron microscopy.

The final experiment scheme is depicted on the graph below (Fig. 26).

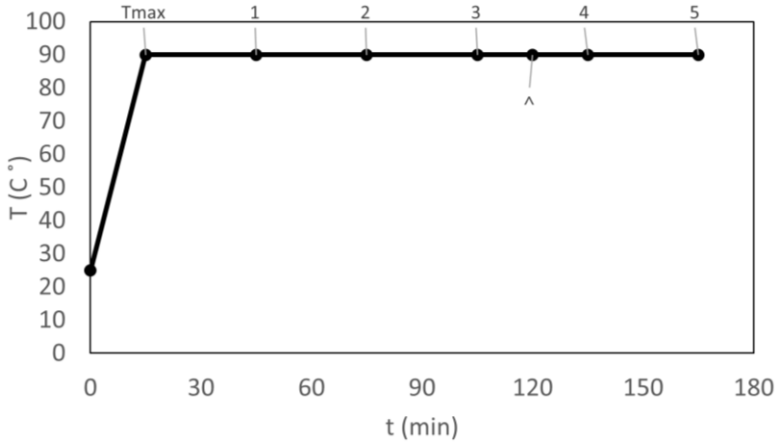

Figure 26. The homogeneous precipitation experiment scheme. The dots mark when the samples for the gravimetric analysis of the residual Ce^{3+} concentrations were taken. The black tick marks the time when the sample of the homogeneously precipitated cerium oxalate decahydrate was taken for the microscopic examination.

The masses of the precipitated cerium oxalate decahydrate from the gravimetry analysis and the corresponding residual Ce^{3+} concentrations are given in Table 3, Table 4, Chapter 5.7.
The number of significant figures is given by the accuracy of the digital laboratory scale.

Homogeneous precipitation from a diluted solution
A homogeneous precipitation experiment with lower concentrations of the reagents was conducted to study the effect of the reagents' concentration on the final morphology of the precipitated product.
200 ml 0,01 mol·dm^{-3} solution of $Ce(NO_3)_3 \cdot 6H_2O$ was prepared in a beaker. The pH of this solution was adjusted to 3,0 (HNO_3 droplets addition). The 10 % excess of oxamic acid was used in this case: 0,285 g of oxamic acid was weighed and added to the beaker. The beaker was placed on a magnetic heater with a hot plate. The solution was constantly magnetically stirred (500 rpm), the temperature was set to 100˚C. The beaker was covered with a watch glass. In 120 min from the start of the experiment, a sample of the suspension formed in the beaker was taken, centrifugated, the pellet was dried in an oven (60 ˚C), the resultant powder sample was weighed and taken for the microscopic examination. At t = 165 min, the heating was stopped, the solution was left to cool down. The precipitated $Ce_2(C_2O_4)_3 \cdot 10H_2O$ was collected by centrifugation, dried, and weighed: $m(Ce_2(C_2O_4)_3 \cdot 10H_2O)$ = 0,2164 g.
Using the rate constant calculated in Chapter 5.7 (T_{max} = 100 ˚C), the oxamic acid immediate concentration at the time moment t = 165 min may be counted: $c_{oxam} = 8{,}52 \cdot 10^{-3}$ mol·dm^{-3}. Therefore, bearing in mind the equivalence in the amount of the emerged oxalate ions and the reacted (decomposed) oxamic acid, we may end up with the value of $1 \cdot 10^{-3}$ mol for the reacted Ce^{3+}species and get to the theoretical mass of the total precipitated $Ce_2(C_2O_4)_3 \cdot 10H_2O$ of 0,3622 g. The yield of the precipitation reaction is following:
Percent yield = 0,2164 / 0,3622 ·100 % = 60 %

The relatively low percent yield may be explained by the losses that occurred during the decantation operations.
The morphology of the powders obtained in the low concentrations homogeneous precipitation experiment is shown in Fig. 53, Chapter 5.7.

Finally, the idea of homogeneous precipitation was tried out for the glyoxylic acid – Ln^{3+} aqueous solution system. The trial was based on the assumption that glyoxylic acid may be oxidized with concentrated HNO_3 under heating (Chapter 3.3). Different molar ratios of the reagents, different pH and temperature conditions were tested. However, no precipitate formation was observed. The oxidation of an aldehydic functionality is an organic reaction, which requires special reaction conditions; the attempts to conduct oxidation in an aqueous medium under the unsophisticated conditions described above were unsuccessful.

5. Results and discussion

5.1 The acids' solubility determination results

The resultant data from the oxamic acid solubility determination experiment (T = 25°C) were statistically evaluated (Table 2). The Q test did not reject any outliers from the data set. The final solubility value was determined as s_{25} = (8,50 ± 0,06) g per 100 g solvent (water),
s_r = 0,6 %.

Table 2. The data used to calculate the oxamic acid solubility in water at room temperature T = 25°C.

№ of the flask	The mass of the clean, dry flask, m_0 [g]	The mass of the analysed solution aliquot, m_a [g]	The mass of the flask with the dry evaporation residue, m_r [g]	The mass of the residue, m_x [g]	The oxamic acid solubility, s_{25} [g per 100 g water]
1	17,4106	2,0350	17,5710	0,1605	8,562
2	25,3030	2,2549	25,4799	0,1769	8,511
3	27,2063	2,5916	27,4089	0,2026	8,480
4	17,1345	2,0588	17,2949	0,1604	8,449
5	14,6601	2,0553	14,8211	0,1610	8,499

The following simple relations were used to count the solubility values:

$$m_r - m_0 = m_x \quad [22]$$

$$s_{25} = \frac{m_x \cdot 100}{m_a - m_x} \quad [23]$$

The meaning of the symbols used in equations 22, 23 is explained in the Table 2 legend.
A powder sample of the evaporation residues from the solubility determination experiment (T = 25°C, oxamic acid) was analyzed with powder XRD diffraction. The diffraction pattern clearly showed one phase identical to that from the diffraction analysis of the pure oxamic acid sample as supplied commercially (Chapter 5.3). Thus, the determined solubility value for T = 25°C was considered valid.
Similar solubility determination experiments were conducted for the elevated temperatures (T = 40°C, T = 60°C, using oil bath heating). However, the XRD patterns of the resultant powders distinctly demonstrated that the solid evaporation residues no longer represented a chemically pure substance. The tentative search and match analysis conducted in Profex [117], and QualX[127] software revealed the presence of more than one phase; several peaks corresponded to the oxammite (ammonium oxalate) reference pattern. The acquired XRD data are not attached as the patterns obtained do not have a satisfying quality: they have a low peak-to-noise ratio and poor reproducibility. Therefore, the determined solubility

values for all the cases except the one described in the previous paragraph were considered invalid and will not be mentioned here.
Within the same experimental setup, an attempt to determine the room temperature solubility was conducted for glyoxylic acid. However, the acid turned out to form gel during the water evaporation using the rotary evaporator. This phenomenon is not surprising as glyoxylic acid is a highly hydrophilic substance [68, 128]. The oligomerization of glyoxylic acid-related compounds (e.g., glyoxal)[129] in aqueous solutions is well-known in the context of environmental chemistry. As for glyoxylic acid itself, its polymerization in aqueous media is also described [75]. In the preparation methods of polyalkylglyoxylates (see Chapter 3.3), unmodified glyoxylate hydrate presence in the reaction mixtures leads to lower molecular weight product formation as glyoxylate tends to enhance the initiation and transfer reactions [74]. The glyoxylate oligomers are also being formed in the process; therefore, to prepare a decent polyalkylglyoxylate, high temperatures are employed to crack the glyoxylate oligomers, and the drying agents are used to remove any liberated water [74].

To summarize, the gelation phenomenon showed by glyoxylic acid concentrated aqueous solutions has a theoretical explanation and empirical background in the literature.

5.2 The pKa values of the studied acids

The pKa values were determined from the experimental data (Fig. 27, 28).
pKa (glyoxylic acid) = 3,18
pKa (oxamic acid) = 3,33
For comparison, pKa_1(oxalic acid) = 1,25; pKa_2(oxalic acid) = 4,14 [130].

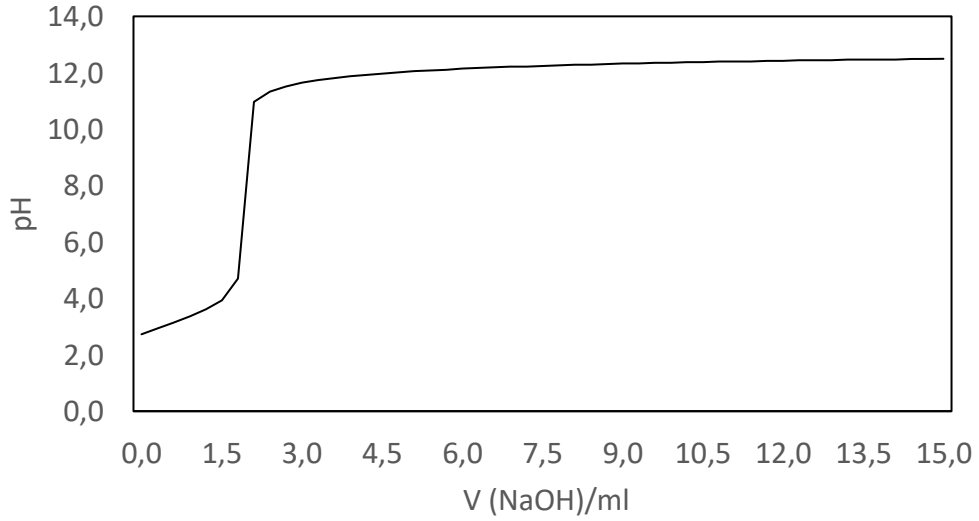

Figure 27. Oxamic acid titration curve

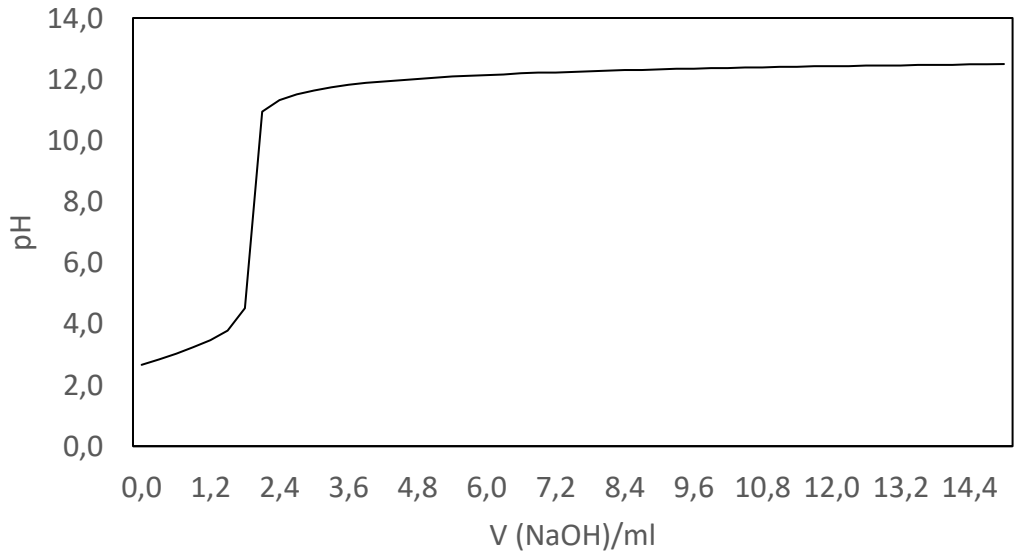

Figure 28. Glyoxylic acid titration curve

5.3 Oxamic acid decomposition - PXRD analysis of the artifacts

In Fig. 29, Fig. 30, and Fig. 31, the refined diffraction patterns of oxamic acid, ammonium oxalate monohydrate, and partially decomposed oxamic acid are shown. The graphs were constructed in OriginLab software. The LeBail method was employed, the following refinements were conducted in Jana2006[118] software. In the refinement process, the calculated profile is fitted to the experimental data by minimizing the differences between the observed and theoretical patterns using a non-linear least square approach [118]. The lattice parameters are: a = 9,4979 Å, b = 5,4379 Å, c = 6,8673 Å, ß = 107,150° for oxamic acid (monoclinic crystal system, space group Cc №9); a = 8,017 Å, b = 10,309 Å, c = 3,735 Å, α = ß = γ = 90° for ammonium oxalate monohydrate (orthorhombic crystal system, space group $P2_12_12$ №18).

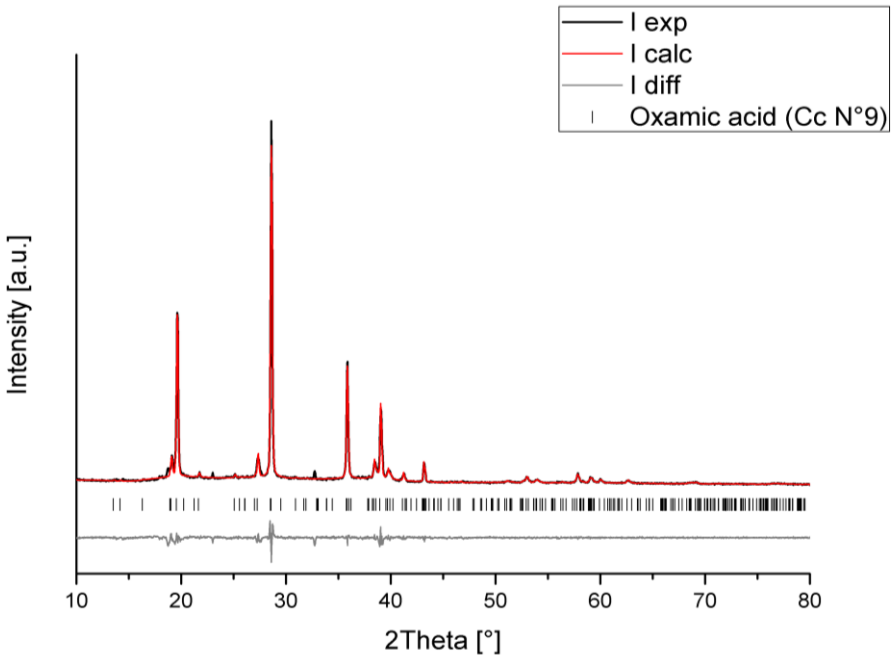

Figure 29. The refined powder roentgen diffraction pattern of oxamic acid. The quality of the fit may be judged by the following values: Rwp = 9,38; GOF = 1,66.

The reflections at 23 and 33 2θ degrees arose from some impurities in the sample. Concerning the positions and the intensities, these peaks cannot be labelled as peaks coming from the minor amounts of ammonium oxalate monohydrate presence.

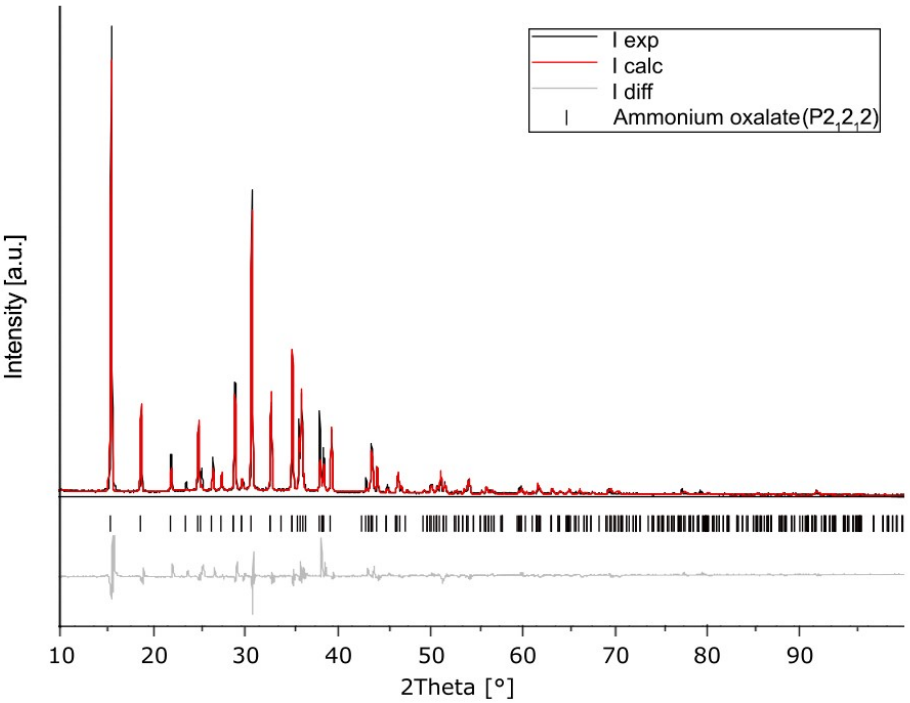

Figure 30. The refined powder roentgen diffraction pattern of ammonium oxalate monohydrate. The quality of the fit may be judged by the following values: Rwp = 18,60; GOF = 3,15.

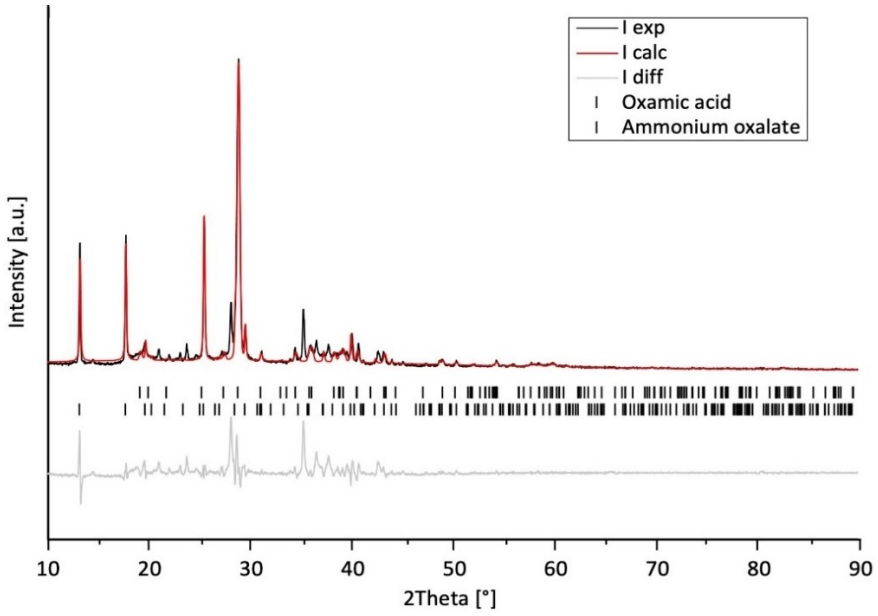

Figure 31. The refined powder roentgen diffraction pattern of a two-phase sample representing a partially decomposed oxamic acid. The quality of the fit may be judged by the following values: Rwp = 23,16, GOF = 4,27.

The relatively high Rwp value implies the somewhat lower preciseness of the fit. This may be explained by the fact that the theoretical profile is calculated from the atomic positions in the ideal structure, and the experimental profile represents the real structure of the two-phase sample, which differs from the ideal model.

5.4 Oxamic acid stability in aqueous solutions – evaluation

To evaluate the results of the experiments undertaken in Chapter 4.5, micro-Raman spectroscopy measurements were conducted (Fig. 32).

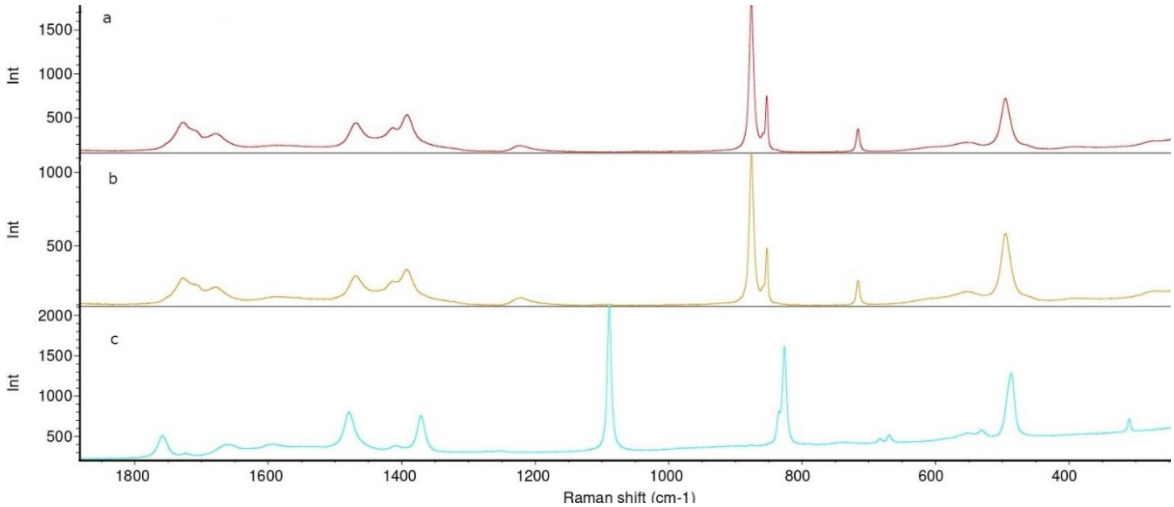

Figure 32. Raman spectra of the ammonium oxalate monohydrate referential sample (a), of the samples 3' and 4' from the study of the temperature effect on oxamic acid decomposition (b), of oxamic acid as suppled commercially (c).

From Fig. 32, it is seen that samples 3' and 4' represent totally decomposed oxamic acid. The analyzed compounds are polar and turned out to be relatively strong scatterers, and the micro-Raman signals were weak. The shorter laser illumination wavelength resulted in a substantial fluorescence interference, large background, and low sensitivity. Therefore, only the low wavenumber "fingerprint" region was used for the analytes' identification. The recorded spectra were compared with the published data on the natural oxalates' Raman spectroscopy[131]. However, the accurate vibrations assignment was not conducted as the Raman measurements turned out to be inapplicable for the kinetics study of the oxamic acid decomposition.

Further, the oxamic acid decomposition kinetics (Fig. 33, 34) were evaluated utilizing quantitative XRD analysis. The experimental setup and sample numbering are described in detail in Chapter 4.5.

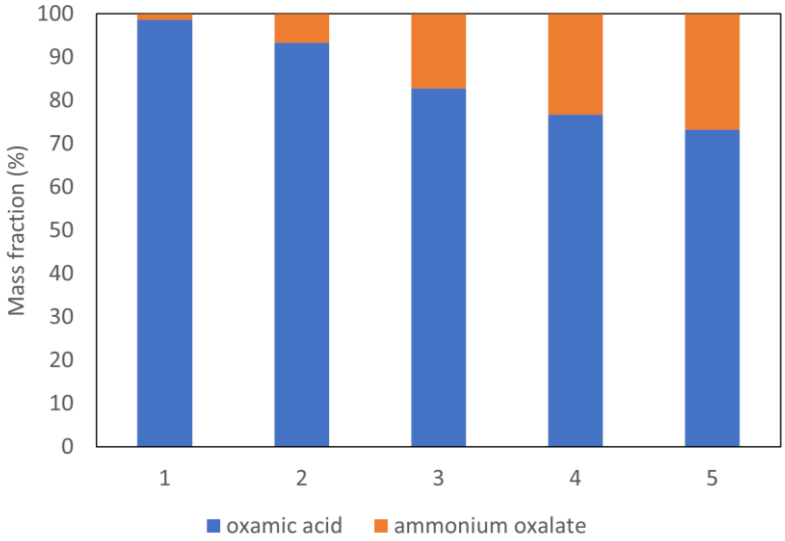

Figure 33. The mass fractions of the phases in the oxamic acid decomposition experiment (T = 90 ˚C) – bar graph representation; the numbers on the horizontal axis stand for the number of the sample (1'', 2'', 3'', 4'' and 5'' – respectively, 30, 60, 90, 120 and 150 min).

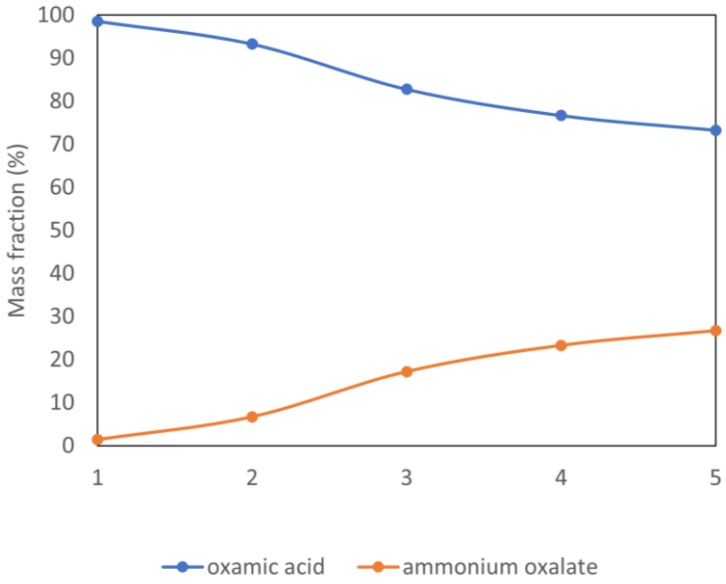

Figure 34. The mass fraction of the phases in the oxamic acid decomposition experiment (T = 90 ˚C) – line graph representation; the numbers on the horizontal axis stand for the number of the sample (1'', 2'', 3'', 4'' and 5'' - respectively, 30, 60, 90, 120 and 150 min).

The mass fraction values were converted to the concentrations, and the trend (Fig. 35) counted from the experimental data was fitted using a non-linear regression model.

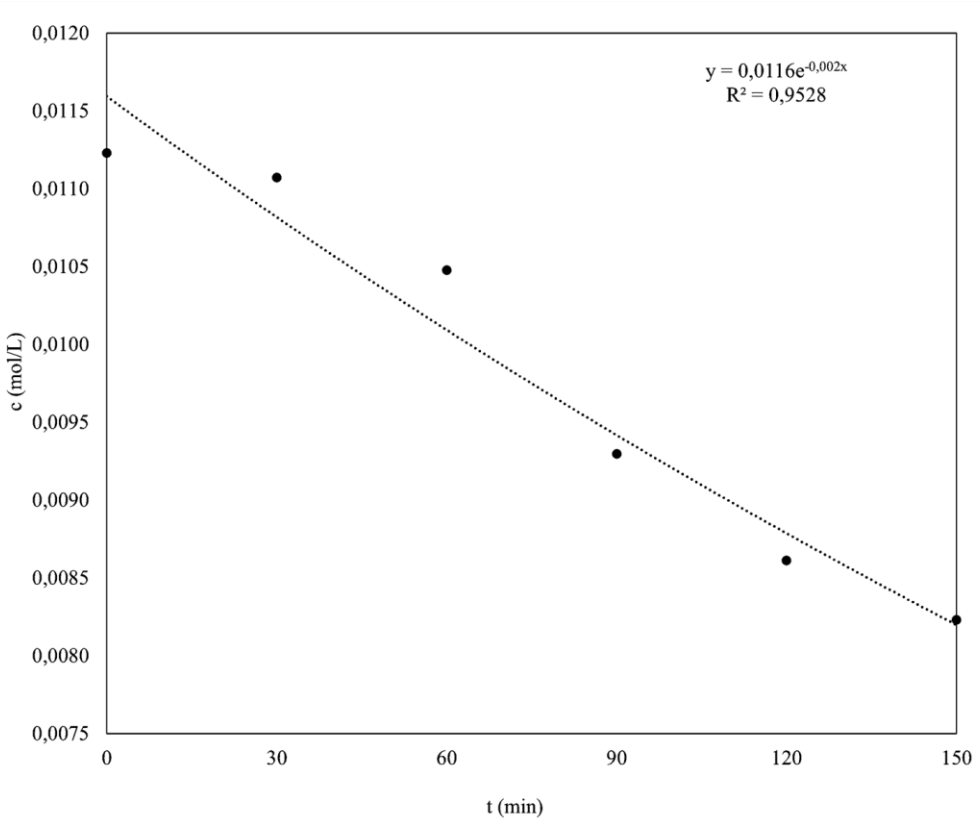

Figure 35. Concentration – Time relationship for oxamic acid in its thermal decomposition experiment, T = 90 ˚C.

The exponential model fitted best to the obtained series of data points, offering the first-order kinetics for the oxamic acid thermal decomposition process. The line of the best-fit equation and the determination coefficient are introduced on the graph. To confirm that the reaction is governed by first-order kinetics, ln(c_{oxam}) values were plotted versus time, and a good linear regression fit was obtained, proving the first-order kinetics of the oxamic acid thermal decomposition reaction. The integrated rate law for the first-order kinetics is given below:

$$c_{oxam} = c_{oxam,o} \cdot e^{-kt} \quad [24]$$

In equation 24, c_{oxam} is the immediate concentration of oxamic acid, $c_{oxam,o}$ is its initial concentration, t represents time, and k is the rate constant.

The rate constant for the oxamic acid decomposition was determined (T = 90˚C):

$k = 2 \cdot 10^{-3}\ min^{-1}$.

5.5 Heterogeneously synthesized lanthanide oxalates characterization

The precipitated lanthanide oxalate compounds (white, fine powder solids), $Ce_2(C_2O_4)_3 \cdot 10H_2O$ and $Gd_2(C_2O_4)_3 \cdot 10H_2O$, were characterized using several methods as described below.

The Ln(III) oxalates decahydrates crystal structure is described in detail in the theoretical part of the work (Chapter 3.2). $Ce_2(C_2O_4)_3 \cdot 10H_2O$ and $Gd_2(C_2O_4)_3 \cdot 10H_2O$ are isomorphous; therefore, the accurate structure of Ce(III) oxalate decahydrate only will be taken into account below. The lattice parameters of the compound are following[132]: space group No.14 ($P2_1/c$; belongs to the monoclinic crystal system), a = 11,3470 Å, b = 9,6300 Å, c = 10,3920 Å, β = 114,52°. The crystal structure of the synthesized $Ce_2(C_2O_4)_3 \cdot 10H_2O$ was drawn in VESTA software (using the crystallography information file taken from COD database [132]); the crystal structure is shown in Fig. 36 and Fig.37.

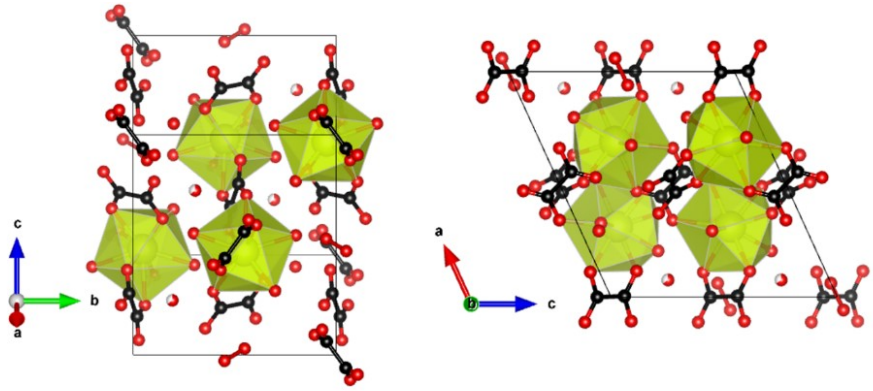

Figure 36. The unit cell of cerium (III) oxalate decahydrate crystal is shown from different perspectives. The light green polyhedra represent the coordination environments of the central cerium atoms (the oxygen coordination polyhedra – distorted tricapped trigonal prisms); carbon atoms are drawn in black, oxygen atoms are drawn in red.

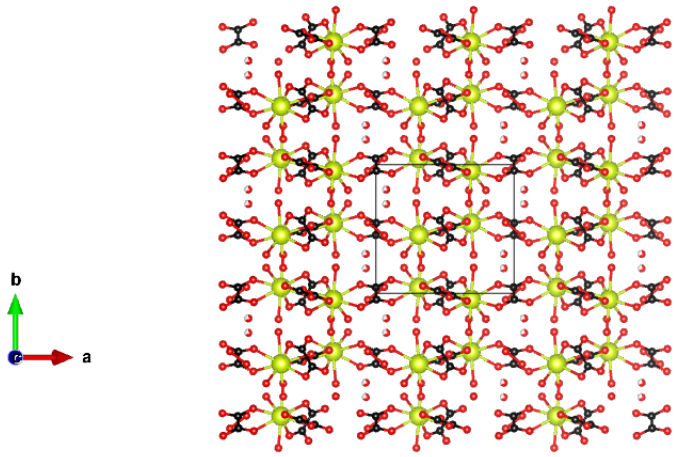

Figure 37. The stacking of the layers along the b-axis in the cerium (III) oxalate decahydrate crystal structure.

The powder X-ray diffraction patterns of the obtained compounds, $Ce_2(C_2O_4)_3 \cdot 10H_2O$ and $Gd_2(C_2O_4)_3 \cdot 10H_2O$, were recorded. The obtained patterns of the synthesized single phases agreed with the XRD patterns of the corresponding oxalates from the database (assessed in the Search-Match Software, Panalytical Xpert Pro). After the identification (assigning all the peaks at the correct positions), the samples' pattern refinement (LeBail fit) was conducted in Jana2006 (Fig. 38, Fig. 39). The graphs were constructed in OriginLab software. The lattice parameters of cerium (III) oxalate decahydrate (Fig. 38) are given

above in the text. The lattice parameters of gadolinium (III) oxalate decahydrate (Fig. 38) are following: a = 8.3803 Å, b = 9.7540 Å, c = 9.4389 Å, ß= 90.23° [132].

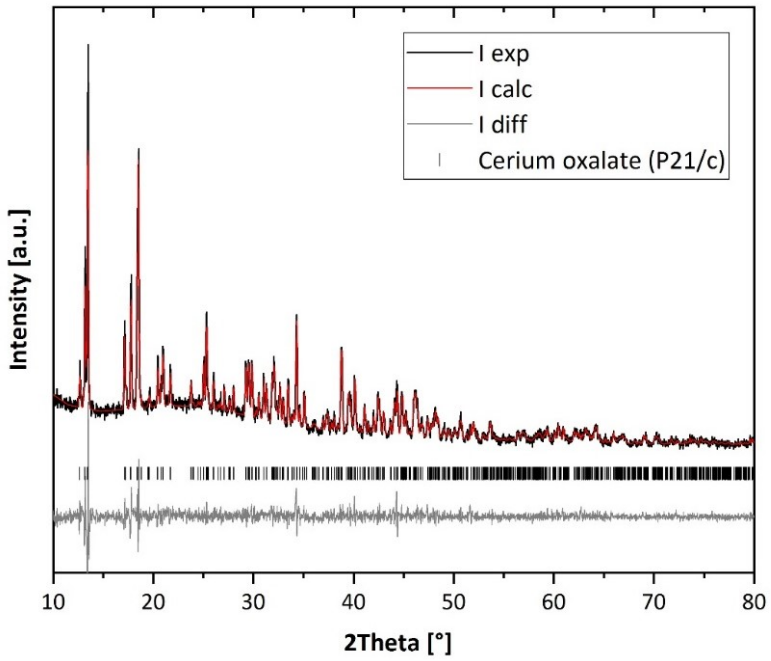

Figure 38. The refined XRD pattern of the sample of $Ce_2(C_2O_4)_3 \cdot 10H_2O$. The quality of the fit may be judged by the following values: Rwp = 8,56; GOF = 1,45.

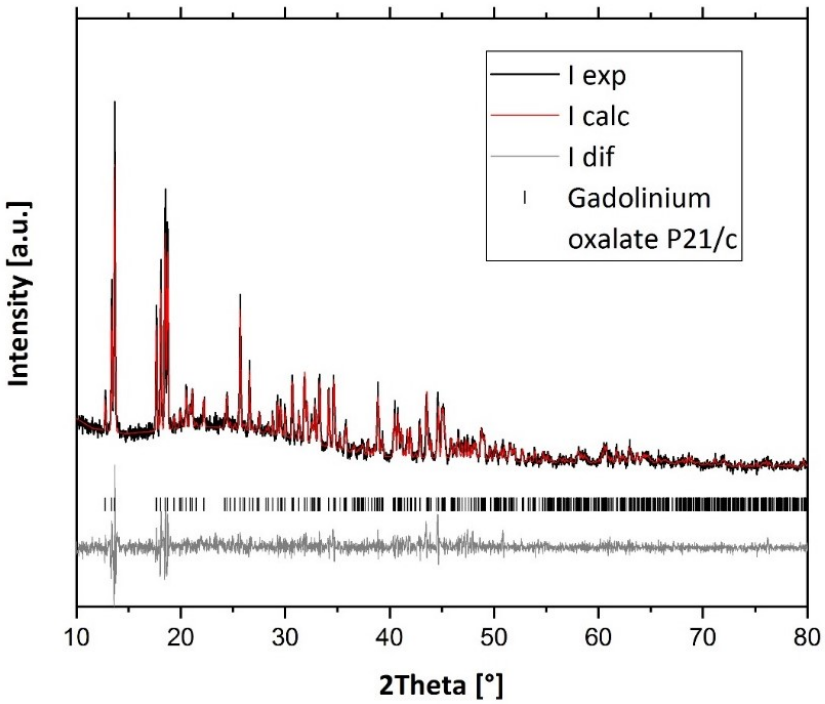

Figure 39. The refined XRD pattern of the sample of $Gd_2(C_2O_4)_3 \cdot 10H_2O$. The quality of the fit may be judged by the following values: Rwp = 9,01; GOF = 1,80.

The Rwp and GOF values imply that the quality of the fits in Fig. 38, Fig. 39 is high: the measured profiles are in good agreement with the calculated ones.

The morphology of the oxalate powders was studied with scanning electron microscopy (SEM). Fig. 40, 41 are showing the obtained microscope images.

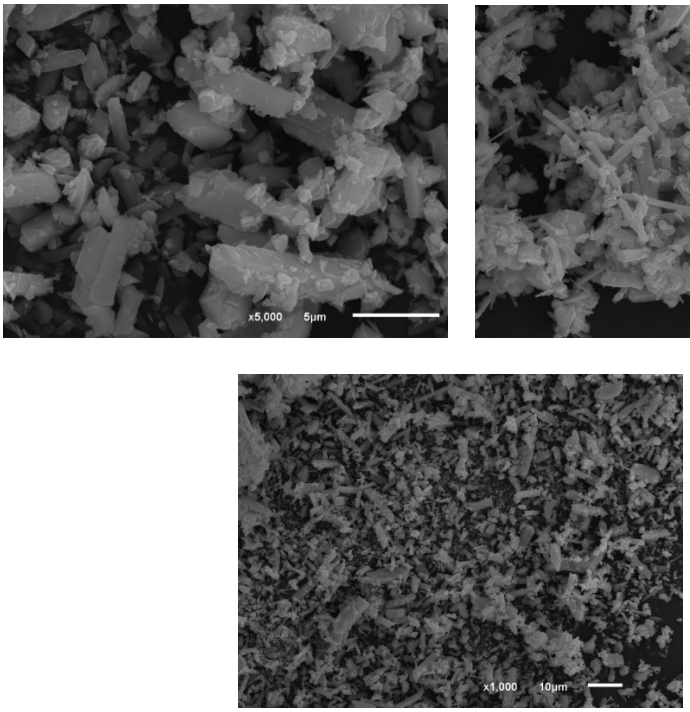

Figure 40. The SEM micrographs showing the morphology of the particles; $Ce_2(C_2O_4)_3 \cdot 10H_2O$

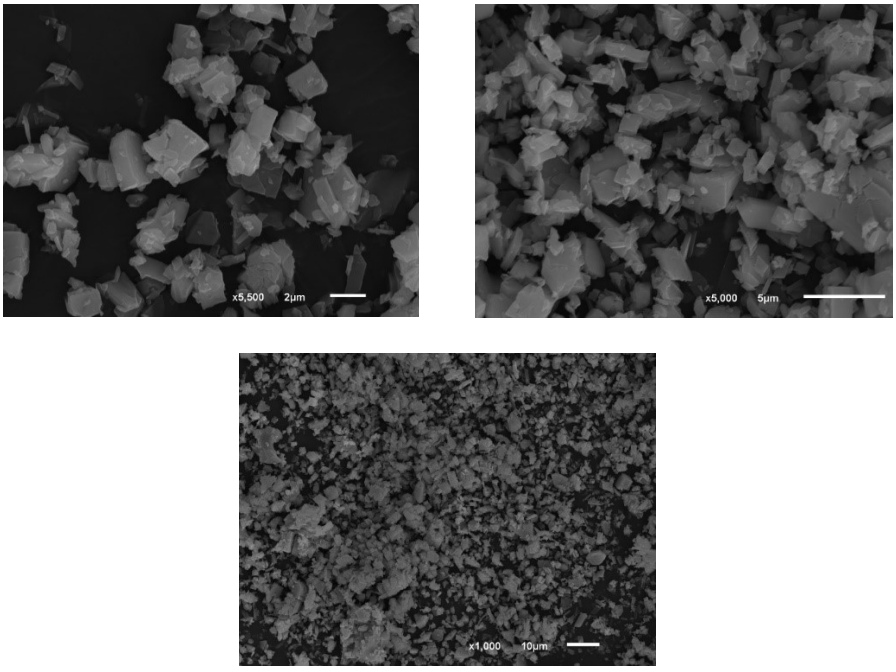

Figure 41. The SEM micrographs showing the morphology of the particles; $Gd_2(C_2O_4)_3 \cdot 10H_2O$

In Fig. 40, 41, the morphology of the particles obtained under the chosen precipitation conditions (described in Chapter 4.6) is shown. It can be observed that the precipitated

anisotropic crystallites are relatively small and randomly oriented. The micrographs of $Ce_2(C_2O_4)_3 \cdot 10H_2O$ show that the obtained precipitates are microcrystalline and frequently cocrystals. The variation of the particles' size in the individual samples (as judged by the eye) may be due to the inhomogeneous oversaturation in the solution. At the sites with lower oversaturation levels, the nucleation rate is naturally slower than the growth rate resulting in larger crystal formation. In both cases, crystals display no preferred orientation, and their shape is also varied: thin flakes, needle-like structures, and thick and solid crystals.
Below, the energy dispersive X-ray microanalysis (EDS) spectra are additionally attached (Fig. 42, 43).

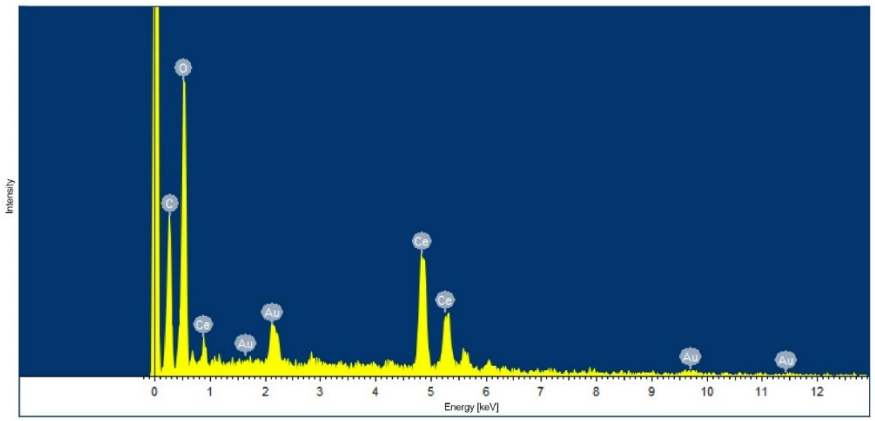

Figure 42. The EDS spectrum of the cerium (III) oxalate decahydrate sample.

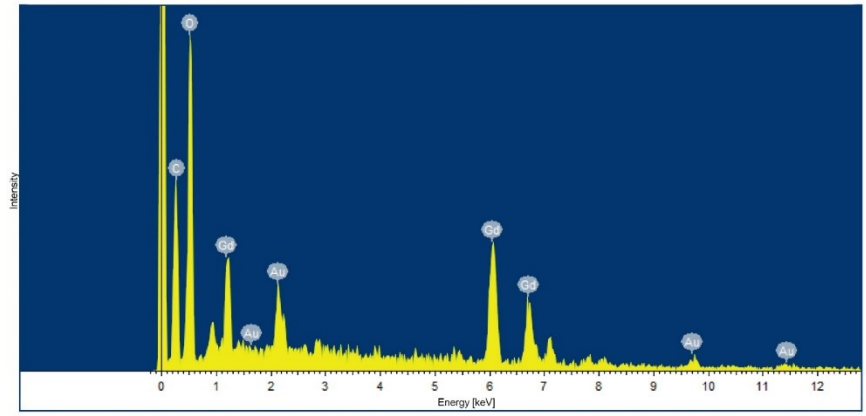

Figure 43. The EDS spectrum of the gadolinium (III) oxalate decahydrate sample.

The energy dispersive X-ray analysis was used for qualitative chemical characterization (elemental analysis) of the samples. It is a technique conventionally associated with electron microscopy. The obtained EDS spectra confirmed the presence of the elements as anticipated according to the chemical formula of the synthesized compounds. However, only high atomic mass elements may be reliably determined by this method (EDS is not suitable for detecting the low atomic number elements). The peaks were assigned automatically. The presence of Au in the samples is due to the sample coating (Au layer)[133].

The synthesized lanthanide (III) oxalate decahydrates were also characterized employing thermogravimetry. A dynamic temperature program in range 25 – 800 ˚C at a heating rate of 3˚C/min under streaming air (20 mL min^{-1}) was executed. At 40˚C, a 20 min isotherm delay was made to dry any absorbed moisture. Fig. 44, Fig. 45 show the TG and DTA curves obtained for cerium (III) and gadolinium (III) oxalate decahydrates.

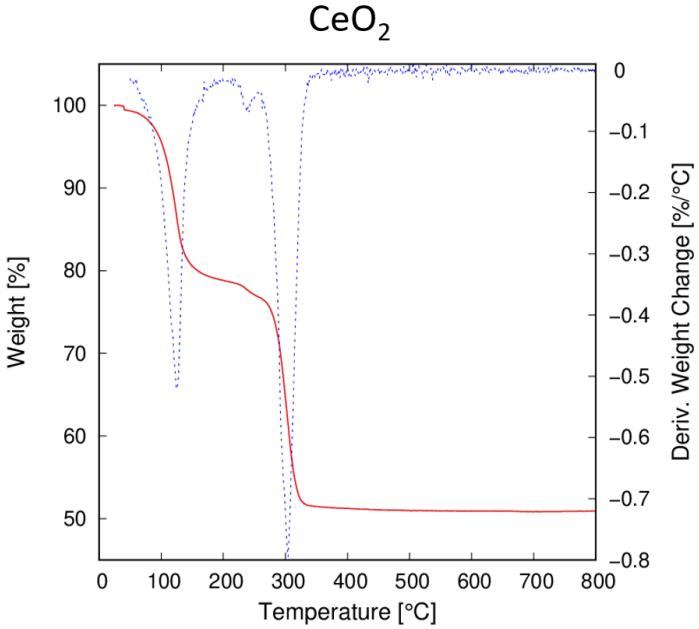

Figure 44. Thermal decomposition of $Ce_2(C_2O_4)_3 \cdot 10H_2O$ – TG (red), DTA (blue dotted) curves.

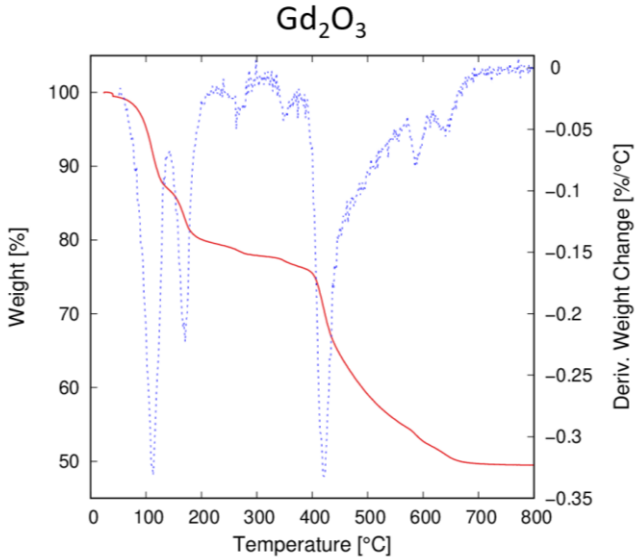

Figure 45. Thermal decomposition of $Gd_2(C_2O_4)_3 \cdot 10H_2O$ – TG (red), DTA (blue dotted) curves.

The TG curves show the mass of a substance as a function of temperature; they provide information about the thermal stability, enable the intermediate products and solid residue composition identification. The DTA curves, the first derivatives of the TG curves, show the rate of change of masses.

The analyzed samples are hydrates; therefore, the water molecules loss was anticipated in the first step. Overall, the courses of the TG curves of both analyzed compounds are, to a certain extent, similar. Based on the current investigation results and the literature[54], it is possible to say that the thermal decomposition of cerium (III) and gadolinium (III) oxalate decahydrates follow a somewhat resembling mechanism.

The $Ce_2(C_2O_4)_3 \cdot 10H_2O$ TG curve has a smooth course: two clear, distinct steps can be seen. The first step (inflection point around 125 ˚C) corresponds to the dehydration, the second (inflection point around 300 ˚C) represents the one-step decomposition to the residue ($Ce_2(C_2O_4)_3 \rightarrow 2CeO_2$). The mass variations are -20,499 % for the first step, -25,392 % for the second. The first step mass variation corresponds to the loss of 8 water molecules. From the second step mass variation, it can be counted that the anhydrous intermediate decomposes forming CeO_2 species.

The $Gd_2(C_2O_4)_3 \cdot 10H_2O$ TG curve shape indicates that water loss, in this case, occurs in two steps (inflection points around 110 ˚C and 170 ˚C). The third step (centred around 450 ˚C) demonstrates a rather uneven course, which may be evidence of a multi-step decomposition process. The anhydrous lanthanide(III) oxalate intermediate may be decomposing through lanthanide(III) carbonate and lanthanide(III) carbonate-oxide formation [54]. However, these details cannot be assessed within the collected data as no complimentary analysis (such as evolved gas analysis) was conducted. The mass variations for the three steps are -12,705 %, -7,406 % (corresponding to the losses of 5 H_2O, 3 H_2O subsequently), and -26,934 %, which indicates the formation of Gd_2O_3 as a final product.

5.6 The oxamic and glyoxylic acids' affinity to lanthanides evaluation

Oxamic acid and glyoxylic acid do not form precipitates with Gd^{3+}, Ce^{3+} in aqueous solutions. Oxamic acid slowly decomposes in aqueous solutions, and Ln^{3+} oxalate decahydrates may be precipitated.

UV-VIS spectra recorded in order to gain a better insight of the processes taking place in the mixed solutions are shown below in Fig. 46, Fig. 47.

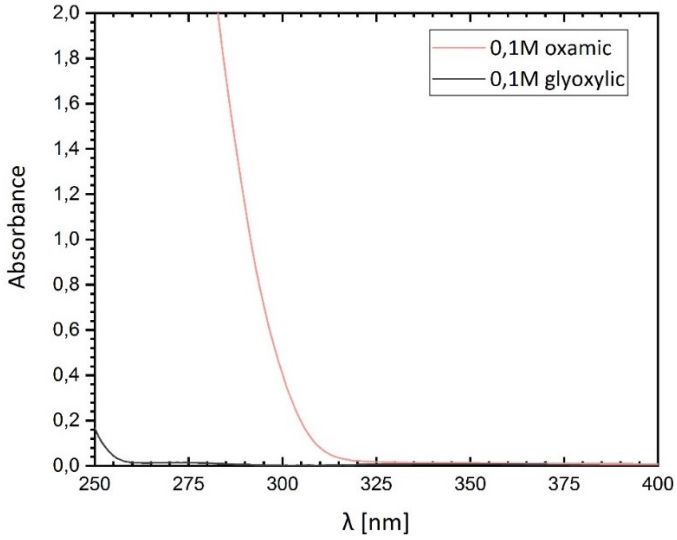

Figure 46. The absorbance spectra of the oxamic and glyoxylic acids' solutions.

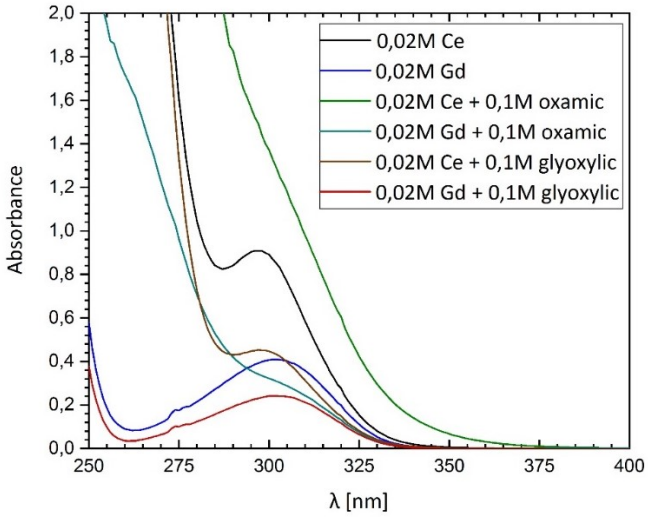

Figure 47. The absorbance spectra of the lanthanide cations' solutions and the mixed samples.

The graph in Fig. 46 shows that oxamic acid and glyoxylic acid samples are spectroscopically silent in the given wavelength range. Fig. 47 shows the absorbance curves of the Ln^{3+} ions in comparison with the absorbance curves of the Ln^{3+}- acids mixture samples. It is seen that the absorption curves have the same course in the following pairs: 0,02 M Ce – 0,02 M Gd; 0,02 M Ce + 0,1 M oxamic acid – 0,02 M Gd + 0,1 M oxamic acid; 0,02 M Ce + 0,1 M glyoxylic acid – 0,02 M Gd + 0,1 M glyoxylic acid. This fact indicates the apparent similarity between the individual lanthanides (cerium and gadolinium) behaviour.

Glyoxylic acid does not affect the shape of the metals' absorbance curves. There is only a decrease in the absorbance seen, as the addition of the glyoxylic acid sample to the metals' solutions increases the volume of the systems decreasing the metal ions concentrations.

The shape changes in the absorption spectra of the samples of the pure (uncoordinated) metal ions due to the oxamic acid addition imply that the coordination of oxamic acid on the metal centres takes place in the solution. The spectra reveal that this type of interaction

occurs in the solution, even if it is generally known that the spectra of the lanthanide species are almost environment independent, as the ligand field effects are mostly negligible for the Ln 4f electrons (4f subshell is extensively shielded by the 5s and 5p orbitals, Chapter 3.1.1).

5.7 Homogeneous precipitation of Ce (III) oxalate decahydrates results

Data from the gravimetry analysis are shown in Table 3 and Table 4. The Tables 3 and 4 were processed into the graph shown in Fig. 48.

Table 3. The data from the gravimetry analysis of the residual Ce^{3+} concentrations; T_{max} = 90 ˚C

Number of the sample	1	2	3	4	5	6
$m(Ce_2(C_2O_4)_3 \cdot 10H_2O)$, g	0,0823	0,0591	0,0499	0,0369	0,0284	0,0093
$c(Ce_2(C_2O_4)_3 \cdot 10H_2O)$, mol/L	0,0568	0,0408	0,0344	0,0255	0,0196	0,0064

Table 4. The data from the gravimetry analysis of the residual Ce^{3+} concentrations; T_{max} = 100 ˚C

Number of the sample	1	2	3	4	5	6
$m(Ce_2(C_2O_4)_3 \cdot 10H_2O)$, g	0,0823	0,0452	0,0289	0,0065	0,0026	0,0021
$c(Ce_2(C_2O_4)_3 \cdot 10H_2O)$, mol/L	0,0568	0,0312	0,0199	0,0045	0,0018	0,0014

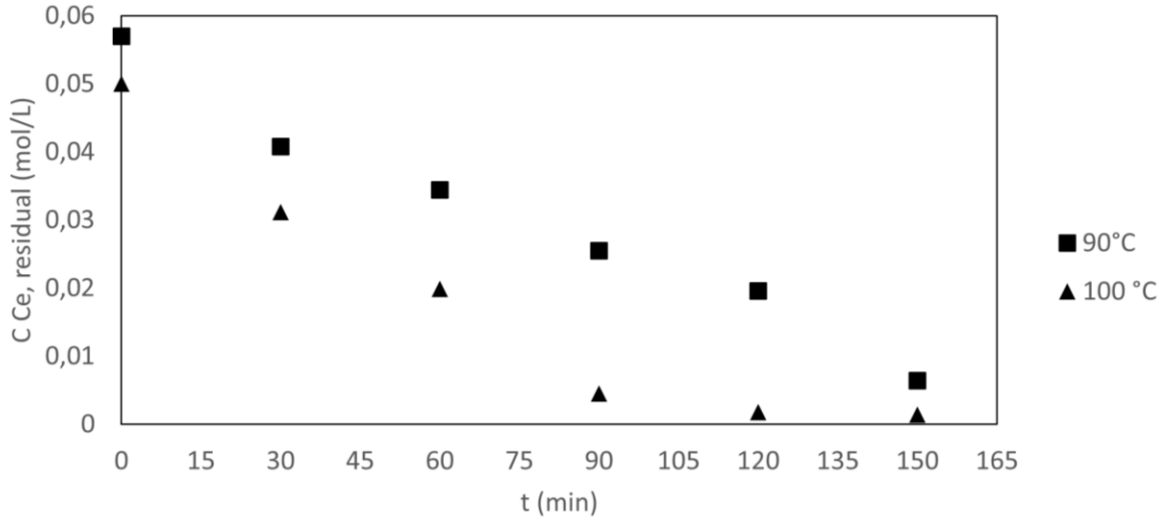

Figure 48. The residual concentrations of Ce^{3+} as a function of time in the homogeneous $Ce_2(C_2O_4)_3 \cdot 10H_2O$ precipitation experiments.

As seen from Fig. 48, the overall rate of the homogeneous precipitation is higher in the second line (depicted with triangles, T_{max} = 100 ˚C), the residual $c_{Ce^{3+}}$ goes down faster. With the increased temperature, the oxamic acid decomposition reaction rate is increased.
The precipitation reaction between Ce^{3+} ions and the newly emerged $C_2O_4^{2-}$ ions is rapid and irreversible. In the whole process, the oxamic acid decomposition is the slowest event and the rate-determining step. In the chosen concentration range (while the precipitation does not completely deplete cerium), the decrease in the concentration of the free Ce^{3+} ions in the solution directly corresponds to the amount of the decomposed oxamic acid. Therefore, from the acquired data, it is possible to estimate the oxamic acid decomposition kinetics tentatively. An approximate trend for the decomposition reaction order estimation may be constructed within the present data. (In Chapter 5.4, the oxamic acid thermal decomposition kinetics is more reliably determined using XRD quantitative analysis). Ideal mixing of the solution and the immediate reaction between Ce^{3+} and oxalate ions must be assumed. The precipitation gravimetry is an analytical technique with limited accuracy, and the multi-step format of the experiment may also be a source of imprecision. The relation between the Ce^{3+} and oxamic acid, resp. oxalate ions, immediate concentrations are given below:
$c_{Ce^{3+}} = c_{Ce^{3+},0} - 0{,}667 \cdot (c_{oxam,0} - c_{oxam})$ – for the stoichiometric ratio Ce^{3+} : oxalate^{2-} = 2 : 3 (Equation 5 , Chapter 3.2)

$$c_{oxam} = \frac{c_{Ce^{3+}} - c_{Ce^{3+},0} + 0{,}667 \cdot c_{oxam,0}}{0{,}667} \qquad [25]$$

$c_{Ce^{3+}}$ and c_{oxam} are the immediate concentrations of Ce^{3+}, oxamic acid; $c_{Ce^{3+},0}$ and $c_{oxam,0}$ are their initial concentrations.
In Fig. 49, Fig. 50, the plots of immediate oxamic acid concentration (counted as described above, Equation 25) versus time are shown. The graphs are constructed for the temperatures T_{max} = 90 ˚C and T_{max} = 100 ˚C correspondingly.

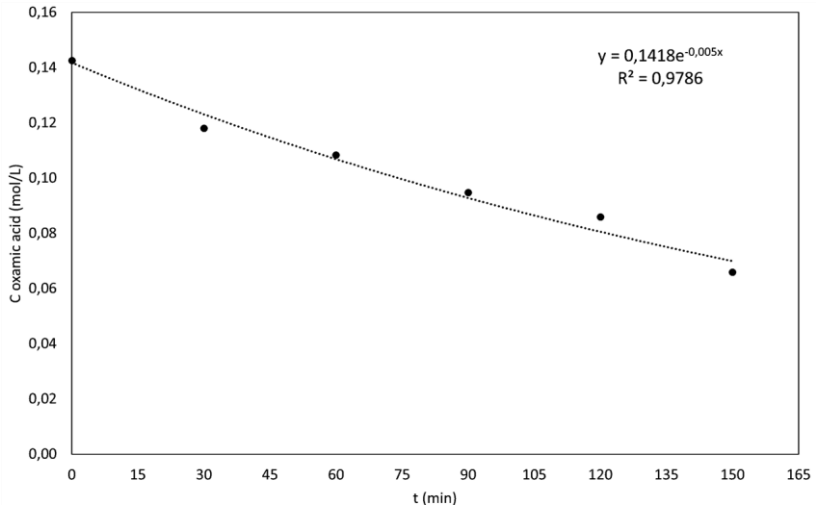

Figure 49. Concentration – time relationship for oxamic acid in homogeneous precipitation experiment, T_{max} = 90 ˚C.

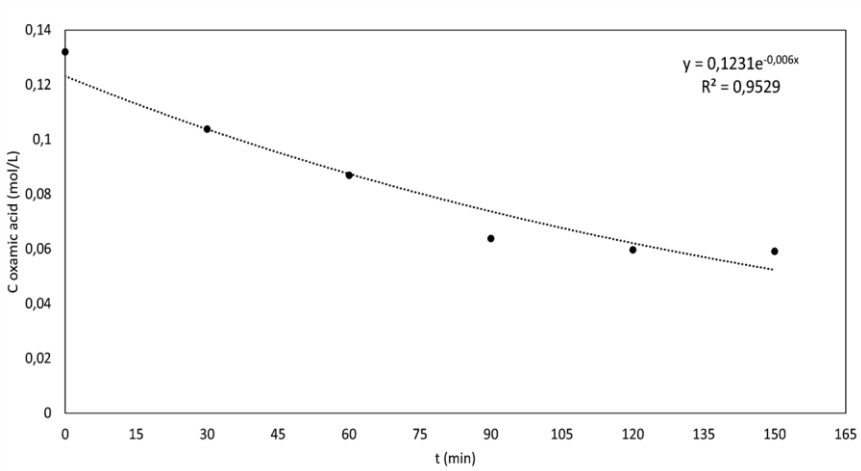

Figure 50. Concentration – time relationship for oxamic acid in homogeneous precipitation experiment, T_{max} = 100 ˚C.

The trends counted from the experimental data were fitted using a non-linear regression model. The first-order kinetics perfectly fits the obtained series of data, which is in good agreement with the results introduced in Chapter 5.4. The values of $\ln(c_{oxam})$, $1/c_{oxam}$, $1/(c_{oxam})^2$ were plotted versus time to exclude the possibility that the other order kinetics governs the reaction. The best linear fits were attained for the $\ln(c_{oxam})$ versus t plots in line with expectations. The rate constants were determined:

$k_1 = 5 \cdot 10^{-3}$ min^{-1} for T = 90 ˚C

$k_2 = 6 \cdot 10^{-3}$ min^{-1} for T = 100 ˚C

The value of k_1 and the rate constant k determined from the quantitative XRD data (pure oxamic acid thermal decomposition experiment, Chapter 5.4) are of the same order of magnitude, but $k_1 > k$. Thus, oxamic acid decomposition runs faster in the presence of Ce^{3+}cations and with HNO_3 added to the system.

The morphology of the oxalate powders obtained in the homogeneous precipitation experiments was studied with scanning electron microscopy. Fig. 51, Fig. 52 are showing the acquired microscope images.

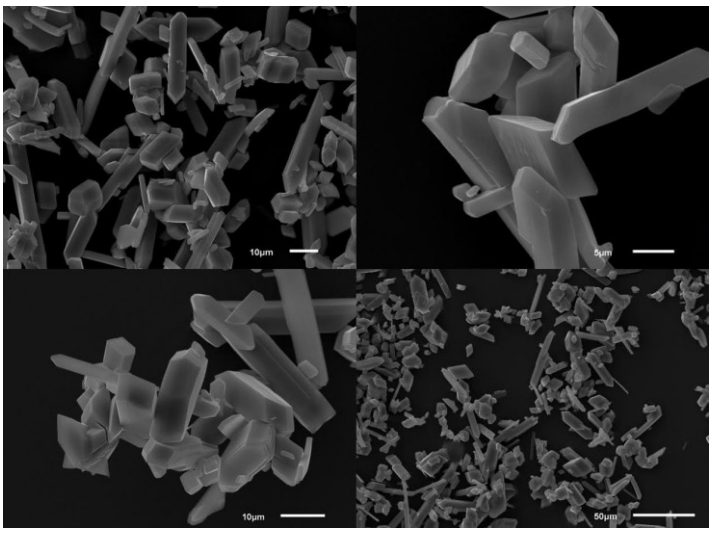

Figure 51. The SEM micrographs showing the morphology of $Ce_2(C_2O_4)_3 \cdot 10H_2O$, homogeneous precipitation, T_{max} = 90 ˚C.

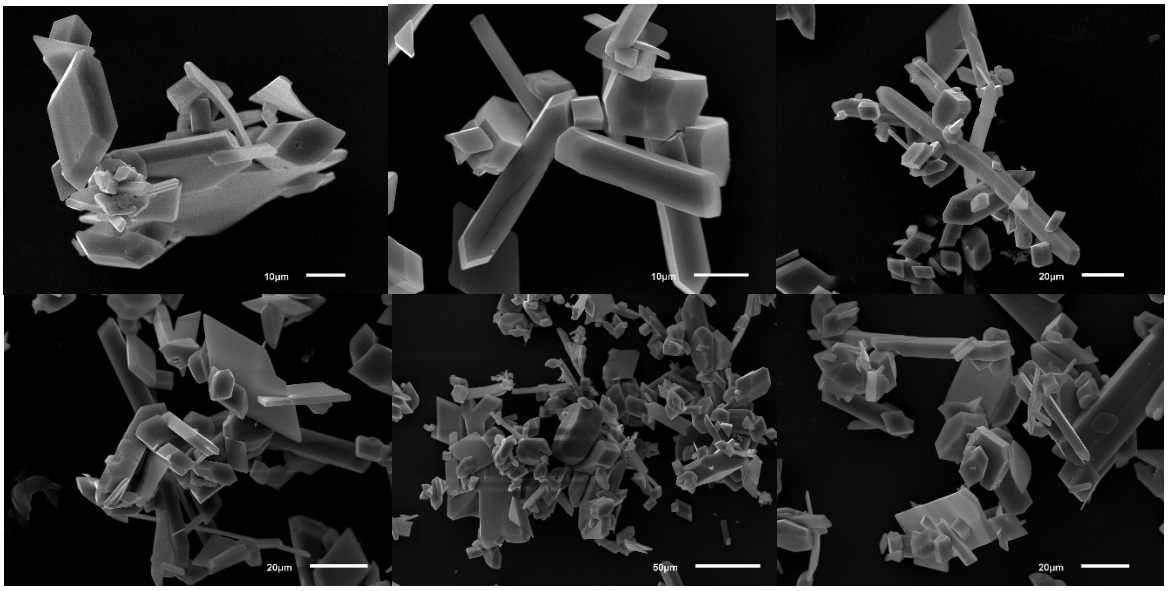

Figure 52. The SEM micrographs showing the morphology of $Ce_2(C_2O_4)_3 \cdot 10H_2O$, homogeneous precipitation, T_{max} = 90 ˚C.

The morphology of the homogeneously precipitated powders may be compared with the heterogeneously precipitated $Ln_2(C_2O_4)_3 \cdot 10H_2O$ powders in Fig. 45, Fig. 46, Chapter 5.5. A prominent difference may be noticed. Significantly larger, well-defined crystals were formed in the case of the homogeneous precipitation, which aligns with the considerations stated in Chapter 4.8. The calculations of the mean crystallite size were not conducted as the particles are highly morphologically anisotropic, and the Debye-Scherrer's approximation would not have yielded reasonable values. However, the differences in crystallite size are apparent. In Fig. 48, Fig. 49, it is seen that the crystallites forming the grains of the monoclinic polycrystalline are irregular-shaped. There is no significant difference between the morphologies obtained for temperatures T_{max} = 90 ˚C and T_{max} = 100 ˚C. Large needle-shaped and platelet-shaped crystals that are characteristic of the monoclinic crystal system are visible.

Homogeneous precipitation from a diluted solution

The effect of the reagents' concentration on the final morphology of the homogeneously precipitated product may be evaluated from Fig. 53.

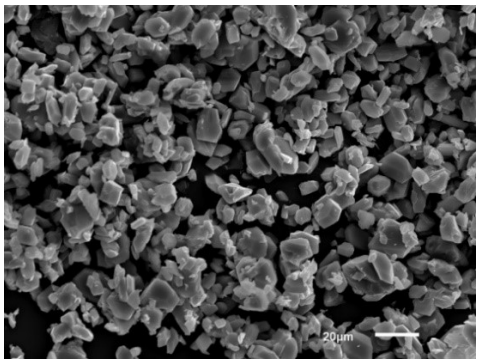

Figure 53. The SEM micrograph showing the morphology of $Ce_2(C_2O_4)_3 \cdot 10H_2O$, homogeneous precipitation, low concentrations.

As seen from Fig. 53, conducting the homogeneous precipitation from a diluted solution did not result in larger crystals formation. On the other hand, smaller and more uniform crystallites were formed. Low concentrations turned out to completely restrict the formation of needle-like microcrystals. Thick monoclinic platelets are the prevalent morphology in this case.

6. Conclusions

A bibliographic review about lanthanides' implementation in radiomedicine was done. Oxamic and glyoxylic acid's behavior in aqueous solutions was a subject of interest in this work. Several physicochemical properties of the concerned compounds were assessed. First, the pKa values were determined for both of the acids. Second, the room temperature solubility was determined for oxamic acid. Within the same experimental setup, it was impossible to specify the same value for glyoxylic acid; gelation under heating was proven for glyoxylic acid. Third, the oxamic and glyoxylic acid's thermal and photochemical stability was evaluated employing conventional laboratory techniques, Raman spectroscopy, and roentgen diffraction analysis. While glyoxylic acid did not show any signs of instability, oxamic acid was proven to undergo decomposition/hydrolysis in aqueous solutions. The kinetics of this process was determined: the rate constants were found for two temperatures. Oxamic acid also slowly (in a timespan of months) hydrolyses in water under ambient conditions.

The affinity of the examined acids to lanthanides in an aqueous solution was tested. Based on the conducted experiments, it is possible to conclude that glyoxylic acid is not suitable for Ln simple separation from the solutions; glyoxylic acid displays no notable interaction with lanthanide species. Oxamic acid may be a precursor of the oxalate anion, and lanthanide (III) oxalate hydrates may be precipitated homogeneously. This procedure appears interesting and promising, considering the outstanding importance of lanthanide (III) oxalates in chemistry and technology. The homogeneous precipitation of cerium (III) oxalate decahydrate was conducted, the process was quantitatively described, and the morphologies of the final homogeneously precipitated products were compared with the morphology of the oxalates synthesized under conventional heterogeneous conditions.

Moreover, the characterization (roentgen diffraction, thermogravimetry, and electron microscopy) of the representative lanthanide (III) oxalate decahydrates was executed. All the concepts and procedures were supported by the theoretical foundation.

7. References

(1) Abraham, F.; Arab-Chapelet, B.; Rivenet, M.; Tamain, C.; Grandjean, S. Actinide Oxalates, Solid State Structures and Applications. *Coord. Chem. Rev.* **2014**, *266–267*, 28–68. https://doi.org/10.1016/j.ccr.2013.08.036.

(2) Zinin, D. S.; Bushuev, N. N. Separate Crystallization of Lanthanide Oxalates and Calcium Oxalates from Nitric Acid Solutions. *Russ. J. Inorg. Chem.* **2018**, *63* (9), 1211–1216. https://doi.org/10.1134/S003602361809022X.

(3) Tyrpekl, V.; Markova, P.; Dopita, M.; Brázda, P.; Vacca, M. A. Cerium Oxalate Morphotypes: Synthesis and Conversion into Nanocrystalline Oxide. *Inorg. Chem.* **2019**, *58* (15), 10111–10118. https://doi.org/10.1021/acs.inorgchem.9b01250.

(4) Manaud, J.; Maynadié, J.; Mesbah, A.; Hunault, M. O. J. Y.; Martin, P. M.; Zunino, M.; Meyer, D.; Dacheux, N.; Clavier, N. Hydrothermal Conversion of Uranium(IV) Oxalate into Oxides: A Comprehensive Study. *Inorg. Chem.* **2020**, *59* (5), 3260–3273. https://doi.org/10.1021/acs.inorgchem.9b03672.

(5) Ellart, M.; Blanchard, F.; Rivenet, M.; Abraham, F. Structural Variations of 2D and 3D Lanthanide Oxalate Frameworks Hydrothermally Synthesized in the Presence of Hydrazinium Ions. *Inorg. Chem.* **2020**, *59* (1), 491–504. https://doi.org/10.1021/acs.inorgchem.9b02781.

(6) Krichen, F.; Walha, S.; Lhoste, J.; Goutenoire, F.; Kabadou, A. Design of Lanthanide Metal Organic Frameworks Incorporating Dicarboxylate Ligands. *J. Porous Mater.* **2019**, *26* (6), 1679–1689. https://doi.org/10.1007/s10934-019-00768-0.

(7) Gergoric, M.; Barrier, A.; Retegan, T. Recovery of Rare-Earth Elements from Neodymium Magnet Waste Using Glycolic, Maleic, and Ascorbic Acids Followed by Solvent Extraction. *J. Sustain. Metall.* **2019**, *5* (1), 85–96. https://doi.org/10.1007/s40831-018-0200-6.

(8) Van de Voorde, M.; Van Hecke, K.; Cardinaels, T.; Binnemans, K. Radiochemical Processing of Nuclear-Reactor-Produced Radiolanthanides for Medical Applications. *Coord. Chem. Rev.* **2019**, *382*, 103–125. https://doi.org/10.1016/j.ccr.2018.11.007.

(9) Nash, K. L. A REVIEW OF THE BASIC CHEMISTRY AND RECENT DEVELOPMENTS IN TRIVALENT F-ELEMENTS SEPARATIONS. *Solvent Extr. Ion Exch.* **1993**, *11* (4), 729–768. https://doi.org/10.1080/07366299308918184.

(10) Götzke, L.; Schaper, G.; März, J.; Kaden, P.; Huittinen, N.; Stumpf, T.; Kammerlander, K. K. K.; Brunner, E.; Hahn, P.; Mehnert, A.; Kersting, B.; Henle, T.; Lindoy, L. F.; Zanoni, G.; Weigand, J. J. Coordination Chemistry of F-Block Metal Ions with Ligands Bearing Bio-Relevant Functional Groups. *Coord. Chem. Rev.* **2019**, *386*, 267–309. https://doi.org/10.1016/j.ccr.2019.01.006.

(11) Bottrill, M.; Kwok, L.; Long, N. J. Lanthanides in Magnetic Resonance Imaging. *Chem. Soc. Rev.* **2006**, *35* (6), 557. https://doi.org/10.1039/b516376p.

(12) Wang, K.; Cheng, Y.; Yang, X.; Li, R. Cell Responses to Lanthanides and Potential Pharmacological Actions of Lanthanides. *Met. Ions Biol. Syst.* **2003**, *40*, 707–751.

(13) Evans, C. H. Interesting and Useful Biochemical Properties of Lanthanides. *Trends Biochem. Sci.* **1983**, *8* (12), 445–449. https://doi.org/10.1016/0968-0004(83)90032-4.

(14) Fricker, S. P. The Therapeutic Application of Lanthanides. *Chem. Soc. Rev.* **2006**, *35* (6), 524. https://doi.org/10.1039/b509608c.
(15) Todorov, L.; Kostova, I.; Traykova, M. Lanthanum, Gallium and Their Impact on Oxidative Stress. *Curr. Med. Chem.* **2019**, *26* (22), 4280–4295. https://doi.org/10.2174/0929867326666190104165311.
(16) IVAN LUKEŠ, ZDENĚK MIČKA. *Anorganická Chemie II (Systematická Část)*, Nakladatelství Karolinum.; Praha; Vol. 2009.
(17) *Werner Centennial*; Kauffman, G. B., Ed.; Advances in Chemistry; AMERICAN CHEMICAL SOCIETY: WASHINGTON, D.C., 1967; Vol. 62. https://doi.org/10.1021/ba-1967-0062.
(18) Bilal, B. A.; Müller, E. Thermodynamic Study of Ce4+ /Ce3+ Redox Reaction in Aqueous Solutions at Elevated Temperatures: 1. Reduction Potential and Hydrolysis Equilibria of Ce4+ in HClO4 Solutions. *Z. Für Naturforschung A* **1992**, *47* (9), 974–984. https://doi.org/10.1515/zna-1992-0908.
(19) MacDonald, M. R.; Bates, J. E.; Ziller, J. W.; Furche, F.; Evans, W. J. Completing the Series of +2 Ions for the Lanthanide Elements: Synthesis of Molecular Complexes of Pr^{2+}, Gd^{2+}, Tb^{2+}, and Lu^{2+}. *J. Am. Chem. Soc.* **2013**, *135* (26), 9857–9868. https://doi.org/10.1021/ja403753j.
(20) Lang, P. F.; Smith, B. C. Ionization Energies of Lanthanides. *J. Chem. Educ.* **2010**, *87* (8), 875–881. https://doi.org/10.1021/ed100215q.
(21) Shannon, R. D. Revised Effective Ionic Radii and Systematic Studies of Interatomic Distances in Halides and Chalcogenides. *Acta Crystallogr. Sect. A* **1976**, *32* (5), 751–767. https://doi.org/10.1107/S0567739476001551.
(22) Jakupec, M. A.; Unfried, P.; Keppler, B. K. Pharmacological Properties of Cerium Compunds. In *Reviews of Physiology, Biochemistry and Pharmacology*; Reviews of Physiology, Biochemistry and Pharmacology; Springer Berlin Heidelberg: Berlin, Heidelberg, 2005; Vol. 153, pp 101–111. https://doi.org/10.1007/s10254-004-0024-6.
(23) Albaaj, F.; Hutchison, A. J. Lanthanum Carbonate for the Treatment of Hyperphosphataemia in Renal Failure and Dialysis Patients. *Expert Opin. Pharmacother.* **2005**, *6* (2), 319–328. https://doi.org/10.1517/14656566.6.2.319.
(24) Haley, T. J. Pharmacology and Toxicology of the Rare Earth Elements. *J. Pharm. Sci.* **1965**, *54* (5), 663–670. https://doi.org/10.1002/jps.2600540502.
(25) Garner, J. P.; Heppell, P. S. J. Cerium Nitrate in the Management of Burns. *Burns* **2005**, *31* (5), 539–547. https://doi.org/10.1016/j.burns.2005.01.014.
(26) Fleisch, H.; Bisaz, S. Mechanism of Calcification: Inhibitory Role of Pyrophosphate. *Nature* **1962**, *195* (4844), 911–911. https://doi.org/10.1038/195911a0.
(27) Hou, C.-C.; Feng, M.; Wang, K.; Yang, X.-G. Lanthanides Inhibit Adipogenesis with Promotion of Cell Proliferation in 3T3-L1 Preadipocytes. *Metallomics* **2013**, *5* (6), 715. https://doi.org/10.1039/c3mt00020f.
(28) Cotton, S. A.; Harrowfield, J. M. Lanthanides: Biological Activity and Medical Applications. In *Encyclopedia of Inorganic and Bioinorganic Chemistry*; Scott, R. A., Ed.; John Wiley & Sons, Ltd: Chichester, UK, 2012; p eibc2091. https://doi.org/10.1002/9781119951438.eibc2091.

(29) Evans, C. H. Application of Ferrography to the Study of Wear and Arthritis in Human Joints. *Wear* **1983**, *90* (2), 281–292. https://doi.org/10.1016/0043-1648(83)90186-2.

(30) Weekes, D. M.; Orvig, C. Harnessing the Bone-Seeking Ability of Ca(II)-like Metal Ions in the Treatment of Metastatic Cancer and Resorption Disorders. *Chem. Soc. Rev.* **2016**, *45* (8), 2024–2031. https://doi.org/10.1039/C5CS00712G.

(31) Prabakaran, S.; Rajan, M.; Lv, C.; Meng, G. Lanthanides-Substituted Hydroxyapatite/Aloe Vera Composite Coated Titanium Plate for Bone Tissue Regeneration. *Int. J. Nanomedicine* **2020**, *Volume 15*, 8261–8279. https://doi.org/10.2147/IJN.S267632.

(32) Kalaivani, S.; Guleria, A.; Kumar, D.; Kannan, S. Bulk Yttria as a Host for Lanthanides in Biomedical Applications: Influence of Concentration Gradients on Structural, Mechanical, Optical, and *in Vitro* Imaging Behavior. *ACS Appl. Bio Mater.* **2019**, *2* (10), 4634–4647. https://doi.org/10.1021/acsabm.9b00718.

(33) Liu, Q. Lanthanides and Cancer. In *Encyclopedia of Metalloproteins*; Kretsinger, R. H., Uversky, V. N., Permyakov, E. A., Eds.; Springer New York: New York, NY, 2013; pp 1103–1110. https://doi.org/10.1007/978-1-4614-1533-6_153.

(34) F. Arambula, J.; Preihs, C.; Borthwick, D.; Magda, D.; L. Sessler, J. Texaphyrins: Tumor Localizing Redox Active Expanded Porphyrins. *Anticancer Agents Med. Chem.* **2011**, *11* (2), 222–232. https://doi.org/10.2174/187152011795255894.

(35) Martin, R. B.; Richardson, F. S. Lanthanides as Probes for Calcium in Biological Systems. *Q. Rev. Biophys.* **1979**, *12* (2), 181–209. https://doi.org/10.1017/s0033583500002754.

(36) Ascenzi, P.; Bettinelli, M.; Boffi, A.; Botta, M.; De Simone, G.; Luchinat, C.; Marengo, E.; Mei, H.; Aime, S. Rare Earth Elements (REE) in Biology and Medicine. *Rendiconti Lincei Sci. Fis. E Nat.* **2020**, *31* (3), 821–833. https://doi.org/10.1007/s12210-020-00930-w.

(37) Norek, M.; Peters, J. A. MRI Contrast Agents Based on Dysprosium or Holmium. *Prog. Nucl. Magn. Reson. Spectrosc.* **2011**, *59* (1), 64–82. https://doi.org/10.1016/j.pnmrs.2010.08.002.

(38) Marturano, V.; Kozlowska, J.; Bajek, A.; Giamberini, M.; Ambrogi, V.; Cerruti, P.; Garcia-Valls, R.; Montornes, J. M.; Tylkowski, B. Photo-Triggered Capsules Based on Lanthanide-Doped Upconverting Nanoparticles for Medical Applications. *Coord. Chem. Rev.* **2019**, *398*, 213013. https://doi.org/10.1016/j.ccr.2019.213013.

(39) Werts, M. H. V. Making Sense of Lanthanide Luminescence. *Sci. Prog.* **2005**, *88* (2), 101–131. https://doi.org/10.3184/003685005783238435.

(40) Sculimbrene, B. R.; Imperiali, B. Lanthanide-Binding Tags as Luminescent Probes for Studying Protein Interactions. *J. Am. Chem. Soc.* **2006**, *128* (22), 7346–7352. https://doi.org/10.1021/ja061188a.

(41) Bandura, D. R.; Baranov, V. I.; Ornatsky, O. I.; Antonov, A.; Kinach, R.; Lou, X.; Pavlov, S.; Vorobiev, S.; Dick, J. E.; Tanner, S. D. Mass Cytometry: Technique for Real Time Single Cell Multitarget Immunoassay Based on Inductively Coupled Plasma Time-of-Flight Mass Spectrometry. *Anal. Chem.* **2009**, *81* (16), 6813–6822. https://doi.org/10.1021/ac901049w.

(42) Knapp, F.; Dash, A. *Radiopharmaceuticals for Therapy*; 2015. https://doi.org/10.1007/978-81-322-2607-9.

(43) Choppin, G.; Liljenzin, J.-O.; Rydberg, J.; Ekberg, C. Chapter 5 - Unstable Nuclei and Radioactive Decay. In *Radiochemistry and Nuclear Chemistry (Fourth Edition)*; Choppin, G., Liljenzin, J.-O., Rydberg, J., Ekberg, C., Eds.; Academic Press: Oxford, 2013; pp 85–123. https://doi.org/10.1016/B978-0-12-405897-2.00005-7.

(44) Neves, M.; Kling, A.; Lambrecht, R. M. UTILIZATION OF LOW POWER RESEARCH REACTORS FOR PRODUCTION OF THERAPEUTIC RADIOPHARMACEUTICALS. 11.

(45) Chaturvedi, S.; Mishra, A. K. Vectors for the Delivery of Radiopharmaceuticals in Cancer Therapeutics. *Ther. Deliv.* **2014**, *5* (8), 893–912. https://doi.org/10.4155/tde.14.57.

(46) Thiele, N. A.; Woods, J. J.; Wilson, J. J. Implementing F-Block Metal Ions in Medicine: Tuning the Size Selectivity of Expanded Macrocycles. *Inorg. Chem.* **2019**, *58* (16), 10483–10500. https://doi.org/10.1021/acs.inorgchem.9b01277.

(47) Rösch, F. Radiolanthanides in Endoradiotherapy: An Overview. *Radiochim. Acta* **2007**, *95* (6). https://doi.org/10.1524/ract.2007.95.6.303.

(48) Van Hoecke, K.; Bussé, J.; Gysemans, M.; Adriaensen, L.; Dobney, A.; Cardinaels, T. Isolation of Lanthanides from Spent Nuclear Fuel by Means of High Performance Ion Chromatography (HPIC) Prior to Mass Spectrometric Analysis. *J. Radioanal. Nucl. Chem.* **2017**, *314* (3), 1727–1739. https://doi.org/10.1007/s10967-017-5538-x.

(49) Choppin, G. R.; Dadgar, A.; Rizkalla, E. N. Thermodynamics of Complexation of Lanthanides by Dicarboxylate Ligands. *Inorg. Chem.* **1986**, *25* (20), 3581–3584. https://doi.org/10.1021/ic00240a009.

(50) Grandjean, S.; Arab-Chapelet, B.; Robisson, A. C.; Abraham, F.; Martin, Ph.; Dancausse, J.-Ph.; Herlet, N.; Léorier, C. Structure of Mixed U(IV)–An(III) Precursors Synthesized by Co-Conversion Methods (Where An=Pu, Am or Cm). *J. Nucl. Mater.* **2009**, *385* (1), 204–207. https://doi.org/10.1016/j.jnucmat.2008.10.039.

(51) Maslennikov, D. V.; Matvienko, A. A.; Sidelnikov, A. A.; Chizhik, S. A. A Study of the Effect of Structural Transformations in the Course of Ce2(C2O4)3·10H2O Thermal Decomposition on the Morphology of CeO2 Obtained. *Mater. Today Proc.* **2017**, *4* (11), 11495–11499. https://doi.org/10.1016/j.matpr.2017.09.036.

(52) Jean-Philippe Gaillard; Sophie Lalleman; Murielle Bertrand; Edouard Plasari. Modelling of Neodymium Oxalate Precipitation by the Method of Classes. *Chem. Eng. Trans.* **2015**, *43*, 781–786. https://doi.org/10.3303/CET1543131.

(53) Modolo, G.; Vijgen, H.; Serrano-Purroy, D.; Christiansen, B.; Malmbeck, R.; Sorel, C.; Baron, P. DIAMEX Counter-Current Extraction Process for Recovery of Trivalent Actinides from Simulated High Active Concentrate. *Sep. Sci. Technol.* **2007**, *42* (3), 439–452. https://doi.org/10.1080/01496390601120763.

(54) Almeida, L. D.; Grandjean, S.; Vigier, N.; Patisson, F. New Insights on the Thermal Decomposition of Lanthanide(III) and Actinide(III) Oxalates: From Neodymium and Cerium to Plutonium. 25.

(55) Lalleman, S.; Bertrand, M.; Plasari, E. Physical Simulation of Precipitation of Radioactive Element Oxalates by Using the Harmless Neodymium Oxalate for

Studying the Agglomeration Phenomena. *J. Cryst. Growth* **2012**, *342* (1), 42–49. https://doi.org/10.1016/j.jcrysgro.2011.01.079.

(56) Zhou, H.-C.; Long, J. R.; Yaghi, O. M. Introduction to Metal–Organic Frameworks. *Chem. Rev.* **2012**, *112* (2), 673–674. https://doi.org/10.1021/cr300014x.

(57) Zhang, K.; Xie, X.; Li, H.; Gao, J.; Nie, L.; Pan, Y.; Xie, J.; Tian, D.; Liu, W.; Fan, Q.; Su, H.; Huang, L.; Huang, W. Highly Water-Stable Lanthanide-Oxalate MOFs with Remarkable Proton Conductivity and Tunable Luminescence. *Adv. Mater.* **2017**, *29* (34), 1701804. https://doi.org/10.1002/adma.201701804.

(58) Fuller, M. J.; Pinkstone, J. Thermal Analysis of the Oxalate Hexahydrates and Decahydrates of Yttrium and the Lanthanide Elements. *J. Common Met.* **1980**, *70* (2), 127–142. https://doi.org/10.1016/0022-5088(80)90222-2.

(59) Suli, L. M.; Ibrahim, W. H. W.; Aziz, B. A.; Deraman, M. R.; Ismail, N. A. A Review of Rare Earth Mineral Processing Technology. *Chem. Eng. Res. Bull.* **2017**, *19*, 20. https://doi.org/10.3329/cerb.v19i0.33773.

(60) Chi, R.; Xu, Z. A Solution Chemistry Approach to the Study of Rare Earth Element Precipitation by Oxalic Acid. *Metall. Mater. Trans. B* **1999**, *30* (2), 189–195. https://doi.org/10.1007/s11663-999-0047-0.

(61) IUPAC Stability Constants Database–Completion of Data Collection up to 2006. *Chem. Int. -- Newsmag. IUPAC* **2006**, *28* (1), 26–26. https://doi.org/10.1515/ci.2006.28.1.26.

(62) Gutz, I. G. R. *CurTiPot – PH and Acid–Base Titration Curves: Analysis and Simulation Freeware*.

(63) Martinj, C. C. S. Solubility of the Rare Earth Oxalates and Complex Ion Formation in Oxalate Solution. 11. Neodymium and Cerium(III). 5.

(64) Ollendorff, W.; Weigel, F. The Crystal Structure of Some Lanthanide Oxalate Decahydrates, Ln2(C2O4)3·10H2O, with Ln = La, Ce, Pr, and Nd. *Inorg. Nucl. Chem. Lett.* **1969**, *5* (4), 263–269. https://doi.org/10.1016/0020-1650(69)80196-0.

(65) Tamain, C.; Arab-Chapelet, B.; Rivenet, M.; Legoff, X. F.; Loubert, G.; Grandjean, S.; Abraham, F. Coordination Modes of Americium in the $Am_2(C_2O_4)_3(H_2O)_6 \cdot 4H_2O$ Oxalate: Synthesis, Crystal Structure, Spectroscopic Characterizations and Comparison in the $M_2(C_2O_4)_3(H_2O)_6 \cdot n\,H_2O$ (M = Ln, An) Series. *Inorg. Chem.* **2016**, *55* (1), 51–61. https://doi.org/10.1021/acs.inorgchem.5b01781.

(66) Michaelides, A.; Skoulika, S.; Aubry, A. CRYSTAL GROWTH AND STRUCTURE OF La2(C204)3 9.5H20. *23* (4), 7.

(67) Trollet, D.; Roméro, S.; Mosset, A.; Trombe, J.-C. Synthèse et structure d'un oxalate de gadolinium ne contenant pas de molécule d'eau libre, [Gd(H2O)3]2(C2O4)3. *Comptes Rendus Académie Sci. - Ser. IIB - Mech.-Phys.-Chem.-Astron.* **1997**, *325* (11), 663–670. https://doi.org/10.1016/S1251-8069(99)80065-7.

(68) Pozdniakov, M. A.; Zhuk, I. V.; Lyapunova, M. V.; Salikov, A. S.; Botvin, V. V.; Filimoshkin, A. G. Glyoxylic Acid: Synthesis, Isolation, and Crystallization. *Russ. Chem. Bull.* **2019**, *68* (3), 472–479. https://doi.org/10.1007/s11172-019-2442-2.

(69) Mattioda, G.; Christidis, Y. Glyoxylic Acid. In *Ullmann's Encyclopedia of Industrial Chemistry*; Wiley-VCH Verlag GmbH & Co. KGaA, Ed.; Wiley-VCH Verlag GmbH

& Co. KGaA: Weinheim, Germany, 2000; p a12_495. https://doi.org/10.1002/14356007.a12_495.

(70) Kumar, R.; Sharma, P.; Mishra, P. Vanillin Derivatives Showing Various Biological Activities. *Int. J. PharmTech Res.* **2012**, *4*.

(71) Takeuchi, Hideo; Yamaguchi, Yuuji. The Hair Cosmetic Material. JP2020/37531.

(72) Alle Bruggink, S. S. M. D. 2001. *Synthesis of β-Lactam Antibiotics*, 1st ed.; Springer, Dordrecht; Vol. 2001.

(73) Eugene, A. J.; Xia, S.-S.; Guzman, M. I. Aqueous Photochemistry of Glyoxylic Acid. *J. Phys. Chem. A* **2016**, *120* (21), 3817–3826. https://doi.org/10.1021/acs.jpca.6b00225.

(74) Fan, B.; Trant, J. F.; Wong, A. D.; Gillies, E. R. Polyglyoxylates: A Versatile Class of Triggerable Self-Immolative Polymers from Readily Accessible Monomers. *J. Am. Chem. Soc.* **2014**, *136* (28), 10116–10123. https://doi.org/10.1021/ja504727u.

(75) Yardley, R. E.; Rabiee Kenaree, A.; Liang, X.; Gillies, E. R. Transesterification of Poly(Ethyl Glyoxylate): A Route to Structurally Diverse Polyglyoxylates. *Macromolecules* **2020**, *53* (19), 8600–8609. https://doi.org/10.1021/acs.macromol.0c01197.

(76) Chan, M. N.; Kreidenweis, S. M.; Chan, C. K. Measurements of the Hygroscopic and Deliquescence Properties of Organic Compounds of Different Solubilities in Water and Their Relationship with Cloud Condensation Nuclei Activities. *Environ. Sci. Technol.* **2008**, *42* (10), 3602–3608. https://doi.org/10.1021/es7023252.

(77) PubChem Compound Summary for CID 15620607, Glyoxylic Acid Monohydrate. *PubChem*; National Center for Biotechnology Information (2021); Vol. Retrieved May 17, 2021.

(78) Lis, T. Structure of Dihydroxyacetic Acid (Glyoxylic Acid Monohydrate), C2H4O4. *Acta Crystallogr. C* **1983**, *39* (8), 1082–1084. https://doi.org/10.1107/S0108270183007465.

(79) Bruhn, K. Sorensen, P.E., Lindelov, F. Kinetics and Equilibria for Thew Reversible Hydration of the Aldehyde Group in Glyoxylic Acid. *Acta Chemica Scandinavica 1974*, 162–168.

(80) Plath, K. L.; Axson, J. L.; Nelson, G. C.; Takahashi, K.; Skodje, R. T.; Vaidaa, V. Gas-Phase Vibrational Spectra of Glyoxylic Acid and Its Gem Diol Monohydrate. Implications for Atmospheric Chemistry. *React. Kinet. Catal. Lett.* **2009**, *96* (2), 209–224. https://doi.org/10.1007/s11144-009-5528-2.

(81) Redington, R. L.; Liang, C.-K. J. Vibrational Spectra of Glyoxylic Acid Monomers. *J. Mol. Spectrosc.* **1984**, *104* (1), 25–39. https://doi.org/10.1016/0022-2852(84)90242-X.

(82) Boga, C.; Taddei, P.; Micheletti, G.; Ascari, F.; Ballarin, B.; Morigi, M.; Galli, S. Formaldehyde Replacement with Glyoxylic Acid in Semipermanent Hair Straightening: A New and Multidisciplinary Investigation. *Int. J. Cosmet. Sci.* **2014**, *36* (5), 459–470. https://doi.org/10.1111/ics.12148.

(83) Pozdniakov, M. A.; Rubtsov, K. V.; Rasskazova, L. A.; Filimoshkin, A. Glyoxylic Acid Separation from Products of Glyoxal Oxidation in the Form of Its Calcium Salt. *Adv. Mater. Res.* **2015**, *1085*, 74–78. https://doi.org/10.4028/www.scientific.net/AMR.1085.74.

(84) Tripathi, G. N. R.; Katon, J. E. Vibrational Spectra and Structure of Crystalline Oxamic Acid and Sodium Oxamate. *Spectrochim. Acta Part Mol. Spectrosc.* **1979**, *35* (5), 401–407. https://doi.org/10.1016/0584-8539(79)80152-X.

(85) Raczyńska, E. D.; Hallmann, M.; Duczmal, K. Quantum-Chemical Studies of Amide–Iminol Tautomerism for Inhibitor of Lactate Dehydrogenase: Oxamic Acid. *Comput. Theor. Chem.* **2011**, *964* (1–3), 310–317. https://doi.org/10.1016/j.comptc.2011.01.017.

(86) Dugarte-Dugarte, A. J.; van de Streek, J.; dos Santos, A. M.; Daemen, L. L.; Puretzky, A. A.; Díaz de Delgado, G.; Delgado, J. M. Structure Determination of Oxamic Acid from Laboratory Powder X-Ray Diffraction Data and Energy Minimization by DFT-D. *J. Mol. Struct.* **2019**, *1177*, 310–316. https://doi.org/10.1016/j.molstruc.2018.09.089.

(87) J.M.Berg, J.L.Tzmoczko,L.Stryer,G.J.Gatto. *Biochemistry*, 7th ed.; W.H.Freeman: New York, NY; Vol. 2012.

(88) O'Carra, P.; Barry, S. [77] Lactate Dehydrogenase: Specific Ligand Approach. In *Methods in Enzymology*; Elsevier, 1974; Vol. 34, pp 598–605. https://doi.org/10.1016/S0076-6879(74)34080-3.

(89) Yang, L.; Liu, L.; Olsen, B. A.; Nussbaum, M. A. The Determination of Oxalic Acid, Oxamic Acid, and Oxamide in a Drug Substance by Ion-Exclusion Chromatography. *J. Pharm. Biomed. Anal.* **2000**, *22* (3), 487–493. https://doi.org/10.1016/S0731-7085(00)00230-2.

(90) Zarzyka-Niemiec, I. Hydroxyalkylation of Oxamic Acid with Propylene Carbonate: Synthesis, Composition, and Properties of Products. *J. Appl. Polym. Sci.* **2008**, *110* (1), 66–75. https://doi.org/10.1002/app.28609.

(91) Kakkar, R.; Pathak, M.; Radhika, N. P. A DFT Study of the Structures of Pyruvic Acid Isomers and Their Decarboxylation. *Org. Biomol. Chem.* **2006**, *4* (5), 886. https://doi.org/10.1039/b516355b.

(92) Wolfs, I.; Desseyn, H. O. Hydrogen Bond Patterns in Solid State Carboxylic Acids. Vibrational Study of the Hydrogen Bond Patterns in Oxamic, Malonamic and Succinamic Acid. *Spectrochim. Acta. A. Mol. Biomol. Spectrosc.* **1995**, *51* (10), 1601–1615. https://doi.org/10.1016/0584-8539(95)01527-2.

(93) Wallace, F.; Wagner, E. Infrared and Far-Infrared Spectra of Solid Oxamic Acid, Deutero-Oxamic Acid and Their Salts. *Spectrochim. Acta Part Mol. Spectrosc.* **1978**, *34* (6), 589–606. https://doi.org/10.1016/0584-8539(78)80058-0.

(94) Aakeröy, C. B.; Hughes, D. P.; Nieuwenhuyzen, M. The Oxamate Anion: A Flexible Building Block of Hydrogen-Bonded Architectures for Crystal Engineering. *J. Am. Chem. Soc.* **1996**, *118* (42), 10134–10140. https://doi.org/10.1021/ja953296v.

(95) ICDD, PDF-4/Organics 2018 (Database), Edited by S. Kabekkodu, International Centre for Diffraction Data, Newtown Square, PA, USA.

(96) Caires, F. J.; Nunes, W. D. G.; Gaglieri, C.; Nascimento, A. L. C. S. do; Teixeira, J. A.; Zangaro, G. A. C.; Treu-Filho, O.; Ionashiro, M. Thermoanalytical, Spectroscopic and DFT Studies of Heavy Trivalent Lanthanides and Yttrium(III) with Oxamate as Ligand. *Mater. Res.* **2017**, *20* (4), 937–944. https://doi.org/10.1590/1980-5373-mr-2016-0633.

(97) Skoulika, S.; Michaelides, A.; Aubry, A. The Structure of Two Gel-Grown Oxamate Complexes: Bis(Oxamato-O,O')Calcium(II) Tetrahydrate and Bis(Oxamato-O,O')Cadmium(II) Tetrahydrate. *Acta Crystallogr. C* **1988**, *44* (5), 931–933. https://doi.org/10.1107/S0108270188000526.

(98) Veltsistas, P. T.; Perlepes, S. P.; Karayannis, M. I.; Tsangaris, J. M. Use of Ethyl Oxamate for Syntheses of Oxamato(-1) and Novel p-Oxamato(-2) Complexes. 5.

(99) Caires, F. J.; Lima, L. S.; Gomes, D. J. C.; Gigante, A. C.; Treu-Filho, O.; Ionashiro, M. Thermal and Spectroscopic Studies of Solid Oxamate of Light Trivalent Lanthanides. *J. Therm. Anal. Calorim.* **2013**, *111* (1), 349–355. https://doi.org/10.1007/s10973-012-2220-y.

(100) Lazaridou, V.; Perlepes, S. P.; Tsangaris, J. M.; Zafiropoulos, Th. F. Synthesis, Physical Properties and Spectroscopic Studies of Oxamato (−1) Lanthanide(III) Complexes. *J. Common Met.* **1990**, *158* (1), 1–14. https://doi.org/10.1016/0022-5088(90)90425-J.

(101) Schoetersd, G. The Complexes of Oxamic Acid with Ni(I1). 6.

(102) Perlepes, S. P.; Zafiropoulos, Th. F.; Kouinis, J. K.; Galinos, A. G. Lanthanide(III) Complexes of Oxamic Acid. *Z. Für Naturforschung B* **1981**, *36* (6), 697–703. https://doi.org/10.1515/znb-1981-0609.

(103) Zafiropoulos, Th. F.; Perlepes, S. P.; Galinos, A. G. Complexes of Oxamic Acid with La(III), Gd(III), Tb(III), Er(III), Tm(III) and Lu(III). *J. Chin. Chem. Soc.* **1983**, *30* (3), 201–206. https://doi.org/10.1002/jccs.198300031.

(104) Vansant, C.; Desseyn, H. O.; Perlepes, S. P. The Synthesis, Spectroscopic and Thermal Study of Oxamic Acid Compounds of Some Metal(II) Ions. *Transit. Met. Chem.* **1995**, *20* (5), 454–459. https://doi.org/10.1007/BF00141516.

(105) Kouinis, J. K.; Velsistas, P. Th.; Tsangaris, J. M. Complexes of Oxamic Acid with Au(III) and Rh(III). *Monatshefte Für Chem. - Chem. Mon.* **1982**, *113* (2), 155–161. https://doi.org/10.1007/BF00799014.

(106) Michaelides, A.; Skoulika, S. Gel Growth of Single Crystals of Complexes of Oxamic Acid with Divalent Metals (Pb2+, Ca2+, Cd2+. *J. Cryst. Growth* **1989**, *94* (1), 208–212. https://doi.org/10.1016/0022-0248(89)90620-9.

(107) Reis, N. V.; Barros, W. P.; Oliveira, W. X. C.; Pereira, C. L. M.; Rocha, W. R.; Pinheiro, C. B.; Lloret, F.; Julve, M.; Stumpf, H. O. Crystal Structure and Magnetic Properties of an Oxamato-Bridged Heterobimetallic Tetranuclear [Ni ^{II} Cu ^{II}] $_2$ Complex of the Rack Type: Crystal Structure and Magnetic Properties of an Oxamato-Bridged Heterobimetallic Tetranuclear [Ni ^{II} Cu ^{II}] $_2$ Complex of the Rack Type. *Eur. J. Inorg. Chem.* **2018**, *2018* (3–4), 477–484. https://doi.org/10.1002/ejic.201700821.

(108) Papadimitriou, C.; Veltsistas, P.; Marek, J.; Derek Woollins, J. The Preparation and X-Ray Structure of [Ho(Oxam)3(H2O)3]4·2.75H2O. *Inorganica Chim. Acta* **1998**, *267* (2), 299–303. https://doi.org/10.1016/S0020-1693(97)05578-3.

(109) G. Veltsistas, P.; D. Papadimitriou, C.; M. Z. Slawin, A.; D. Woollins, J. Synthesis, Characterization and X-Ray Structural Determination of the Nine-Coordinate Tris-Aqua Tetra-Oxamato Neodymium(III) Complex [Nd(Hoxm)3(H2oxm)·2.5H2O]. *J. Chem. Res. Synop.* **1999**, No. 3, 222–223. https://doi.org/10.1039/A809526D.

(110) Packer, J.; Thomson, A. L.; Vaughan, J. 864. The Hydrolysis of Amides of Dibasic Acids. Part II. The Acid Hydrolysis of Oxamide and Oxamic Acid. *J. Chem. Soc. Resumed* **1952**, No. 0, 4516–4518. https://doi.org/10.1039/JR9520004516.

(111) Raju, B.; Sivasankar, B. N. Spectral, Thermal and X-Ray Studies on Some New Bis-Hydrazine Lanthanide(III) Glyoxylates. *J. Therm. Anal. Calorim.* **2008**, *94* (1), 289–296. https://doi.org/10.1007/s10973-007-8953-3.

(112) Vikram, L.; Sivasankar, B. N. Spectral, Thermal and X-Ray Studies on Some New Bis-Hydrazine Metal Glyoxylates and Bis-Hydrazine Mixed Metal Glyoxylates. *Thermochim. Acta* **2007**, *452* (1), 20–27. https://doi.org/10.1016/j.tca.2006.10.001.

(113) Pradeep, R.; Sivasankar, B. N. Synthesis, Characterization, Thermal Degradation, X-Ray and DNA Binding Studies on Metal(II) and Mixed Metal Hydrazone Glyoxylate Dihydrates: A Typical One Step Aqueous Condensation Reaction. *Asian J. Chem.* **2017**, *29* (8), 1746–1752. https://doi.org/10.14233/ajchem.2017.20609.

(114) Niculescu, M.; Pascariu, M.-C.; Muntean, C.; Sasca, V.; Lupa, L.; Milea, M.-S.; Birzescu, M. Thermal and Spectroscopic Analysis of Co(II)–Fe(III) Polyglyoxylate Obtained through the Reaction of Ethylene Glycol with Metal Nitrates. *J. Therm. Anal. Calorim.* **2018**, *131* (1), 127–136. https://doi.org/10.1007/s10973-016-6079-1.

(115) Masoudpanah, S. M.; Mirkazemi, S. M.; Shabani, S.; Dolat Abadi, P. T. The Effect of the Ethylene Glycol to Metal Nitrate Molar Ratio on the Phase Evolution, Morphology and Magnetic Properties of Single Phase BiFeO3 Nanoparticles. *Ceram. Int.* **2015**, *41* (8), 9642–9646. https://doi.org/10.1016/j.ceramint.2015.04.029.

(116) Caizer, C. Structural and Magnetic Properties of Nanocrystalline Zn0.65Ni0.35Fe2O4 Powder Obtained from Heteropolynuclear Complex Combination. *Mater. Sci. Eng. B* **2003**, *100* (1), 63–68. https://doi.org/10.1016/S0921-5107(03)00075-8.

(117) Doebelin, N.; Kleeberg, R. Profex: A Graphical User Interface for the Rietveld Refinement Program BGMN. *J. Appl. Crystallogr.* **2015**, *48* (5), 1573–1580. https://doi.org/10.1107/S1600576715014685.

(118) Petříček, V.; Dušek, M.; Palatinus, L. Crystallographic Computing System JANA2006: General Features. *Z. Für Krist. - Cryst. Mater.* **2014**, *229* (5), 345–352. https://doi.org/10.1515/zkri-2014-1737.

(119) Opekar, F.; Jelinek, I.; Rychlovsky, P.; Plzak, Z. *Základní analytická chemie*, 1st ed.; Nakladatelstvi Karolinum: Praha, 2002.

(120) Nývlt, J. Kinetics of Nucleation in Solutions. *J. Cryst. Growth* **1968**, *3–4*, 377–383. https://doi.org/10.1016/0022-0248(68)90179-6.

(121) Sangwal, K. A Novel Self-Consistent Nývlt-like Equation for Metastable Zone Width Determined by the Polythermal Method. *Cryst. Res. Technol.* **2009**, *44* (3), 231–247. https://doi.org/10.1002/crat.200800501.

(122) Nagy, Z. K.; Fujiwara, M.; Woo, X. Y.; Braatz, R. D. Determination of the Kinetic Parameters for the Crystallization of Paracetamol from Water Using Metastable Zone Width Experiments. *Ind. Eng. Chem. Res.* **2008**, *47* (4), 1245–1252. https://doi.org/10.1021/ie060637c.

(123) Mota, F. L.; Teychéne, S.; Biscans, B. Measurement of the Nucleation and Growth Kinetics of Some Middle Distillate Fuels and Their Blends with a Model Biodiesel

Fuel. *Ind. Eng. Chem. Res.* **2014**, *53* (7), 2811–2819. https://doi.org/10.1021/ie402984p.

(124) Dixit, M.; Subbanna, G. N.; Kamath, P. V. Homogeneous Precipitation from Solution by Urea Hydrolysis: A Novel Chemical Route to the α-Hydroxides of Nickel and Cobalt. *J. Mater. Chem.* **1996**, *6* (8), 1429–1432. https://doi.org/10.1039/JM9960601429.

(125) Huang, J.; Chen, C.; Huang, Z.; Fu, J.; Chen, S.; Jiang, Y.; Lu, L.; Xia, Y.; Zhao, X. Preparation and Growth Mechanism of the Flower-like Whiskers of γ-, θ-, and α-Al2O3 Phases by Homogeneous Precipitation/Calcination Method. *Ceram. Int.* **2021**, *47* (12), 16943–16949. https://doi.org/10.1016/j.ceramint.2021.03.004.

(126) Britannica, T. Editors of Encyclopaedia. Chemical precipitation https://www.britannica.com/science/chemical-precipitation (accessed 2021 -06 -16).

(127) Altomare, A.; Corriero, N.; Cuocci, C.; Falcicchio, A.; Moliterni, A.; Rizzi, R. QUALX2.0: A Qualitative Phase Analysis Software Using the Freely Available Database POW-COD. *J. Appl. Crystallogr.* **2015**, *48*. https://doi.org/10.1107/S1600576715002319.

(128) Dahman, Y. Chapter 3 - Smart Nanomaterials**By Yaser Dahman, Adil Kamil, and Daniel Baena. In *Nanotechnology and Functional Materials for Engineers*; Dahman, Y., Ed.; Micro and Nano Technologies; Elsevier, 2017; pp 47–66. https://doi.org/10.1016/B978-0-323-51256-5.00003-4.

(129) Avzianova, E.; Brooks, S. D. Raman Spectroscopy of Glyoxal Oligomers in Aqueous Solutions. *Spectrochim. Acta. A. Mol. Biomol. Spectrosc.* **2013**, *101*, 40–48. https://doi.org/10.1016/j.saa.2012.09.050.

(130) Bjerrum, J., 1909-1992 (viaf)18272890; Sillén, L. G., 1916-1970 (viaf)50275565; Schwarzenbach, G. K., 1904-1978 (viaf)112365539; Berecki-Biedermann, C. (viaf)311208776. *Stability constants of metal-ion complexes, with solubility products of inorganic substances. 2 : Inorganic ligands*; London : Chemical society, 1958.

(131) Frost, R. L.; Weier, M. L. The “cave” Mineral Oxammite - a High Resolution Thermogravimetry and Raman Spectroscopic Study. *Neues Jahrb. Für Mineral. - Monatshefte* **2004**, *2004* (1), 27–48. https://doi.org/10.1127/0028-3649/2004/2004-0027.

(132) Gražulis, S.; Chateigner, D.; Downs, R. T.; Yokochi, A. F. T.; Quirós, M.; Lutterotti, L.; Manakova, E.; Butkus, J.; Moeck, P.; Le Bail, A. Crystallography Open Database – an Open-Access Collection of Crystal Structures. *J. Appl. Crystallogr.* **2009**, *42* (4), 726–729. https://doi.org/10.1107/S0021889809016690.

(133) Newbury, D. E. Mistakes Encountered during Automatic Peak Identification in Low Beam Energy X-Ray Microanalysis. *Scanning* **2007**, *29* (4), 137–151. https://doi.org/10.1002/sca.20009.